JUPITER'S DECAMETRIC FLUX: A CONSISTENT TWO-DIMENSIONAL ANALYSIS, 1957-1970

By
HUGH RICHARD MILLER

A DISSERTATION PRESENTED TO THE GRADUATE COUNCIL OF
THE UNIVERSITY OF FLORIDA
IN PARTIAL FULFILLMENT OF THE REQUIREMENTS FOR THE
DEGREE OF DOCTOR OF PHILOSOPHY

UNIVERSITY OF FLORIDA
1970

ACKNOWLEDGEMENTS

The author wishes to express his sincere appreciation to Dr. A. G. Smith for suggesting the topic of this dissertation, and for his advice and assistance in the analysis of the data and the writing of this dissertation. Appreciation is also expressed to Drs. T. D. Carr and G. R. Lebo for the many useful discussions on the calibration systems employed, and to Drs. F. E. Dunnam and F. B. Wood, the other members of the Supervisory Committee. Messrs. C. N. Oisson, R. J. Leacock, W. W. Richardson, J. Levy, and J. May provided valuable assistance and advice during the entire development of this dissertation. Mrs. Judith Lipofsky aided the author in the computer programming that was necessary for the data analysis. The untiring efforts of Mrs. Gail Pokrant in the typing of this manuscript are deeply appreciated. A special note of appreciation is due the author's wife for her continuing faith and encouragement. It is to her that this dissertation is dedicated.

TABLE OF CONTENTS

LIST OF TABLES

LIST OF FIGURES

Abstract of Dissertation Presented to the
Graduate Council of the University of Florida in Partial Fulfillment
of the Requirements for the Degree of Doctor of Philosophy

JUPITER'S DECAMETRIC FLUX: A CONSISTENT TWO-DIMENSIONAL ANALYSIS, 1957-1970

By

Hugh Richard Miller

December, 1970

Chairman: Dr. A. G. Smith
Major Department: Astronomy

The decametric radiation from Jupiter received from 1957 to 1969 at the University of Florida and its associated field station located at Maipu, Chile, has been analyzed at frequencies ranging from 15 MHz to 27.6 MHz. A consistent analysis of the flux density was undertaken for approximately seventy-five yearly sets of data in order that the individual and joint effects of several geometrical parameters could be determined.

A two-dimensional analysis of the flux density as a simultaneous function of the longitude of the central meridian and the position of Io from superior geocentric conjunction was made. The well-known Io-related "sources," A, B, and C, were easily located on the two-dimensional flux contour maps which were constructed. The flux from Io-related source B did not exhibit any bifurcation as had previously been reported for probability studies. Io-related source D was observed at a frequency of 15 MHz.

A definite symmetry about the Earth-Jupiter line was observed which appears to be associated with these four sources. It was observed that if the positions of Io and the north magnetic pole associated with Io-related source A are reflected through the Earth-Jupiter line, they are then located at positions for which radiation associated with Io-related source B is highly probable. A similar relationship relative to the Earth-Jupiter line exists for Io-related sources C and D where reflected parameters are the position of Io and the position of Jupiter's south magnetic pole.

The two-dimensional analysis of the flux density was also used in an attempt to determine if there exist simultaneous favorable positions of Io and Europa and Io and Ganymede for which the intensity of the radiation is enhanced. It appears that there is no significant effect due either to Europa or Ganymede.

A study was made of the flux density versus sunspot number, Jovicentric declination of the Earth, and brightness of the coronal 5303 Å line (used as an alternative index of solar activity), in an attempt to determine which of these parameters appears to have more influence on the observed 11-year cycle of the Jovian radiation probability. A limited positive correlation was observed between the flux density and the brightness of the coronal line, indicating that solar activity may exert a more important influence on the decametric radiation than does the Jovicentric declination. However, the results presented here are far from conclusive.

A pulse-height analysis of the Jupiter flux data was also carried out. In this analysis, the average flux density of the three peak pulses received in a five-minute interval was plotted versus the number of five-minute intervals. It was found that the number decreased exponentially as the flux density increased out to a value of 73×10^{-22} $w/m^2/cps$. At this point, the number of intervals in which the flux density exceeded the above value suddenly increased. This may be due either to a resonance phenomenon, or it may represent the onset of a different class of pulses. The analysis is not complete enough at the present time to determine which of the above possibilities is more likely.

CHAPTER I

INTRODUCTION

Early Radio Observations of Jupiter

In 1955, Burke and Franklin[1] made a discovery which focused the attention of radio astronomy on the giant planet Jupiter. They observed on their records a strange type of interference at 22 Mc/s which occurred each night, but always four minutes later. Any object on the celestial sphere rises approximately four minutes later on each successive night. When Burke and Franklin attempted to determine what celestial body was in the antenna beam, they found that Jupiter was always at this position.

The interference which is received from Jupiter is very sporadic and occurs in what are called "noise storms." The length of these noise storms varies from only a few seconds to several hours. An example of a Jovian noise storm is shown in Fig. 1.[2]

Shortly after the discovery that Jupiter was the source of the decameter wavelength radiation, several groups, including the University of Florida in 1956, began monitoring this radiation at a frequency of 18 Mc/s.[3,4] Other groups which also monitored the decametric radiation were the National Bureau of Standards,[5,6] Carnegie Institution,[7,8,9,10] Ohio State University,[11,12,13] Yale,[14,15] and the

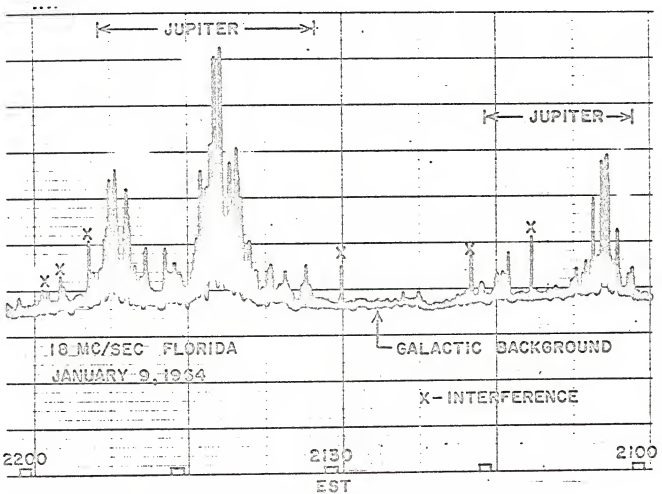

Fig. 1. Record of a typical Jovian noise storm at 18 MHz.

University of Colorado.[16, 17, 18] A good review of the early work has been given by Douglas.[19]

In 1958, another non-thermal component of the radiation received from Jupiter was observed at decimeter wavelengths.[20] The decimetric radiation is believed to be much better understood than the decametric radiation. It is thought to be synchrotron radiation from particles trapped by Jupiter's magnetic field in radiation belts similar to the Earth's Van Allen belts.[21, 22, 23, 24] A recent review of the decimetric radiation received from Jupiter can be found in a paper by Carr and Smith.[4]

Periodicities in the Decametric Radiation

There were numerous periodicities observed in the analysis of the decametric component of the radiation. One of the first of these was that Jupiter did not emit with the same intensity for all longitudes facing the Earth, but had a much higher probability of radiating when certain longitudes were facing Earth. This early work, which was done by Shain,[25] led to the definition of a "radio period" of $9^h55^m30^s$, which is different from the optical rotation periods of Jupiter. There are two such optical rotation rates associated with Jupiter: they are referred to as System I (equatorial regions of Jupiter), which has a period of $9^h50^m30^s$; and System II (regions of higher latitude), which has a period of $9^h55^m40^s.6$.

It was found that the longitude dependence of the reception probability had very distinct characteristic maxima and minima which were reproduced regularly for extended periods of time. It was also found that the features of the longitude dependence are relatively unchanged for the frequency range from 15 Mc/s to 27.6 Mc/s, although the probability of emission changes greatly over this frequency range as demonstrated in Fig. 2.

Carr et al.[26] have referred to the maxima in reception probability as "sources" and designated them as shown in Fig. 3 and Fig. 4. The values of the longitude of the central meridian corresponding to the source positions refer to the position of the central meridian facing the Earth and not necessarily to the actual locations of the sources on Jupiter.

Carr et al.[27] found that the sources drifted when the rotation rate determined by Shain was used. However, they found that the sources were stable in a coordinate system rotating with a constant period of $9^h55^m28.^s8$, which was later revised[26] to $9^h55^m29.^s35$. Douglas[28] independently arrived at a value for the period of $9^h55^m29.^s37$. This latter value was adopted by the International Astronomical Union.[28] This is now defined as System III (1957) and will be referred to just as "System III" for the remainder of this dissertation.

Recent Radio Rotation Rate Information

Smith[29] and Douglas and Smith[14] independently observed, early in 1961, an abrupt change in the radio rotation period of Jupiter. It

Fig. 2. Typical variation of the probability of emission with frequency.

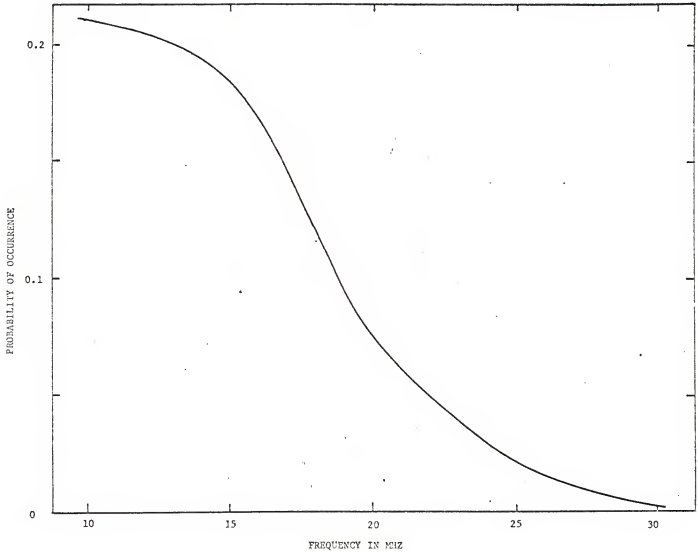
0.2
0.1
0
PROBABILITY OF OCCURRENCE
10
15
20
25
30
FREQUENCY IN MHZ

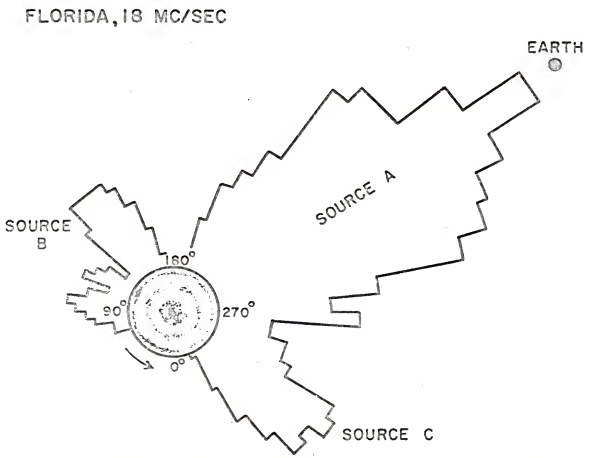

Fig. 3. Probability histogram for the 18 MHz data taken at the Florida station in 1962, plotted in polar coordinates (after Lebo 52).

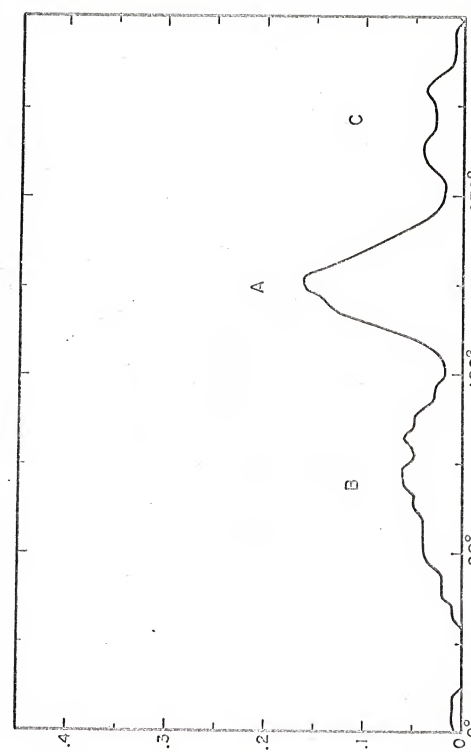

Fig. 4. 22 MHz smoothed histogram of Florida and Chile data 1958 to 1961 (after Six[54]).

appeared that the rotational period had changed by approximately one second. Carr and Gulkis[30] and more recently Carr and Donivan[31] do not believe that the observed change in the rotational period of Jupiter is a real change in the period of rotation. Their analysis indicates that the observed variations in the period are due to the change in the Jovicentric declination of the Earth. Register[32] also has shown that the University of Florida data exhibit consistent correlation with this model.

Theories of the Decametric Radiation Versus Solar Activity

There have been many theories proposed for the mechanism responsible for the decametric radiation received from Jupiter. Those which appear to give the best agreement with observations depict radiation belts similar to the Earth's Van Allen belts where charged particles are trapped by the Jovian magnetic field. When particles are lost out of these radiation belts, it is assumed that the belts are replenished from the charged particles in the solar wind. If this is indeed the source of the charged particles for the radiation belts, one might expect increased radiation at the maximum of the sunspot cycle. However, this is not observed. In fact, a long-term negative correlation of the reception probability with solar activity has been seen since early observations. In view of this, an analysis of the correlation between the flux density of the emitted decametric radiation and solar activity has been made by the author and this will be discussed later.

Another point of view is that presented by Carr,[33] Carr and Donivan,[31] and Douglas,[34] in which they argue that the activity variation is due to the change in the Jovicentric declination of the Earth, which has a period the same as Jupiter's orbital period of 11.86 years. They argue that the Jovicentric declination of the Earth in 1958 was such that it caused a minimum in the reception of decametric radiation, and that it is only coincidental that this also occurs at the maximum of the sunspot cycle, which has a mean period of 11 years.

The Io Effect

In 1964, Bigg[35] made a discovery that shed some light on the mystery of why radiation from a source was not always received when the longitude corresponding to that source was facing the Earth. He found that the intensity of the radiation was greatly enhanced when Io, the innermost Galilean satellite, was at certain positions. Lebo et al.,[36] Dulk,[37] and Duncan confirmed this discovery. This dependence is illustrated in Fig. 5 and Fig. 6, showing the dependence of the reception probabilities on both the position of Io and the central meridian longitude. A similar analysis has been made by the author using the received flux densities at decameter wavelengths and this will be discussed later.

Effects of Other Jovian Satellites

Effects similar to the Io effect have been searched for by several groups, but nothing conclusive has been found. In particular, an increase in the emission probability of the decametric radiation as a function of

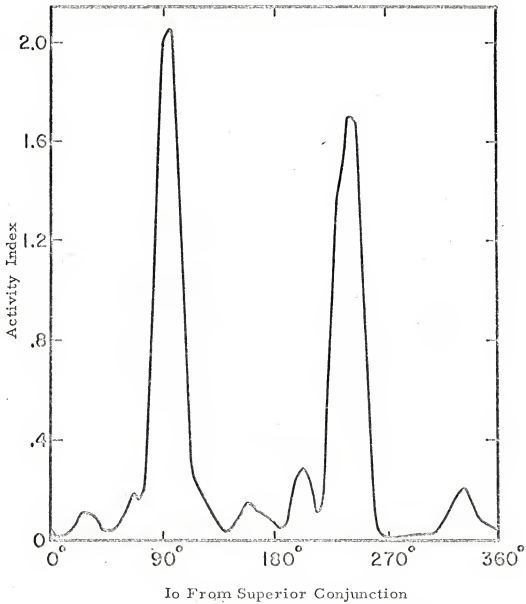

Fig. 5. Typical example of the dependence of the activity index upon position of Io from superior geocentric conjunction (after Lebo, Smith, and Carr[35]).

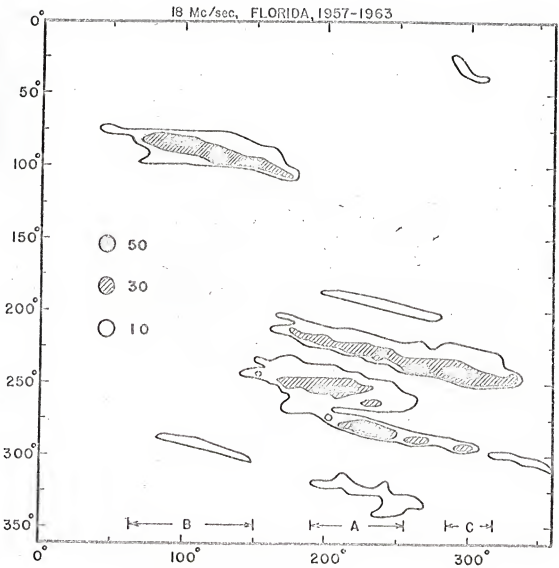

Fig. 6. Example of the dependence of the decametric component of the radiation upon both System III longitude and position of Io from superior geocentric conjunction (after Lebo, Smith, and Carr[35]).

position from superior conjunction for Europa and Ganymede has been searched for. It is very difficult to isolate possible effects of the inner three Galilean satellites since their periods are very near the exact ratio of 1:2:4. Lebo et al.[36] gave evidence of an effect due to Europa and Ganymede. Dulk[38] found no detectable effect of any of the satellites, except Io, on the reception probabilities. An analysis of a coupled effect between Io and both Europa and Ganymede versus flux density has been made by the author and this will be discussed later in this dissertation.

Recent Theories for Decametric Radiation

Since 1964, theories explaining the decametric radiation received from Jupiter have had to account for the Io effect. Gledhill[39] introduced a theory which assumes that Io generates waves at or near the plasma frequency as it moves through the plasma. However, this theory appears to have a serious defect in that it does not account for the high plasma densities that are necessary.

Ellis[40] postulated local disturbances in Jupiter's exosphere that allowed groups of electrons to be accelerated along the magnetic field lines. The electrons spiraling around the field lines emitted at the cyclotron frequency.

Warwick[41] assumed a disturbance in Jupiter's magnetic field lines in its radiation belt. This disturbance allows high velocity electrons to escape from the radiation belts along the lines of force, generating Cerenkov radiation.

However, possibly the most widely accepted theory at present is that of Goldreich and Lynden-Bell,[42] in which they picture Io as a unipolar generator.

This theory assumes that Jupiter's main magnetic field permeates Io. Other assumptions include perfect conductivity along the field lines and zero conductivity across them. This implies that the plasma inside the flux tube which passes through Io will act as though it were rigidly attached to the satellite. As Io rotates through Jupiter's magnetic field, a current due to electrons photo-ejected at the surface of Io will be generated and will flow down one side of this flux tube, cross over in the ionosphere, and flow back up the other side of the flux tube to Io. The current-carrying electrons will be weakly relativistic, having energies of a few keV. Goldreich and Linden-Bell argue that due to a relativistic mass change of the radiating electrons, they will emit coherent cyclotron radiation.

Purpose of the Present Analysis

The present analysis attempts a consistent, two-dimensional study of the flux densities received from Jupiter at decameter wavelengths. Other parameters which will be studied as a function of flux density are the yearly sunspot number and the Jovicentric declination of the Earth. A search has been made for a coupled effect between Io and Europa, and between Io and Ganymede, using an analysis similar to that used in showing the simultaneous dependence of Io and the position of the central meridian longitude on the flux density.

A large amount of data has been collected at the University of Florida Radio Observatory and at its associated field stations at Maipu and Huanta in Chile. A number of people have previously analyzed parts of these data. These include T. D. Carr,[43] N. E. Chatterton,[44] N. F. Six,[45] G. R. Lebo,[46] I. Shever,[2] H. I. Register,[32] and others.[47,48] The previous work of G. R. Lebo and H. I. Register in particular was used extensively as a basis for the present study.

CHAPTER II

DATA COLLECTION AND CALIBRATION SYSTEMS

The data collected for the present analysis were gathered at three stations--one in Florida and two in Chile. The Florida station began operation in 1956 on the University campus, and in 1952 it was moved to Bivens Arm, which is located in Gainesville. This station was finally moved to a more remote site near Old Town, Florida, after the 1967 apparition. The University of Florida also has two field stations in Chile, located at Huanta and Maipu (Fig. 7), which are operated co-operatively with the University of Chile. The station at Maipu began operation in 1959 and the one at Huanta in 1963.

Signal Detection and Instrumentation

The radio frequency signals which are emitted from Jupiter are received by antenna arrays designed to operate at specific wavelengths. The effective area of these arrays is a critical parameter which must be determined in order to calculate values of the flux density. The effective area of an antenna may be calculated using the equation of Kraus[49] for a lossless antenna:

$$A_e = \frac{D\lambda^2}{4\pi} \qquad (1)$$

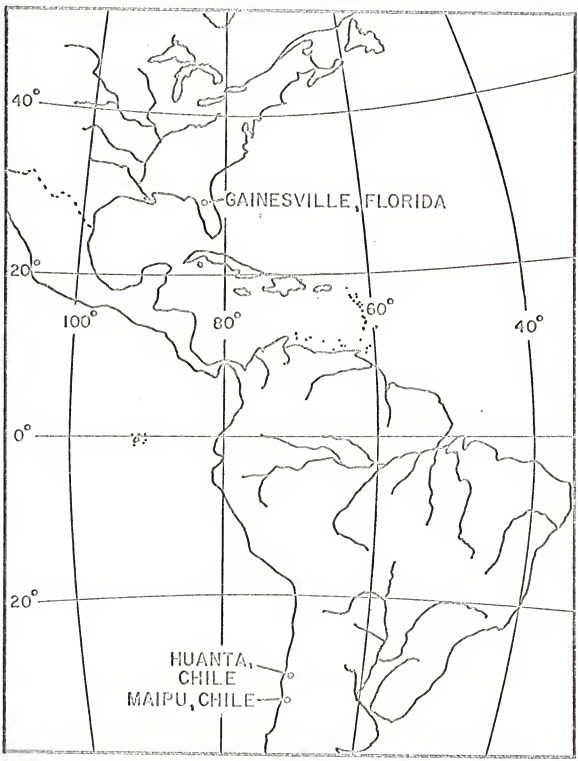

Fig. 7. Map indicating location of observing stations.

where A_e is the effective area of the antenna, D is the directivity of the antenna, and λ is the wavelength for which the antenna was designed. The gain, G, of an antenna is equal to the directivity of that antenna if the antenna is 100% efficient. However, if the antenna is not lossless, the gain is related to the directivity by the equation[50]

$$G = kD \tag{2}$$

where k takes on a range of values from zero to one. Values for the effective areas of the antennas used in the collection of the data for the present analysis have previously been calculated and tabulated in H. I. Register's dissertation.[32]

The signals received from the antennas are detected by short-wave receivers. At the present time, the University of Florida station is using Collins Type 75S-1 receivers. The output from the receivers is amplified and then connected both to an audio system and to a Texas Instruments roll-chart recorder. The Texas Instruments recorder has adjustable chart speeds: six inches per hour is used when ordinary activity from Jupiter is being observed and three inches per minute for polarimeter studies. When activity from Jupiter is observed, high speed Brush recorders and/or tape recorders are also used to record the noise storm. An automatic timer incorporated in the system is calibrated against WWV and marks the roll-chart records automatically.

The galactic background and the Jovian activity are calibrated at the present time using a Hewlett-Packard 461A amplifier as a noise generator. Calibration systems and techniques will be discussed in more detail later in this chapter.

Observing Techniques

The activity from Jupiter occurs in what are usually termed "noise storms," which are recorded on the Texas Instruments roll-chart recorders. The Jovian noise storms must be distinguished by the observer from interference such as radio stations, lightning, air-conditioner switching, etc.

Noise storms may last from only a few seconds to more than an hour. Two distinct types of noise bursts are received from Jupiter. One type is "L-bursts," which are those bursts having a duration exceeding one-tenth of a second. The other type, termed "S-bursts," usually has a duration of only a few milliseconds. S-bursts are most often received from sources B and C and very seldom received from source A. When one listens to the audio output from the receiver, the L-bursts have a "swishing" character while the S-bursts have a "spitting" or "popping" character. These characteristics enable the observer to distinguish Jovian activity from interference.

Data Storage

The Jovian data recorded by the Texas Instruments roll-chart recorders are reduced at the University of Florida and punched on IBM cards. The roll-chart records and the data cards are kept on file at the University for future reference and analysis. A complete description of the format for the data decks, known as the "intermediate" data deck, is given by H. I. Register in his dissertation.[32]

Flux Density Calculation

In order that one may calculate the flux density of a pulse received from Jupiter, one must either use some kind of calibration system or use the galactic background as a reference.

First, let us consider the system shown in Fig. 8 and define the following parameters:

P_c - Power per unit bandwidth generated by the calibrator

P_r - Power per unit bandwidth reaching the receiver from the calibrator

P_J' - Total received celestial power per unit bandwidth

P_J - Power per unit bandwidth received from Jupiter

P_G - Power per unit bandwidth received from the galaxy

S_J' - Total flux density

S_J - Flux density of the radiation received from Jupiter

A_e - Effective area of antenna (m^2)

C - Attenuation of attenuator (decibels)

The attenuation, C, of the signal calibrator which reaches the receiver is given by the following equation:

$$C = 10 \log \frac{P_c}{P_r} . \tag{3}$$

Using Eq. (3), one finds that the power per unit bandwidth reaching the receiver from the calibrator is given by:

$$P_r = P_c 10^{-C/10} . \tag{4}$$

The total power per unit bandwidth reaching the receiver from Jupiter is given by:

Fig. 8. Sample system used in reception and calibration of radiation received from Jupiter.

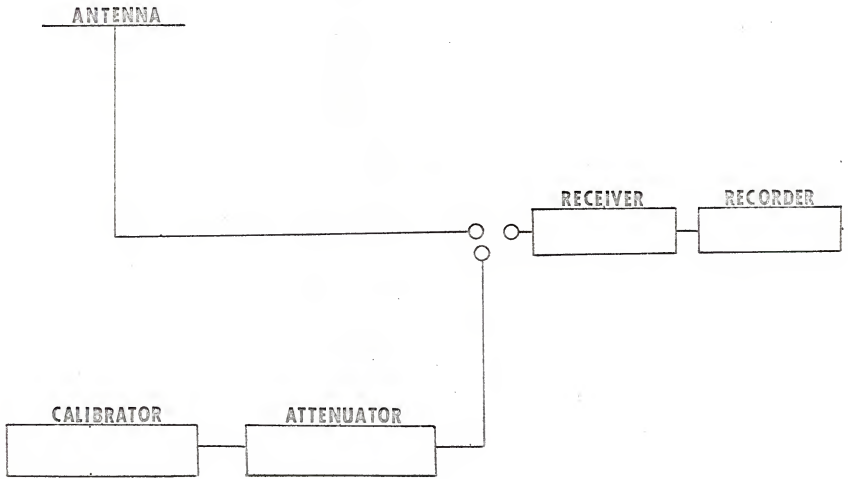
ANTENNA
RECEIVER
RECORDER
CALIBRATOR
ATTENUATOR

$$P_J' = P_J + P_G . \tag{5}$$

However, if one uses the calibrator to determine the power per unit bandwidth received from Jupiter, the power reaching the receiver from the calibrator must also equal the power of the signal from Jupiter. It then follows that

$$P_J = P_c 10^{-C/10} - P_G . \tag{6}$$

The net power per unit bandwidth received from Jupiter is also given by

$$P_J = S_J A_e / 2 \tag{7}$$

where the 1/2 is introduced because the antenna is sensitive to only one of two linearly polarized components of the radiation. Therefore the flux density of the received radiation can be written in the form

$$S_J = 2(P_c 10^{-C/10} - P_G)/A_e . \tag{8}$$

One may also use an equivalent calibrator current, i, defined as that current through a noise diode which will generate a specified shot noise output to a matched load resistor. This relationship is given by

$$P = eiR/2 \tag{9}$$

where e is the charge of the electron and R is the value of the load resistor. The 1/2 is used since only one half of the a. c. plate current reaches the receiver.

Let us now define the following quantities:

G_R - Galactic background level from zero (per cent full scale)

D - Deflection due to Jupiter (per cent full scale)

b - Attenuation factor of the transmission lines

i - Equivalent calibrator current

R - Load resistance

K - Constant depending on the overall gain of the receiver

N - Constant depending on the detector characteristics

The total flux density received from Jupiter may now be written as:

$$S'_J = \frac{2P'_J}{A_e b} \tag{10}$$

where P'_J is also the power per unit bandwidth reaching the receiver from the calibrator.

An empirical equation which has been found to give a good fit between the power per unit bandwidth expressed as an equivalent calibrator current and the pen deflection, D, is given by:

$$i = KD^N . \tag{11}$$

A square-law detector will correspond to N=1, while a plate detector corresponds to N=2.

Combining Eqs. (9), (10), and (11), one may write the following expression for the flux density:

$$S'_J = \frac{eRK}{bA_e}(D^N) . \tag{12}$$

A representative value for the galactic flux density is 10^{-20} $w/m^2/cps$,[51] which will correspond to a deflection G on the roll-chart records. Then the net flux density from Jupiter may be written as:

$$S_J = \frac{eRK}{bA_e}(D^N - C^N). \qquad (13)$$

The problem of calculating the flux densities has now been reduced, in large part, to a determination of the constant K for the particular receiver systems employed.

Calibrations

There have been three calibration systems used at the University of Florida station, beginning with the 1962 apparition. Prior to this time, all calculations of the flux density of the Jovian pulses were made using the galactic background as a reference.

The three calibrators are designated as calibrator A, calibrator B, and calibrator C. Calibrator A consists of a pair of Sylvania 5722 noise diodes connected in parallel, with an output impedance of 52 ohms. This calibrator is used as a standard. Calibrator B adds a stage of power amplification to the calibrator A circuit by means of a cathode follower adjusted for a 52-ohm output impedance. Calibrator B can be attenuated over a range of values from 0 db to -132 db. Calibrator C consists of a Hewlett-Packard 461A amplifier which is periodically standardized against calibrator A. The Hewlett-Packard 461A amplifier has been found to have a very stable, flat noise spectrum in the decametre region. This characteristic makes it an ideal noise generator to calibrate the Jovian decametric pulses.

A number of different calibration systems have been used at the field station located at Maipu, Chile. Calibrator A' at Maipu is identical

to the Florida calibrator A, except that it has an output impedance of 75 ohms. Calibrators B'_1, B'_2, and B'_3 were similar to the Florida calibrator B but used different arrangements of amplifiers and attenuators. The values of the output impedances of these calibrators ranged from 75 ohms to 450 ohms. A detailed discussion of these calibrators may be found in G. R. Lebo's dissertation.[52] Calibrator C' used the parallel arrangement of noise diodes followed by an amplification stage which has an output impedance of 450 ohms. This is followed by an impedance transformer which is adjusted for 75 ohms output impedance. Calibrator D' uses a Hewlett-Packard 461A amplifier as the noise generator and is identical to the Florida calibrator C except that it has a terminating resistor of 75 ohms, while the Florida calibrator has a 52-ohm terminating resistor.

Table 1 indicates the dates when each calibrator was in use, both for the Maipu and the Florida Station.

Calculations Using Calibrators and Galactic Background

The flux density calculations in the present work have drawn heavily upon the previous work of H. I. Register[32] and G. R. Lebo.[52] The flux density calculations of Register for the 1965-69 Florida data were not modified, but his calculations for the 1962-65 Florida data at frequencies of 15 MHz, 22.2 MHz, and 27.6 MHz were modified to take into account the different calibrators used in this period.

TABLE 1

Dates and Stations at Which Each Calibrator Was Used

Epoch	Station	Calibrator
1962.7	Florida	A
1963.8	Florida	B
1964.8	Florida	B and C
1965.9	Florida	C
1967.0	Florida	C
1968.0	Florida	C
1969.0	Florida	C
1962.6	Maipu	A', B'_1, B'_2
1963.7	Maipu	B'_3
1964.9	Maipu	C'
1966.0	Maipu	C'

Previous work by Tiberi[53] greatly facilitated the above modification. Tiberi experimentally investigated the relationship between equivalent calibrator A currents in milliamperes and the attenuation for calibrator B in decibels at frequencies of 15 MHz, 18 MHz, 22.2 MHz, and 27.6 MHz, as shown in Figs. 9-12. It was found empirically that the following equation fits the data taken by Tiberi:

$$I_A^{-1} = 10^{B/m + K} \tag{14}$$

where I_A is the equivalent calibrator A current in amperes, B is the attenuation of calibrator B in db, and m and K are constants for a particular frequency which is obtained from the data.

Now we wish to obtain a relationship between calibrator B and calibrator C. We may do this in the following manner. If one obtains a plot of the attenuation of both calibrators B and C versus the pen deflection on the roll chart records, one may write parametric equations for the attenuation of these calibration systems in terms of the pen deflection. When one combines these two equations, eliminating the pen deflection parameter, the following equation is the result:

$$C = \alpha B + \gamma \tag{15}$$

where C is the attenuation of calibrator C, and B is the attenuation of calibrator B and α and γ are constants which may be determined from information comparing the calibrators found both in the Florida Radio Observatory log books and the roll chart records.

Fig. 9. Equivalent current on calibrator A for a given attenuation on calibrator B at a frequency of 15 MHz.

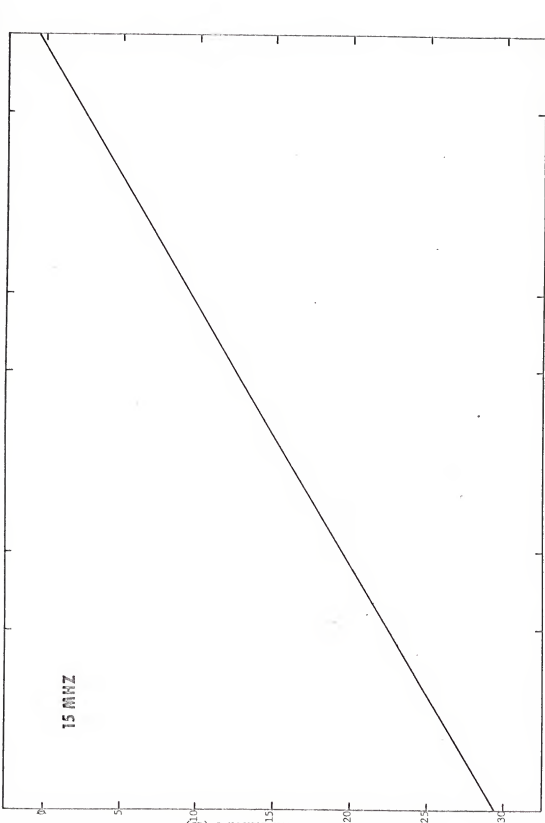
15 MHZ
ATTENUATION OF CALIBRATOR B (dB)
0
5
10
15
20
25
30
1
5
10
50
100
500
1000
EQUIVALENT CALIBRATOR A CURRENT (mA)

Fig. 10. Equivalent current on calibrator A for a given attenuation on calibrator B at a frequency of 18 MHz.

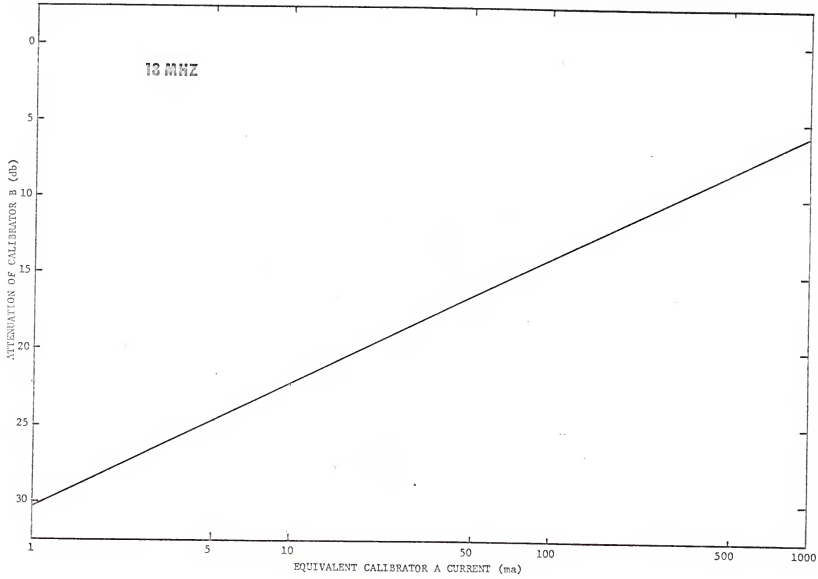
18 MHZ
ATTENUATION OF CALIBRATOR B (db)
0
5
10
15
20
25
30
1
5
10
50
100
500
1000
EQUIVALENT CALIBRATOR A CURRENT (ma)

Fig. 11. Equivalent current on calibrator A for a given attenuation on calibrator B at a frequency of 22.2 MHz.

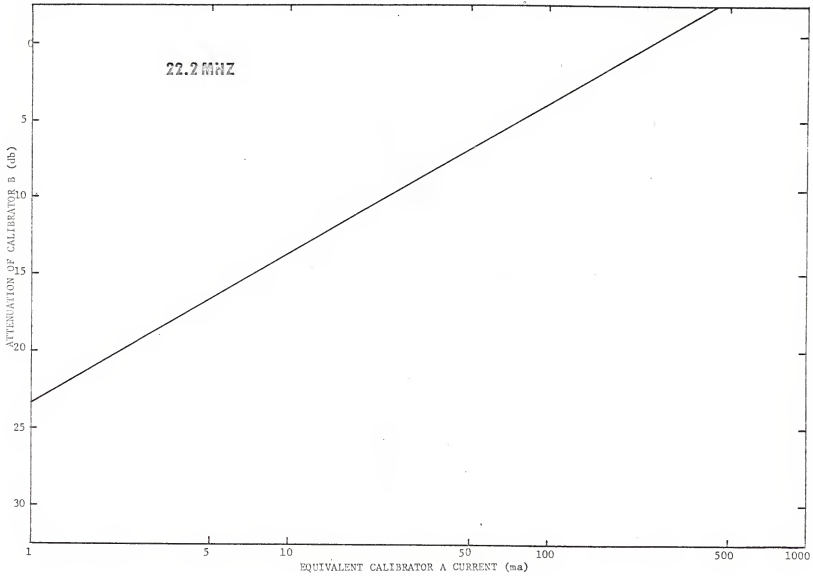
22.2 MHZ
0
5
10
15
20
25
30
ATTENUATION OF CALIBRATOR B (db)
1
5
10
50
100
500
1000
EQUIVALENT CALIBRATOR A CURRENT (ma)

Fig. 12. Equivalent current on calibrator A for a given attenuation on calibrator B at a frequency of 27.6 MHz.

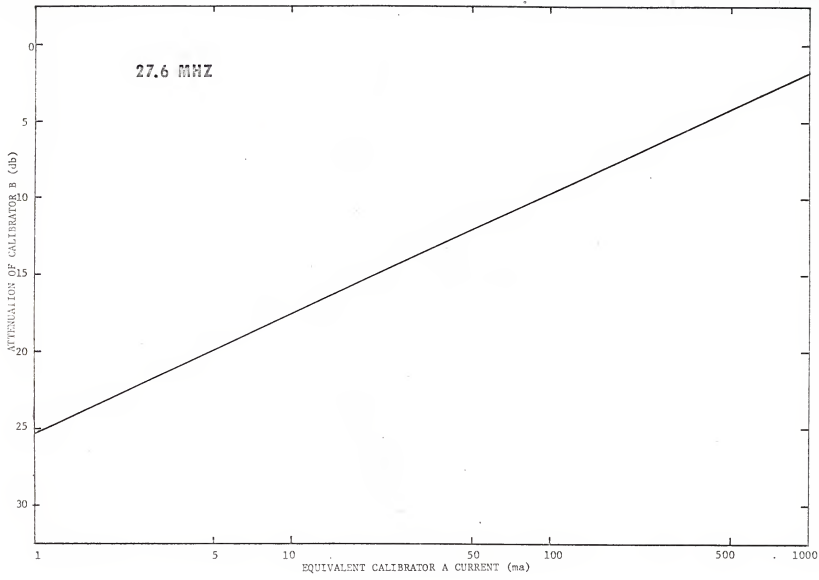
27.6 MHZ
ATTENUATION OF CALIBRATOR B (db)
0
5
10
15
20
25
30
1
5
10
50
100
500
1000
EQUIVALENT CALIBRATOR A CURRENT (ma)

One may calculate the flux density in a consistent manner, using the relationships obtained in Eqs. (14) and (15) for all the Florida data from 1962 to 1969, except for the data at 18 MHz for 1962-65.

The work of C. R. Lebo and N. F. Six was used extensively in the analysis of the remainder of the Florida data and the data collected in Chile. These workers calculated the flux density of the decametric radiation by using the galactic background as a reference. A discussion of this analysis is given in the dissertations of Six[54] and Lebo.[52] Lebo has performed a two-dimensional analysis of the activity index and probability of emission for the decametric radiation; his activity index is defined as the probability of occurrence weighted through multiplication by the received flux density. To calculate the flux density for each five-degree square zone for a particular apparition, one divides the activity index of that zone by the probability of emission for that zone. Thus one is not calculating the flux density received in a five-minute interval, but the total flux density received in a five-degree square zone for the complete apparition.

To compare flux densities calculated as above with the storm-by-storm analysis, the Florida data at 22.2 MHz for the 1964 and 1965 apparitions were analyzed using both methods. When a comparison was made at the positions of the sources, there was less than an 8% difference. Therefore, one may claim that the two methods do not differ significantly.

CHAPTER III

DATA ANALYSIS

Method

The dependence of the flux density on several pairs of geometric variables has been plotted in one-dimensional histograms and in two-dimensional contour maps.

In the one-dimensional analysis, the "flux density" for a five-minute interval of time during which activity is observed is calculated by averaging the flux densities for the three peak pulses in the interval and designating this average as the flux density for the five-minute interval. The five-minute interval of activity can be associated with a particular value of one of the geometric variables. If the radiation is received more than once at this position, the flux densities associated with the radiation received at that position are summed to give a total flux density for that particular position. The summations are performed over certain periods of time, usually one or more apparitions. Hereafter,

unless otherwise specified, the term "flux density" will mean the summation of the flux density at a particular value of the geometric variable over a specified period of time; it should be noted that this definition differs from the common connotation of the term.

In the two-dimensional analysis, the flux received for each five-minute interval of observing time was given an importance number which represents the mean intensity of the three peak pulses received in that interval. This number is a positive integer arrived at by dividing the mean flux density for the three peaks by ten and rounding off to the next highest integer. This division by ten and rounding off to the next highest integer was performed solely for the purpose of facilitating the computer processing of the data. The importance number was then stored in a two-dimensional array that represented the values of two of the geometric variables. If the radiation was

observed more than once at the same location in the two-dimensional array, a new importance number was assigned to this location which was the sum of all the importance numbers for radiation received at this location. When all of the five-minute intervals of activity for a given period of time had been stored in this manner, the importance numbers were normalized to integer values between zero and ten, so that the position with the highest importance number now is given the value of ten. The flux density associated with a particular position in the two-dimensional array may be inferred from the normalized summed importance numbers by taking into account the normalization factors utilized in the preceding analysis.

The variables analyzed in both the one-dimensional histogram analysis and in the two-dimensional contour analysis were: position of the central meridian longitude, System III (1957); position of Io from superior geocentric conjunction; position of Europa from superior geocentric conjunction; and position of Ganymede from superior geocentric conjunction. Each of these variables was analyzed in terms of the flux density from a five-degree zone. In the one-dimensional analysis, the position of only one variable must be satisfied at the time of reception of radiation for that zone to be credited with the value of the flux density while in the two-dimensional analysis, the positions of two variables must be satisfied for a five-degree by five-degree zone to be credited with an importance number derived from the flux density.

Since a large amount of data, covering several years for each frequency, were analyzed, all zones for each pair of variables were observed for approximately equal periods of time as previously shown by Register.[32] Therefore, the positions of the peaks shown in the contour analysis are not due to observations having been made only at preferred values for certain pairs of the variables.

The two-dimensional contour analysis is a powerful tool which enables one to determine the combined effect of pairs of variables on the flux density. A large number of the two-dimensional contour maps have been produced from many apparations for frequencies ranging from 15 MHz to 27.6 MHz. Table 2 indicates by the symbol "X" in an appropriate column the apparition and the observing station for which two-dimensional contour maps have been produced.

One-Dimensional Analysis

One-dimensional flux density histograms have been produced for the following variables: position of Io from superior geocentric conjunction; position of the central meridian longitude, System III (1957). In these histograms, the flux that was received at Maipu from 1960 to 1966 and at Florida from 1957 to 1969 for a particular value of one of the geometric variables is summed for each frequency. The summed flux density is then plotted versus one of the geometric variables. The resulting histogram is a profile of the relative rate of Jovian emission as a function of central meridian longitude, System III.

TABLE 2

Two-Dimensional Contour Maps Produced

Frequency	Mean Epoch	Observing Station	
		Florida	Maipu
15 MHz	1961.5		X
"	1962.6		X
"	1962.7	X	
"	1963.8	X	
"	1964.9	X	
"	1965.9	X	
"	1967.0	X	
"	1968.0	X	
"	1969.0	X	
18 MHz	1957.1	X	
"	1958.1	X	
"	1959.1	X	
"	1960.2	X	
"	1961.6	X	X
"	1962.6		X
"	1962.7	X	
"	1963.7		X
"	1963.8	X	
"	1964.8	X	
"	1964.9		X
"	1965.9	X	
"	1966.0		X
"	1967.0	X	
"	1968.0	X	
"	1969.0	X	
22.2 MHz	1958.1	X	
"	1959.2	X	
"	1960.2	X	
"	1960.4		X
"	1961.5	X	X
"	1962.8	X	
"	1963.7		X
"	1963.8	X	

TABLE 2 continued

Frequency	Mean Epoch	Observing Station	
		Florida	Maipu
22.2 MHz	1964.8	X	
"	1964.9		X
"	1965.9	X	X
"	1967.0	X	
"	1968.0	X	
"	1969.0	X	
27.6 MHz	1961.6	X	
"	1962.5		X
"	1962.7	X	
"	1963.7		X
"	1963.8	X	
"	1964.8	X	
"	1965.9	X	
"	1967.0, 1968.0, 1969.0	X	

The "sources," A, B, and C, which were discussed in Chapter I, are clearly visible on the histograms of summed flux density versus the longitude of the central meridian, System III (1957), as shown in Figs. 13-16. Source A is located in the longitude range from 200°-20°. Several facts can be deduced from these histograms. It was found that the flux density from sources A and C decreased relative to that from source B as the frequency at which the radiation was monitored was increased. Register[32] observed a similar effect in his studies of the emission probability. A "double peak" character of source B is observed at frequencies of 22.2 MHz and 27.6 MHz as seen in Figs. 15 and 16. This character is not evident at 15 MHz and 18 MHz. Source B_1 appears to occur at a System III longitude of 130° and source B_2 at a System III longitude of 150°. The "double peak" character of source B also has previously been observed in studies of emission probabilities by Olsson and Smith.[55]

There are two positions of Io from superior geocentric conjunction at which a very pronounced increase in the summed flux density is observed. These positions are centered about Io located either at 90° or 240° from superior geocentric conjunction as shown in Figs. 17-20. When Io is near 90°, radiation from source B is observed, and when it is near 240°, radiation from sources A and C is received. It is also observed that as one increases the frequency at which the radiation is monitored, the flux density when Io is near 240° decreases relative to the flux density when Io is near 90°. This behavior is in

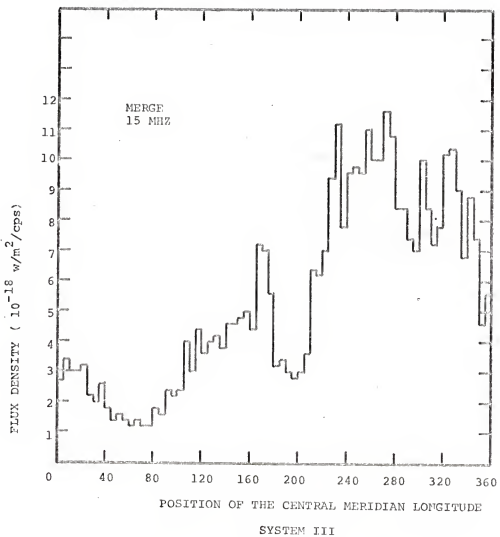

Fig. 13. Long-term histogram of summed flux density at 15 MHz as a function of central meridian longitude, merged for radiation received at Maipu from 1962 to 1965 and at Florida from 1961 to 1969.

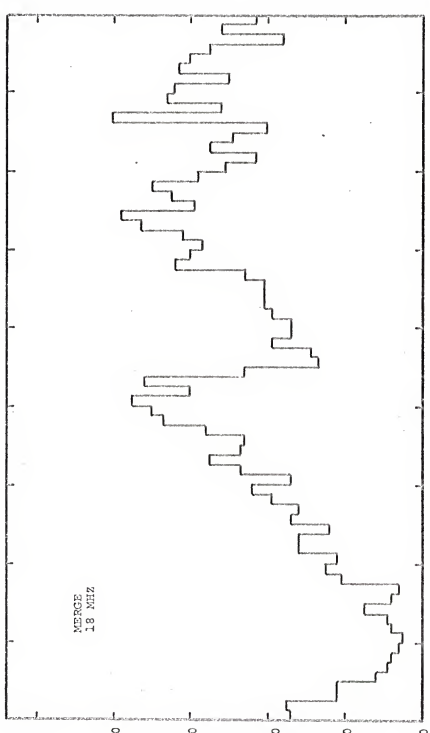

Fig. 14. Long-term histogram of summed flux density at 18 MHz as a function of central meridian longitude, merged for radiation received at Maipu from 1960 to 1966 and at Florida from 1957 to 1969.

Fig. 15. Long-term histogram of summed flux density at 22.2 MHz as a function of central meridian longitude, merged for radiation received at Maipu from 1960 to 1965 and at Florida from 1958 to 1969.

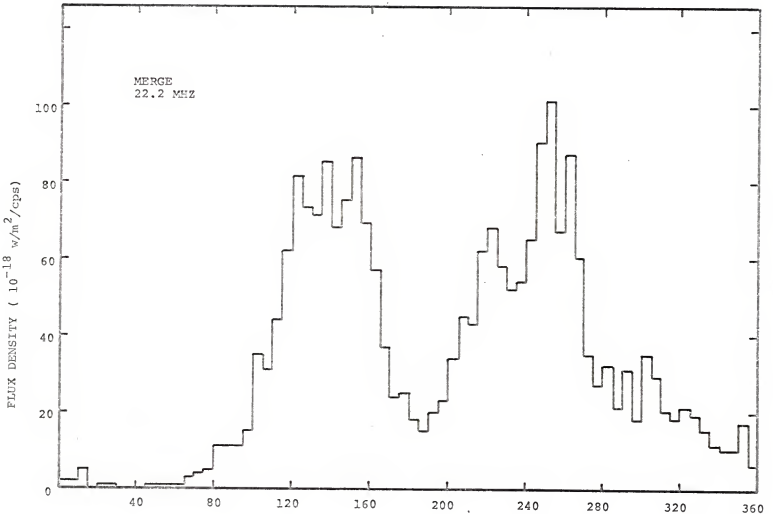
MERGE
22.2 MHZ
FLUX DENSITY (10^{-18} w/m^2/cps)
0
20
40
60
80
100
40
80
120
160
200
240
280
320
360
POSITION OF THE CENTRAL MERIDIAN LONGITUDE SYSTEM III

Fig. 16. Long-term histogram of summed flux density at 27.6 MHz as a function of central meridian longitude, merged for radiation received at Maipu from 1962 to 1964 and at Florida from 1961 to 1969.

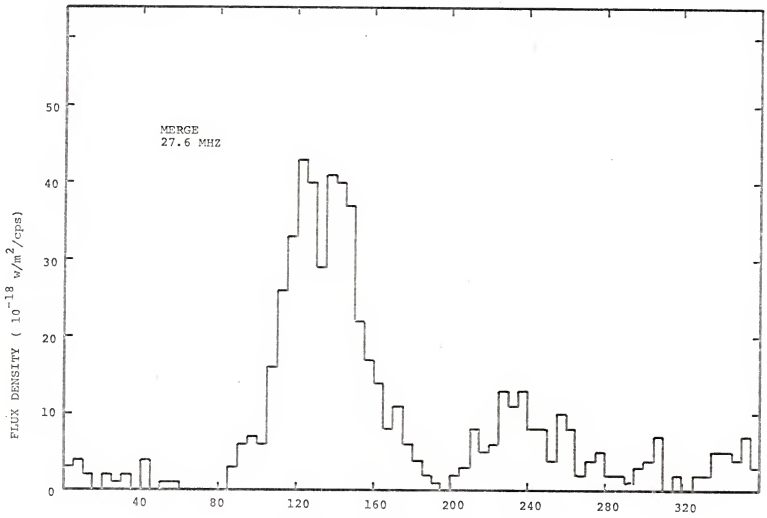
MERGE
27.6 MHZ
FLUX DENSITY (10^{-18} w/m^2/cps)
0
10
20
30
40
50
40
80
120
160
200
240
280
320
POSITION OF THE CENTRAL MERIDIAN LONGITUDE SYSTEM III

Fig. 17. Long-term histogram of summed flux density at 15 MHz as a function of Io position, merged for radiation received at Maipu from 1962 to 1965 and at Florida from 1961 to 1969.

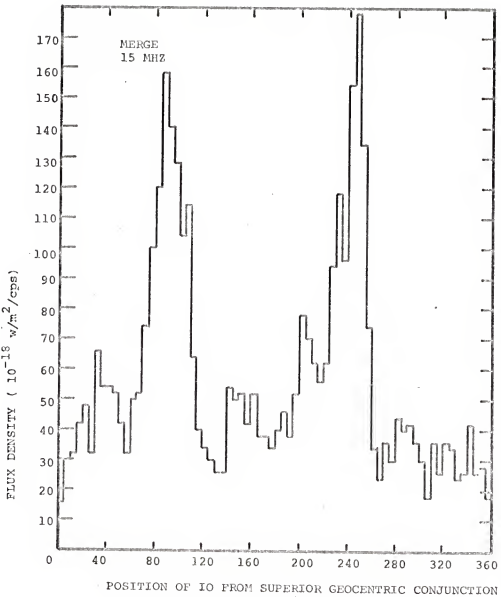
MERGE
15 MHZ
FLUX DENSITY (10^{-15} w/m^2/cps)
POSITION OF IO FROM SUPERIOR GEOCENTRIC CONJUNCTION
0
10
20
30
40
50
60
70
80
90
100
110
120
130
140
150
160
170
40
80
120
160
200
240
280
320
360

Fig. 18. Long-term histogram of summed flux density at 18 MHz as a function of Io position, merged for radiation received at Maipu from 1960 to 1966 and at Florida from 1957 to 1969.

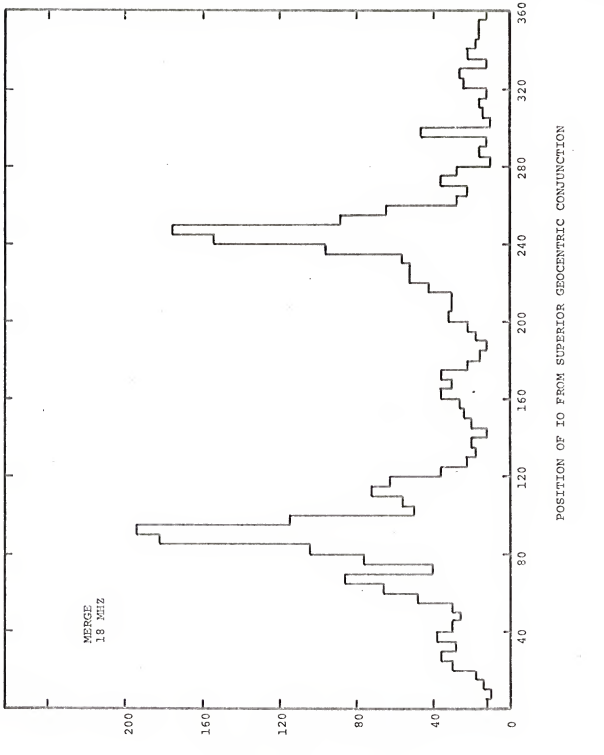
MERGE
18 MHz
FLUX DENSITY (10^{-18} w/m^2/cps)
0
40
80
120
160
200
40
80
120
160
200
240
280
320
360
POSITION OF IO FROM SUPERIOR GEOCENTRIC CONJUNCTION

Fig. 19. Long-term histogram of summed flux density at 22.2 MHz as a function of Io position, merged for radiation received at Maipu from 1960 to 1965 and at Florida from 1958 to 1969.

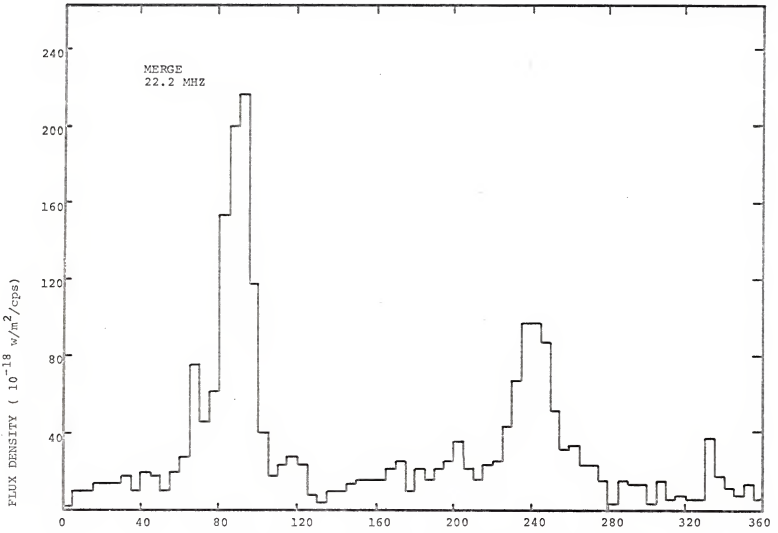
MERGE
22.2 MHZ
240
200
160
120
80
40
0
40
80
120
160
200
240
280
320
360
FLUX DENSITY (10^{-18} w/m2/cps)
POSITION OF IO FROM SUPERIOR GEOCENTRIC CONJUNCTION

Fig. 20. Long-term histogram of summed flux density at 27.6 MHz as a function of Io position, merged for radiation received at Maipu from 1962 to 1964 and at Florida from 1961 to 1969.

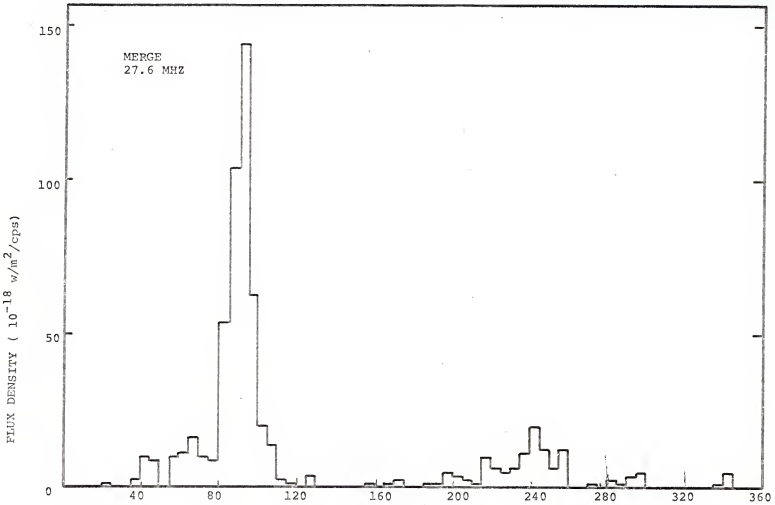
MERGE
27.6 MHZ
150
100
50
0
40
80
120
160
200
240
280
320
360
FLUX DENSITY (10^{-18} w/m^2/cps)
POSITION OF IO FROM SUPERIOR GEOCENTRIC CONJUNCTION

good agreement with that found by Register[32] for the probability of emission. This, combined with the behavior of sources A and C relative to source B on the longitude versus summed flux density histograms, indicates that at least a component of the flux density associated with each of these sources is Io-related.

There is also an indication of another Io position at which the flux density is enhanced, although not nearly as pronounced as the two previously mentioned positions. This increase in the flux density is observed when Io is located between 330^{o} and 350^{o} from superior geocentric conjunction. This is observed only at the frequencies 22.2 MHz and 27.6 MHz, and the effect appears to be decreasing with increasing frequency.

Two-Dimensional Analysis

The data for several years have been merged in two-dimensional contour maps in which the importance numbers derived from the flux density for the data collected at Maipu from 1960 to 1966 and at Florida from 1957 to 1969 are plotted as contours on the two-dimensional plane representing the position of Io from superior geocentric conjunction and the longitude of the central meridian. Figs. 21, 22, and 23 are examples of the two-dimensional contour maps drawn in perspective. These have been produced as an aid to the reader in visualizing the two-dimensional analysis. These figures may be compared to Figs. 25, 27, and 57 which are two-dimensional representations of the same data. The maps were produced as two-dimensional number arrays on the IBM

Fig. 21. Typical two-dimensional contour map, shown in perspective, for the flux density* at 18 MHz merged for radiation received at Maipu from 1960 to 1966 and at Florida from 1957 to 1969.

*For definition of "flux density" as employed here, see discussion on on page 38.

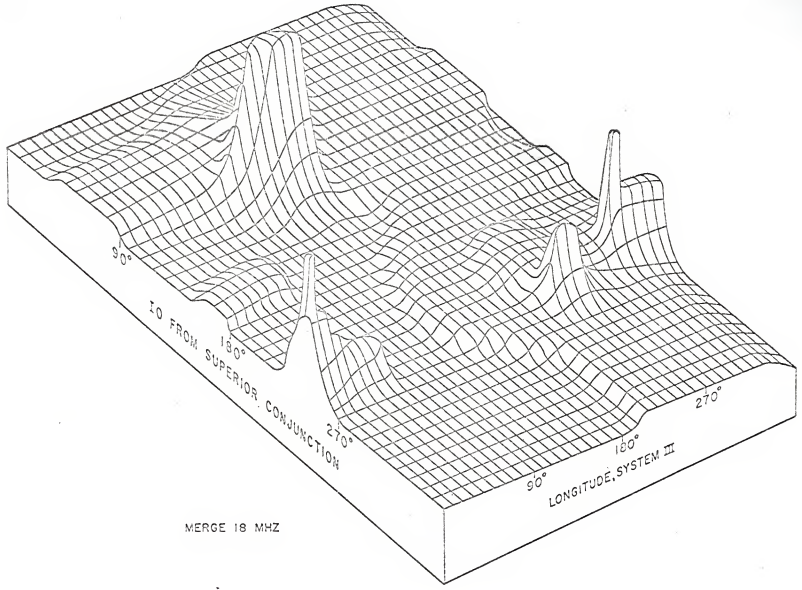
90°
180°
270°
IO FROM SUPERIOR CONJUNCTION
90°
180°
270°
LONGITUDE, SYSTEM III

MERGE 18 MHZ

Fig. 22. Typical two-dimensional contour map, shown in perspective, for the flux density* at 27.6 MHz merged for radiation received at Maipu from 1962 to 1964 and at Florida from 1961 to 1969.

*For definition of "flux density" as employed here, see discussion on page 33.

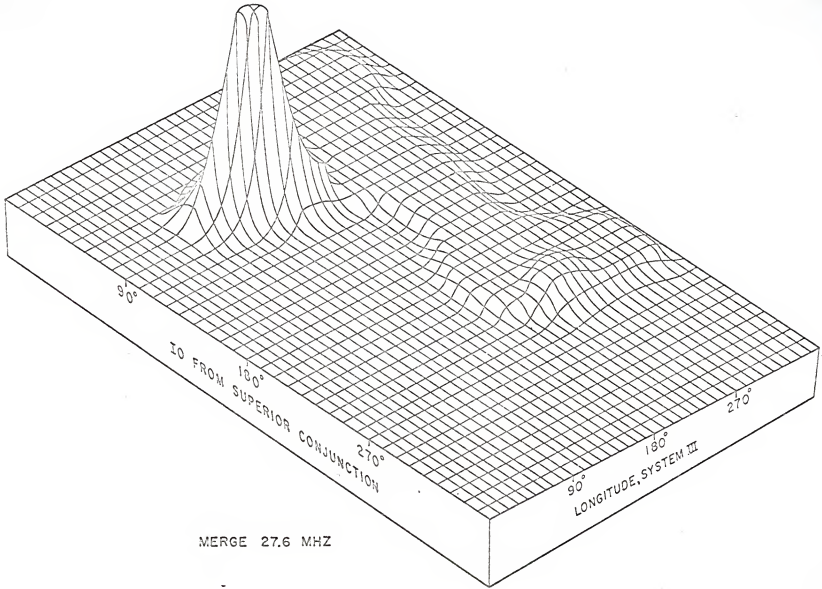

MERGE 27.6 MHZ

Fig. 23. Typical* two-dimensional contour map, shown in perspective, for the flux density at 22.2 MHz for the 1965.9 apparition at Florida.

*For definition of "flux density" as employed here, see discussion on page 38.

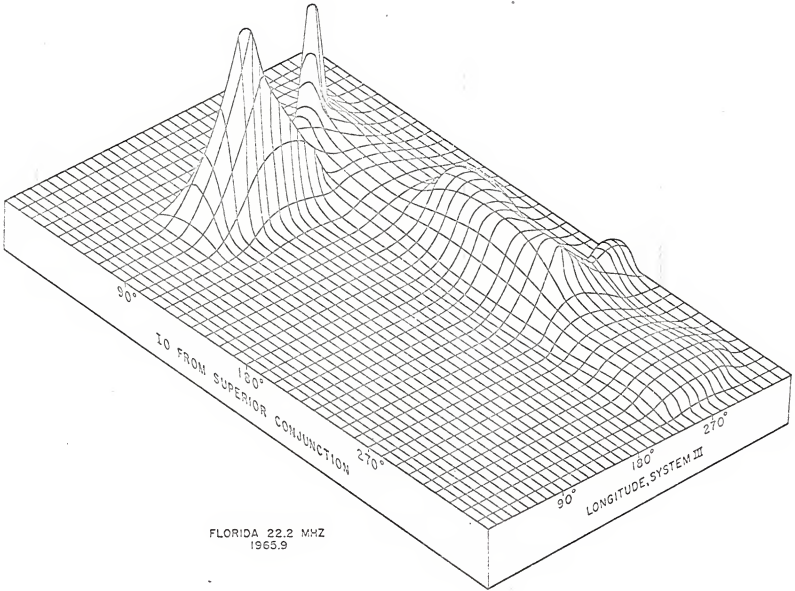

FLORIDA 22.2 MHZ
1965.9

360/65 computer at the University of Florida and then hand-plotted as contours of equal flux density. The contour maps produced for 15 MHz, 18 MHz, 22.2 MHz, and 27.6 MHz are shown in Figs. 24-27. The merging of the data was necessary in order to smooth out the short-term fluctuations and to emphasize the long-term permanent features.

Two-dimensional contour maps were produced for most of the individual apparitions during which observations were made. Only those years in which the scarcity of data made the contour maps uninformative were deleted. However, the flux density during those apparitions for which maps were not produced has nevertheless been included in the merged contour maps.

It is seen that the distribution of the flux density is not homogeneous but is concentrated in "peaks" and "ridges." The peaks indicate an increase in the flux density when both coordinates are simultaneously near favorable positions. The ridges run approximately vertical on the page, indicating a dependence on the longitude of the central meridian and essentially no dependence on the position of Io. The radiation which is received in the peak positions is generally referred to as "Io-related" radiation and that which is received in the ridges outside the peaks is referred to as "non-Io-related" radiation. This convention will be followed for the remainder of this dissertation.

Although the two-dimensional contour maps have many similarities, there are also noticeable differences which may be observed at different frequencies. The details of the features of these contour maps are discussed in the following sections.

Fig. 24. 15 MHz contour map of the flux density* merged from 1961 to 1969 for Florida and 1962 to 1965 for Maipu as a function of central meridian longitude and Io position.

*For definition of "flux density" as employed here, see discussion on page 38.

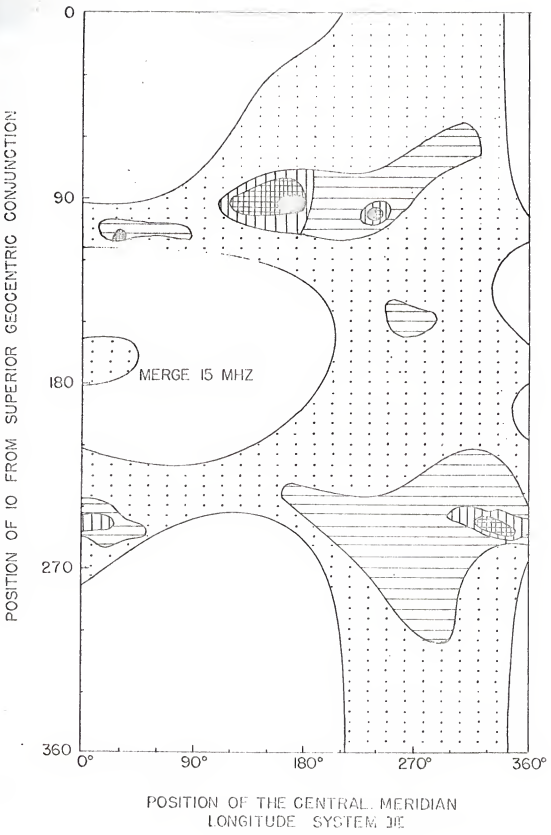
0
90
180
270
360
MERGE 15 MHZ
0°
90°
180°
270°
360°
POSITION OF IO FROM SUPERIOR GEOCENTRIC CONJUNCTION
POSITION OF THE CENTRAL MERIDIAN
LONGITUDE SYSTEM III

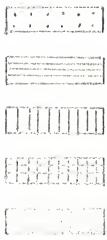

Fig. 25. 18 MHz contour map of the flux density* merged from 1957 to 1969 for Florida and 1960 to 1966 for Maipu as a function of central meridian longitude and Io position.

*For definition of "flux density" as employed here, see discussion on page 38

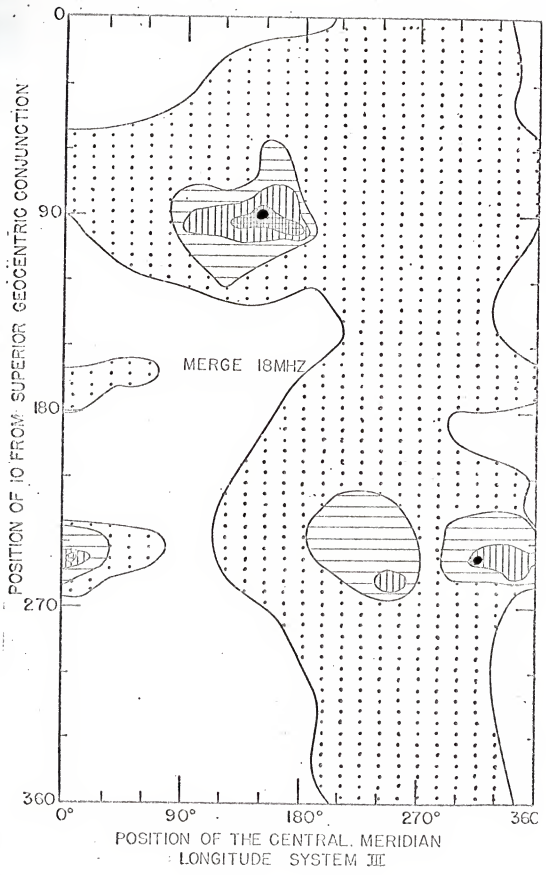
0
90
180
270
360
POSITION OF IO FROM SUPERIOR GEOCENTRIC CONJUNCTION
MERGE 18MHZ
0°
90°
180°
270°
360
POSITION OF THE CENTRAL MERIDIAN
LONGITUDE SYSTEM III

Fig. 26. 22.2 MHz contour map of the flux density* merged from 1958 to 1969 for Florida and 1960 to 1965 for Maipu as a function of central meridian longitude and Io position.

*For definition of "flux density" as employed here, see discussion on page 38.

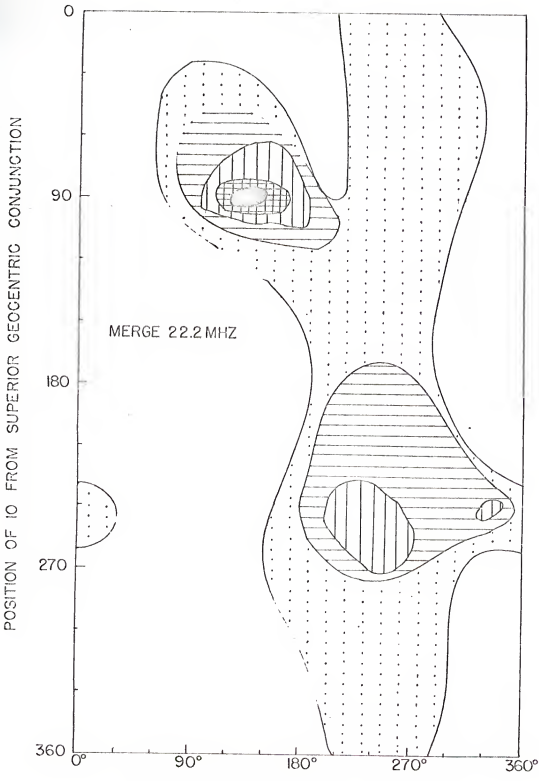
0
90
180
270
360
MERGE 22.2 MHZ
POSITION OF IO FROM SUPERIOR GEOCENTRIC CONJUNCTION
0°
90°
180°
270°
360°
POSITION OF THE CENTRAL MERIDIAN
LONGITUDE SYSTEM III

Fig. 27. 27.6 MHz contour map of the flux density* merged from 1961 to 1967 for Florida and 1962 to 1964 for Maipu as a function of central meridian longitude and Io position.

*For definition of "flux density" as employed here, see discussion on page 38.

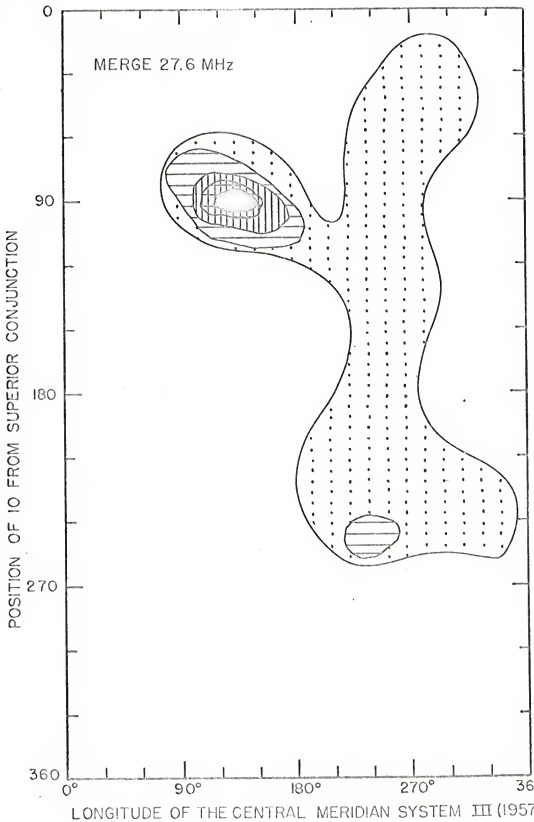
MERGE 27.6 MHz
0
90
180
270
360
POSITION OF IO FROM SUPERIOR CONJUNCTION
0°
90°
180°
270°
360
LONGITUDE OF THE CENTRAL MERIDIAN SYSTEM III (1957)

Io-Related Source A

Io-related source A may be identified at all frequencies. However, it is more prominent at frequencies of 18 MHz and above than at 15 MHz.

Io-related source A occurs at longitudes of the central meridian (System III) which range from 180° to 270°, and at positions of Io from superior geocentric conjunction which range from 215° to 270°. It should be noted that Jupiter's north magnetic pole (longitude of the north magnetic pole is 200°) is located between the Earth-Jupiter line and the Io-Jupiter line when Io-related source A is observed.

The distribution of the flux density within the source is homogeneous except for a small peak which occurs at 18 MHz and is localized at positions of Io from superior conjunction near 255° and positions of the central meridian longitude which range from 245° to 260°. At frequencies of 18 MHz and 22.2 MHz, the contours of equal flux density surrounding the Io-related source A peak tend to slope toward higher values of both Io and the longitude of the central meridian. A similar effect was observed by Register[32] in his studies of the probability of emission for Io-related source A.

The total area occupied by Io-related source A on the two-dimensional contour maps decreased with increasing frequency. The range of central meridian longitudes at 18 MHz for which Io-related source A radiation is received is 180°-270°, and at 27.6 MHz it is 215°-260°. The corresponding range of positions of Io from superior

geocentric conjunction varies from 215^{o}-265^{o} at 18 MHz to 240^{o}-260^{o} at 27.6 MHz. Therefore, the total area occupied by Io-related source A diminishes from 4,500 square degrees at 18 MHz to 900 square degrees at 27.6 MHz. There is good agreement between the behavior in the two-dimensional analysis of Io-related source A and that in the one-dimensional histograms which indicated that the Io-favored zone centered about Io=240^{o} shrinks with frequency.

Io-related source A exhibits a relatively sharp cut-off at Io=265^{o}. A more gradual cut-on of this source is observed at Io=$225^{o}\pm10^{o}$.

Io-Related Source B

Io-related source B is the most predictable and the most powerful of the decametric "sources" on Jupiter. It is the only one of the Io-related sources which can be definitely identified at all frequencies from 15 MHz to 27.6 MHz, and it is the most prominent feature on the two-dimensional contour maps at frequencies of 22.2 MHz and 27.6 MHz.

Io-related source B demonstrates a very strong Io-dependence and it is observed only when Io is near 90^{o} from superior geocentric conjunction. It has a maximum range of Io positions of $\pm20^{o}$. The longitude of the central meridian is in the range 90^{o}-180^{o} when Io-related source B radiation is received. It should again be noted that Io-related source B is received when Jupiter's north magnetic pole is located between the Earth-Jupiter line and the Io-Jupiter line. This

is a geometry similar to that found when Io-related source A is received.

There is a relatively sharp cut-on of Io-related source B when Io is near 70° from superior geocentric conjunction, and a sharp cut-off of Io-related source B radiation when Io is near 110°. There is also a sharp cut-off of the Io-related source B radiation when the central meridian longitude is near 180°.

Io-related source B shows essentially no frequency dependence in either its location or size, in sharp contrast to the behavior of Io-related source A. The range of Io positions for Io-related source A is larger than that for Io-related source B, but B is active over a wider range of central meridian longitudes.

Register[32] has indicated in a previous two-dimensional analysis of the emission probability that Io-related source B is bifurcated. The two-dimensional analysis of the flux density indicates no bifurcation of B for contour maps composed of data that are merged from several years. Several two-dimensional contour maps for single apparitions which do show some bifurcation of Io-related source B will be discussed in a later section of this chapter.

Io-Related Source C

Io-related source C may be observed at the frequencies 15 MHz, 18 MHz, and 22.2 MHz. It is a very prominent Io-related source at 15 MHz and 18 MHz, but it has entirely disappeared at a frequency of 27.6 MHz.

Io-related source C is strongly Io-dependent, centered about Io near 245° from superior geocentric conjunction. It exhibits a very sharp cut-on at an Io-position of 240°, and a very sharp cut-off at 255°. Register,[32] in his earlier analysis of the emission probability, indicated a more gradual cut-on located near an Io position of 220° from superior geocentric conjunction. It appears that the two-dimensional contour maps of the flux density yield a better definition of source C relative to the position of Io from superior geocentric conjunction than the two-dimensional arrays of emission probability.

Io-related source C is not as well defined relative to the longitude of the central meridian. There is a gradual cut-on of C when the longitude of the central meridian is near 295°, and a gradual cut-off when the longitude is near 25°. The cut-on occurs shortly after Jupiter's south magnetic pole appears on the hemisphere facing the Earth, and the cut-off occurs as the south magnetic pole crosses the Earth-Jupiter line.

Other Io-Related Radiation

A relatively sharp increase in the flux density is observed when Io is near 105° from superior geocentric conjunction and the longitude of the central meridian is between 20° and 100°. This "peak" in the flux density is observed only at a frequency of 15 MHz. This may be the Io-related source D which has previously been observed at frequencies

of 15 MHz and below. The positions of Io and Jupiter's south magnetic pole for Io-related source D would be approximately the same as for Io-related source C if they were reflected through the Earth-Jupiter line (Fig. 28). This indicates that the radiation received from Io-related sources C and D may originate from a single source, but that the radiation is beamed in different directions.

Io-related source B terminates relatively abruptly at a central meridian longitude of 90^{o}. This is near the longitude for which Io-related source D is observed. However, since the sources occur at slightly different Io-positions, one source would not be observed at the same time as the other.

Another "peak" in the flux density also appears at a frequency of 15 MHz when Io is near 140^{o} from superior geocentric conjunction and the longitude of the central meridian is near 270^{o}. It would be interesting to determine if this "source" is part of non-Io-related source A, or if it is radiation from one of the other sources that is beamed in a different direction.

A third "peak" in the flux density is observed when the longitude of the central meridian is near 235^{o} and Io is near 100^{o} from superior geocentric conjunction. Note that this peak occurs at the longitude of source A but at the Io-position of source B. It is possible that this peak is due to "leakage" radiation from Io-related source B. It would be interesting to compare the spectral characteristics and the polarization of this peak with those for Io-related source B and non-Io-related

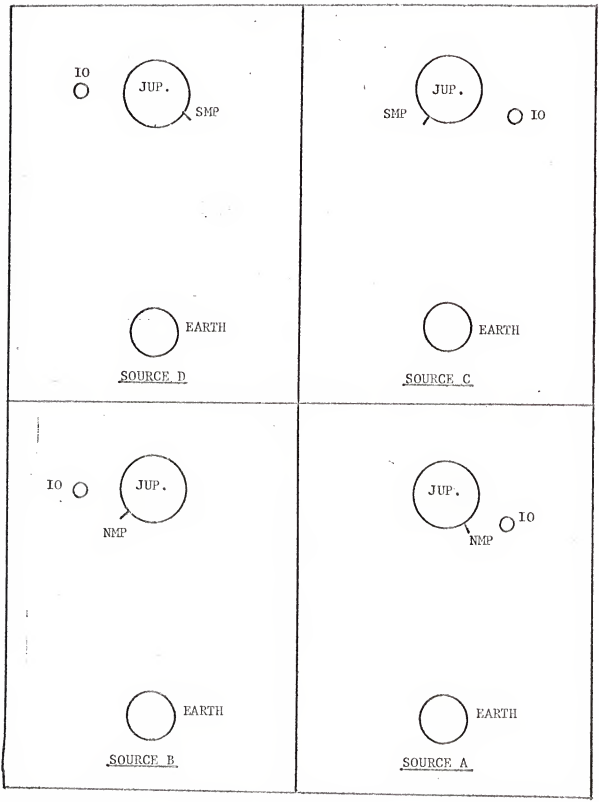

Fig. 28. The symmetrical location of Io and the north magnetic pole about the Earth-Jupiter line for each of the Io-related sources.

source A. This should give one insight into the problem of determining the source of the radiation.

Non-Io-Related Radiation

Radiation which is non-Io-related is relatively scarce at 27.6 MHz but increases as the frequency is decreased to 15 MHz, where it represents the majority of the radiation received from Jupiter at decametric wavelengths. However, as the non-Io-related component of the radiation increases, the Io-related component also increases.

The major change in the non-Io-related component of the radiation occurs for the range of central meridian longitudes from 219^{o} to 20^{o}. Non-Io-related source A exhibits a uniform distribution of the flux density for positions of the central meridian longitude between 200^{o} and 280^{o}. There appears to be a sharp decrease in the flux density received at the frequencies 22.2 MHz and 27.6 MHz when the position of the central meridian longitude is greater than 280^{o}. This decrease in the flux density appears to be more gradual for the frequencies 15 MHz and 18 MHz and to extend to longitudes of the central meridian near 20^{o}.

It is observed that the contours of equal flux density associated with the non-Io-related ridge tend to slope toward higher values of both Io and the longitude of the central meridian. This behavior is observed for the frequency range 15 MHz-22.2 MHz. Therefore, the non-Io-related radiation associated with source A exhibits a behavior similar to that observed in Io-related source A, which was discussed

earlier. This same tendency for the radiation to occur at increasingly higher longitude and Io positions is also observed in Io-related source B at frequencies of 22.2 MHz and 27.6 MHz. This sloping of the contour lines is due to the combined motion of Io about Jupiter and Jupiter's rotation. In other words, it is the "time line" of the motion of Io about Jupiter versus the rotation of the longitude system with the surface of the planet.

Two-Dimensional Analysis for Individual Apparitions

For some time it has been suggested that Io-related source B is in fact two sources. The two-source character was not apparent from the two-dimensional analysis of the flux density merged over several apparitions. However, the bifurcation was observable on several of the two-dimensional contour maps which were produced for single apparitions, as is demonstrated in Figs. 29-34. It should also be noted that the bifurcation is observed at all frequencies from 15 MHz to 27.6 MHz, and it is most apparent in Figs. 29, 30, and 34. This is in good agreement with the previous work by Olsson and Smith.[55] However, the Io positions of sources B_1 and B_2 are interchanged at 15 MHz for the 1964.8 apparition as shown in Fig. 29. This may be due to the influence of a strong Io-related source D, which is also observed in this apparition for Io near 105°.

An increase in the flux density is observed when Io is near 100° and the central meridian longitude is between 180° and 270°. Examples

Fig. 29. Two-dimensional contour map of the flux density* at 15 MHz at Florida for the 1964.9 apparition.

*For definition of "flux density" as employed here, see discussion on page 38.

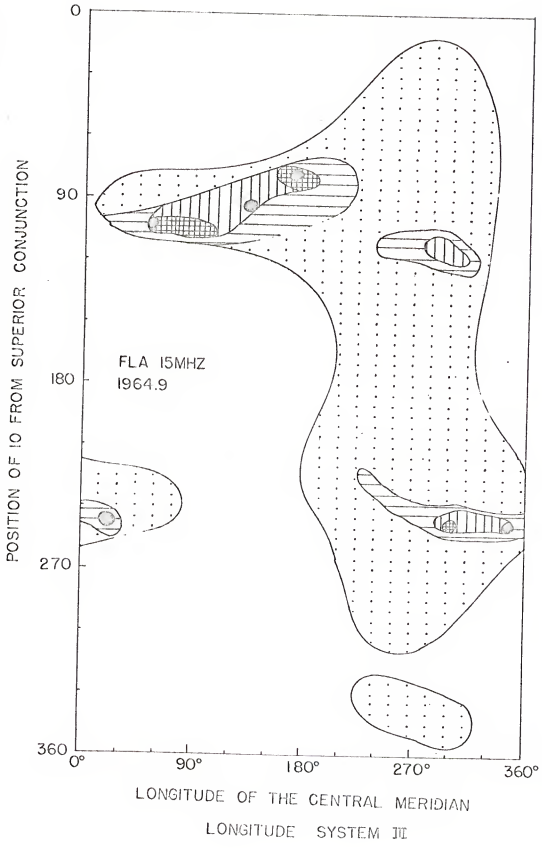
0
90
180
270
360
POSITION OF IO FROM SUPERIOR CONJUNCTION
FLA 15MHZ
1964.9
0°
90°
180°
270°
360°
LONGITUDE OF THE CENTRAL MERIDIAN
LONGITUDE SYSTEM III

Fig. 30. Two-dimensional contour map of the flux density* at 15 MHz at Florida for the 1968.0 apparition.

*For definition of "flux density" as employed here, see discussion on page 38.

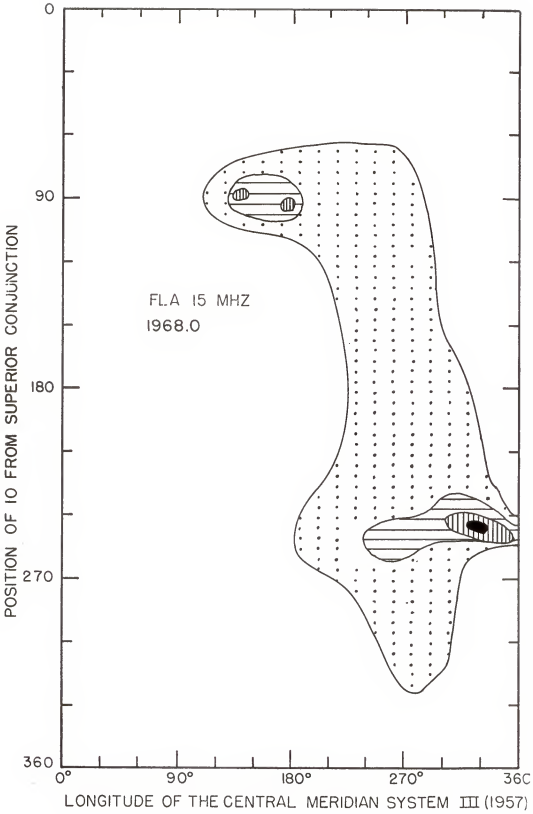
FL.A 15 MHZ
1968.0
POSITION OF IO FROM SUPERIOR CONJUNCTION
0
90
180
270
360
0°
90°
180°
270°
360
LONGITUDE OF THE CENTRAL MERIDIAN SYSTEM III (1957)

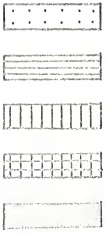

Fig. 31. Two-dimensional contour map of the flux density* at 18 MHz at Maipu for the 1963.7 apparition.

*For definition of "flux density" as employed here, see discussion on page 38.

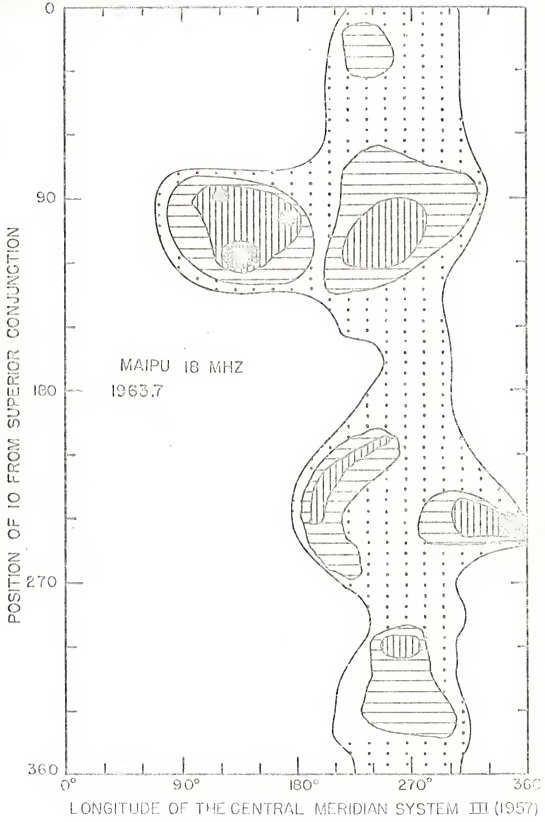
0
90
180
270
360
MAIPU 18 MHZ
1963.7
POSITION OF IO FROM SUPERIOR CONJUNCTION
0°
90°
180°
270°
360
LONGITUDE OF THE CENTRAL MERIDIAN SYSTEM III (1957)

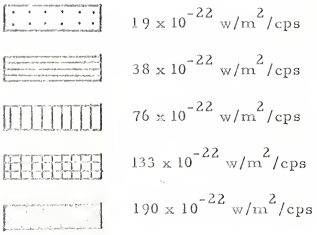

Fig. 32. Two-dimensional contour map of the flux density* at 22.2 MHz at Maipu for the 1963.7 apparition.

*For definition of "flux density" as employed here, see discussion on page 38.

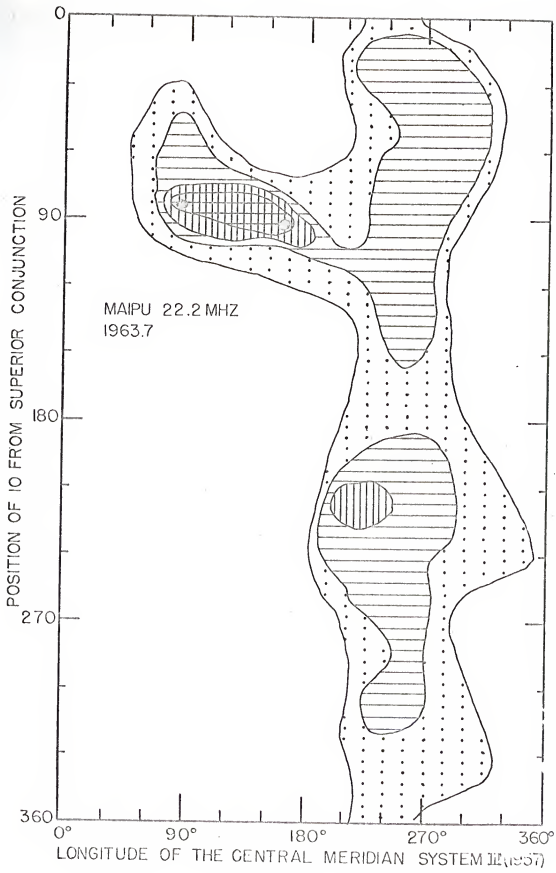
MAIPU 22.2 MHZ
1963.7
POSITION OF IO FROM SUPERIOR CONJUNCTION
0
90
180
270
360
0°
90°
180°
270°
360°
LONGITUDE OF THE CENTRAL MERIDIAN SYSTEM III (1957)

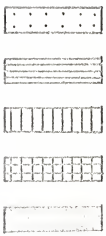

Fig. 33. Two-dimensional contour map of the flux density* at 22.2 MHz at Maipu for the 1964.9 apparition.

*For definition of "flux density" as employed here, see discussion on page 38.

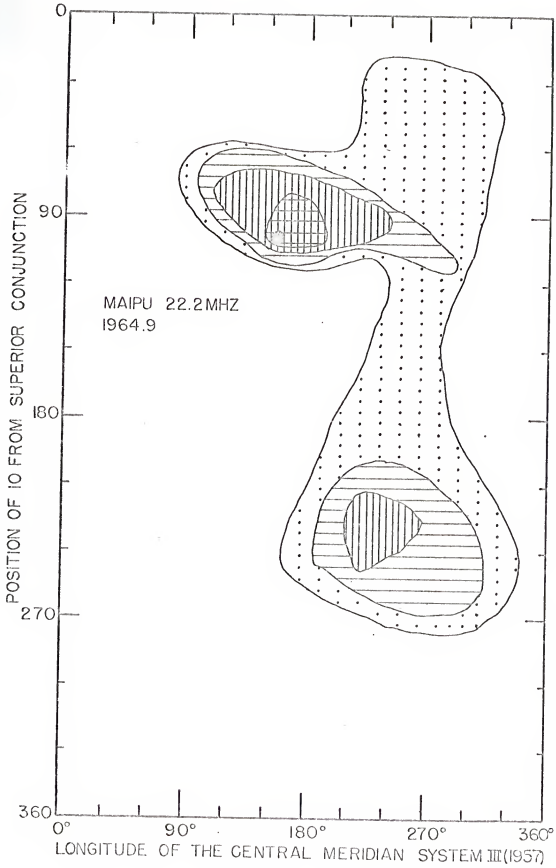
0
90
180
270
360
POSITION OF IO FROM SUPERIOR CONJUNCTION
MAIPU 22.2MHZ
1964.9
0°
90°
180°
270°
360°
LONGITUDE OF THE CENTRAL MERIDIAN SYSTEM III(1957)

Fig. 34. Two-dimensional contour map of the flux density* at 27.6 MHz at Florida for the 1967.0 apparition.

*For definition of "flux density" as employed here, see discussion on page 38.

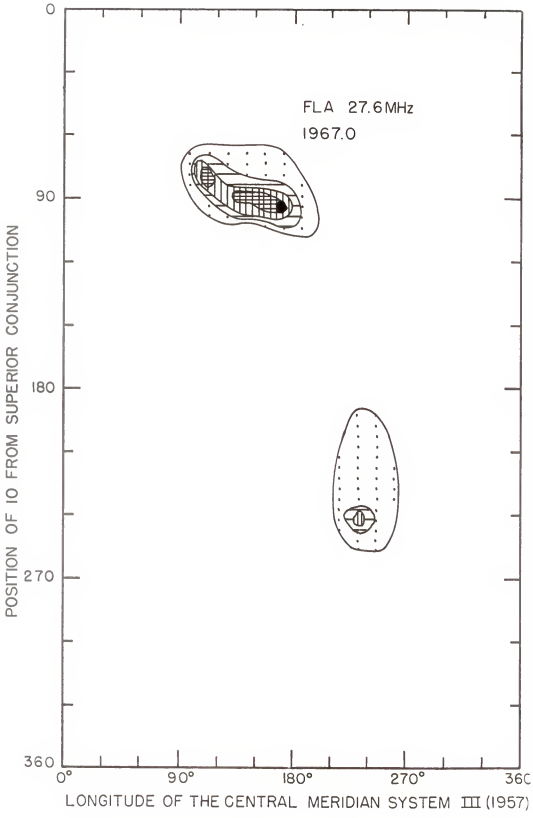
FLA 27.6MHz
1967.0
0
90
180
270
360
POSITION OF IO FROM SUPERIOR CONJUNCTION
0°
90°
180°
270°
360
LONGITUDE OF THE CENTRAL MERIDIAN SYSTEM III (1957)

of this are shown in Fig. 33 and Figs. 35-44. This increase is not seen at frequencies greater than 22.2 MHz. In most cases, the location of this intensification appears as though it is an extension of Io-related source B into the non-Io-related source A longitude region. It would be interesting to determine if the polarization and spectral characteristics of this radiation are the same as that for Io-related source B or for non-Io-related source A. There is also the possibility that this radiation originates from the same source as Io-related source A, but that it is beamed in a different direction.

Another "peak" of the flux density is observed on the two-dimensional contour maps (Figs. 29, 31, and 45-52) when Io is near 115° and the central meridian longitude ranges from 270° to 300°. This peak is observed at all frequencies from 15 MHz to 27.6 Mhz, but it apparently reaches its maximum intensity and size at 18 MHz. As the frequency is increased from 18 MHz to 27.6 MHz, both the intensity and size of the peak decrease.

The flux density is also significantly intensified for the central meridian longitude centered about 250° and a range of Io-positions from 300° to 330°. This radiation is not observed for frequencies greater than 22.2 MHz. The radiation has the appearance of a small source separated from Io-related source A but occurring at the same central meridian longitudes (Figs. 29, 31, 48, and 53). It also has the same general frequency dependence at Io-related source A. A study of the polarization and other characteristics of the radiation

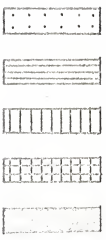

Fig. 35. Two-dimensional contour map of the flux density* at 15 MHz at Florida for the 1965.9 apparition.

*For definition of "flux density" as employed here, see discussion on page 38.

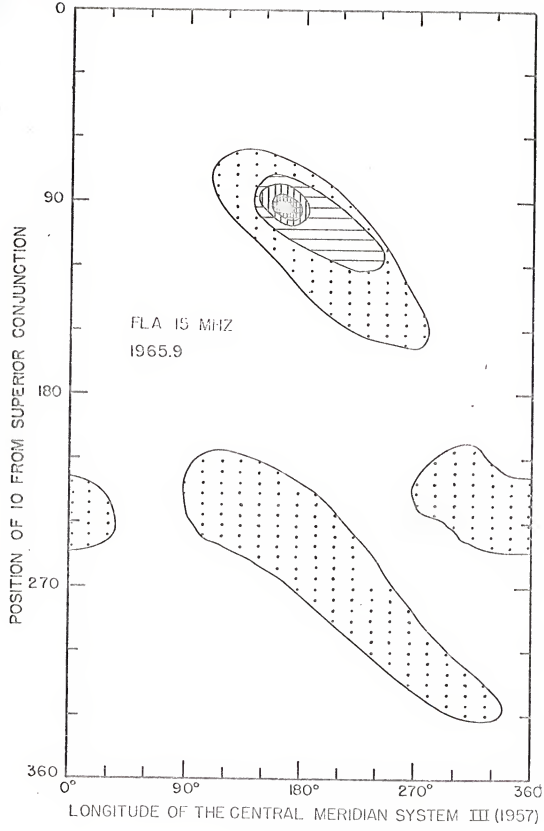
0
90
180
270
360
POSITION OF IO FROM SUPERIOR CONJUNCTION
FLA 15 MHZ
1965.9
0°
90°
180°
270°
360
LONGITUDE OF THE CENTRAL MERIDIAN SYSTEM III (1957)

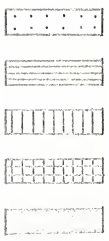

Fig. 36. Two-dimensional contour map of the flux density* at 15 MHz at Florida for the 1967.0 apparition.

*For definition of "flux density" as employed here, see discussion on page 38.

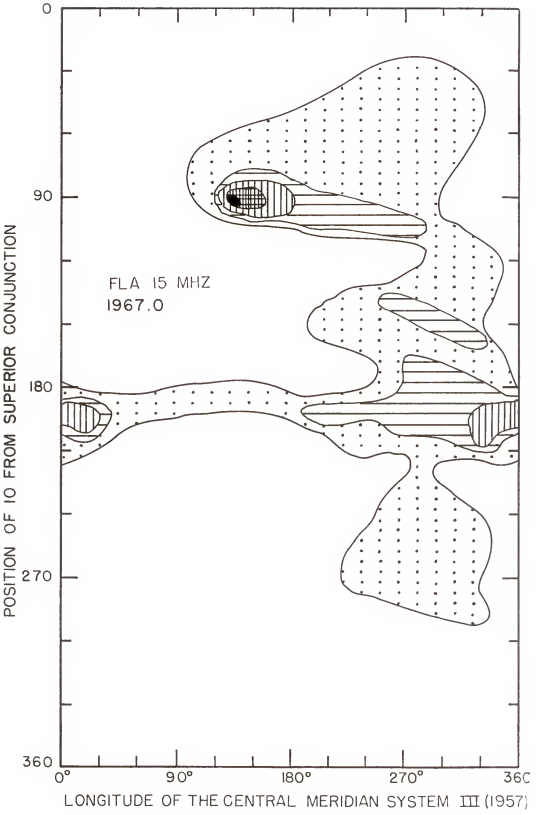
FLA 15 MHZ
1967.0
POSITION OF IO FROM SUPERIOR CONJUNCTION
0
90
180
270
360
0°
90°
180°
270°
360
LONGITUDE OF THE CENTRAL MERIDIAN SYSTEM III (1957)

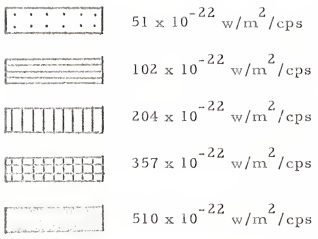

Fig. 37. Two-dimensional contour map of the flux density* at 15 MHz at Florida for the 1969.0 apparition.

*For definition of "flux density" as employed here, see discussion on page 38.

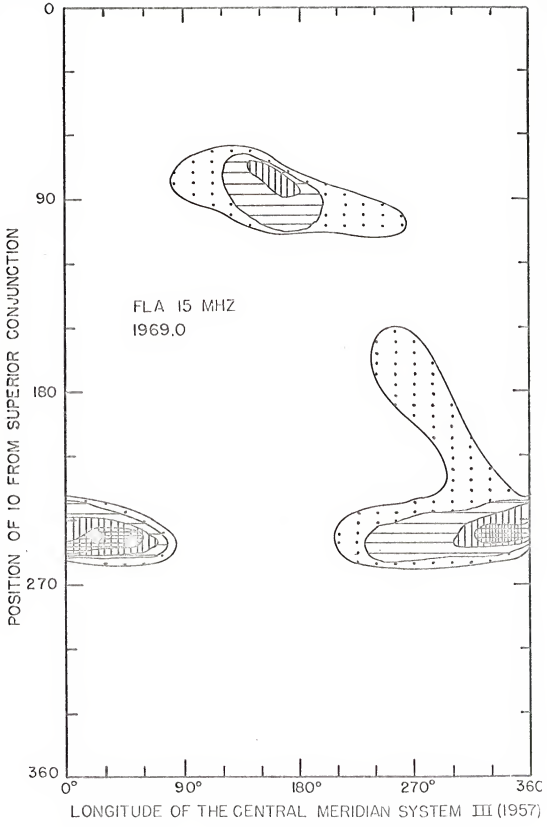
0
90
180
270
360
POSITION OF IO FROM SUPERIOR CONJUNCTION
FLA 15 MHZ
1969.0
0°
90°
180°
270°
360
LONGITUDE OF THE CENTRAL MERIDIAN SYSTEM III (1957)

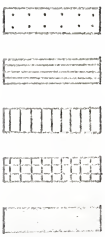

Fig. 38. Two-dimensional contour map of the flux density* at 18 MHz at Florida for the 1959.1 apparition.

*For definition of "flux density" as employed here, see discussion on page 38.

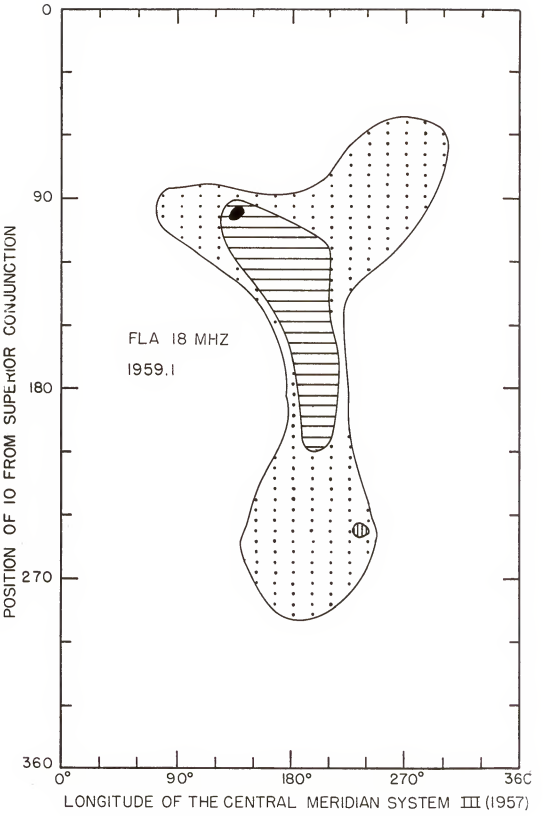
0
90
180
270
360
POSITION OF IO FROM SUPERIOR CONJUNCTION
FLA 18 MHZ
1959.1
0°
90°
180°
270°
360
LONGITUDE OF THE CENTRAL MERIDIAN SYSTEM III (1957)

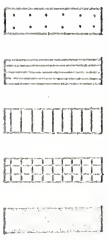

Fig. 39. Two-dimensional contour map of the flux density* at 18 MHz at Florida for the 1961.6 apparition.

*For definition of "flux density" as employed here, see discussion on page 38.

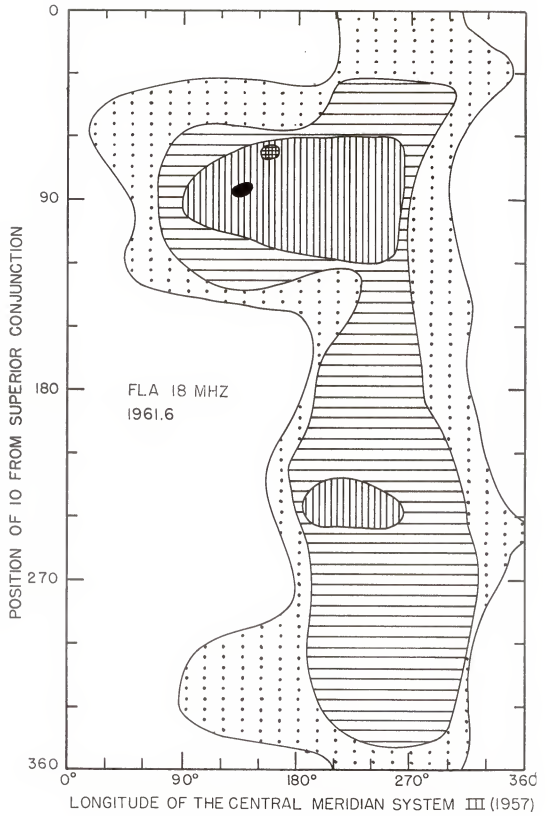
0
90
180
270
360
POSITION OF IO FROM SUPERIOR CONJUNCTION
FLA 18 MHZ
1961.6
0°
90°
180°
270°
360
LONGITUDE OF THE CENTRAL MERIDIAN SYSTEM III (1957)

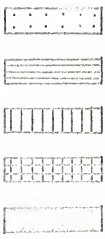

Fig. 40. Two-dimensional contour map of the flux density* at 18 MHz at Florida for the 1967.0 apparition.

*For definition of "flux density" as employed here, see discussion on page 38.

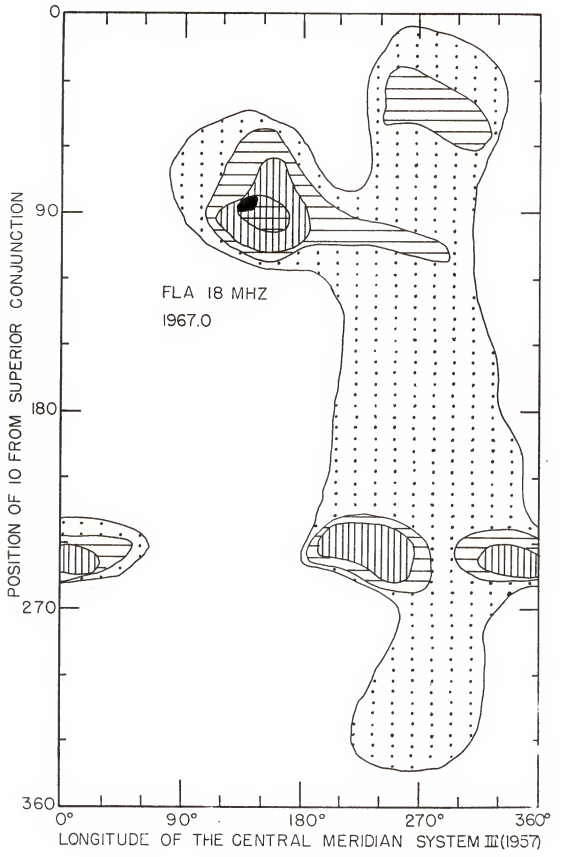
FLA 18 MHZ
1967.0
POSITION OF IO FROM SUPERIOR CONJUNCTION
0
90
180
270
360
0°
90°
180°
270°
360°
LONGITUDE OF THE CENTRAL MERIDIAN SYSTEM III (1957)

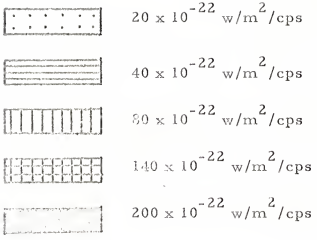

Fig. 41. Two-dimensional contour map of the flux density* at 18 MHz at Florida for the 1968.0 apparition.

*For definition of "flux density" as employed here, see discussion on page 38.

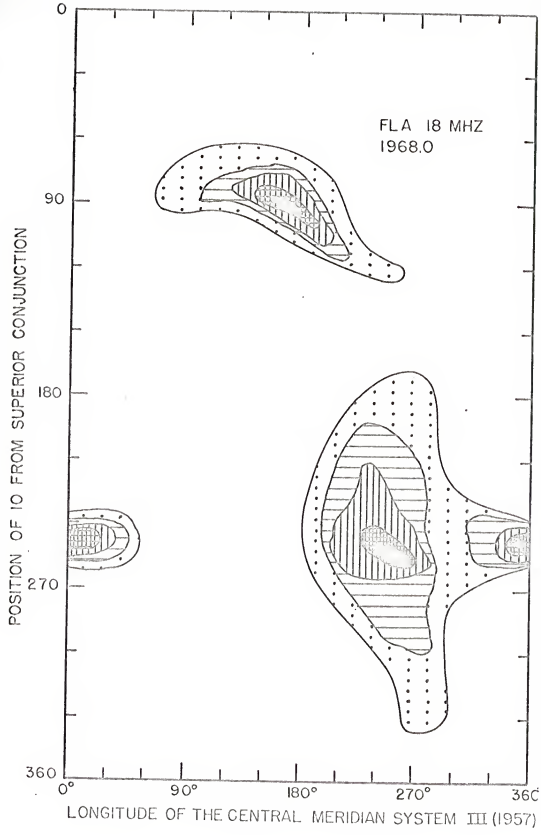
FLA 18 MHZ
1968.0
0
90
180
270
360
POSITION OF IO FROM SUPERIOR CONJUNCTION
0°
90°
180°
270°
360
LONGITUDE OF THE CENTRAL MERIDIAN SYSTEM III (1957)

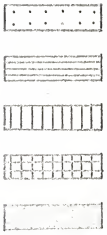

Fig. 42. Two-dimensional contour map of the flux density* at 18 MHz at Maipu for the 1962.6 apparition.

*For definition of "flux density" as employed here, see discussion on page 38.

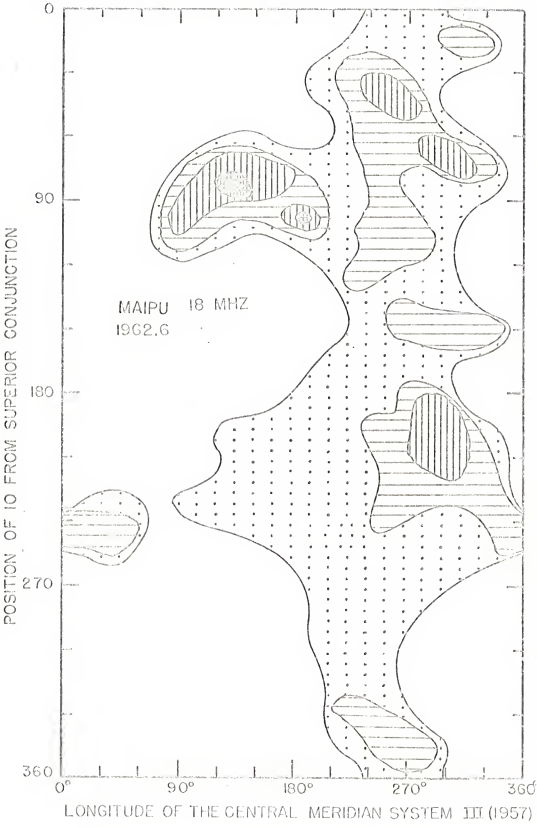
MAIPU 18 MHZ
1962.6
POSITION OF IO FROM SUPERIOR CONJUNCTION
0
90
180
270
360
0°
90°
180°
270°
360°
LONGITUDE OF THE CENTRAL MERIDIAN SYSTEM III (1957)

Fig. 43. Two-dimensional contour map of the flux density* at 22.2 MHz at Florida for the 1961.5 apparition.

*For definition of "flux density" as employed here, see discussion on page 38.

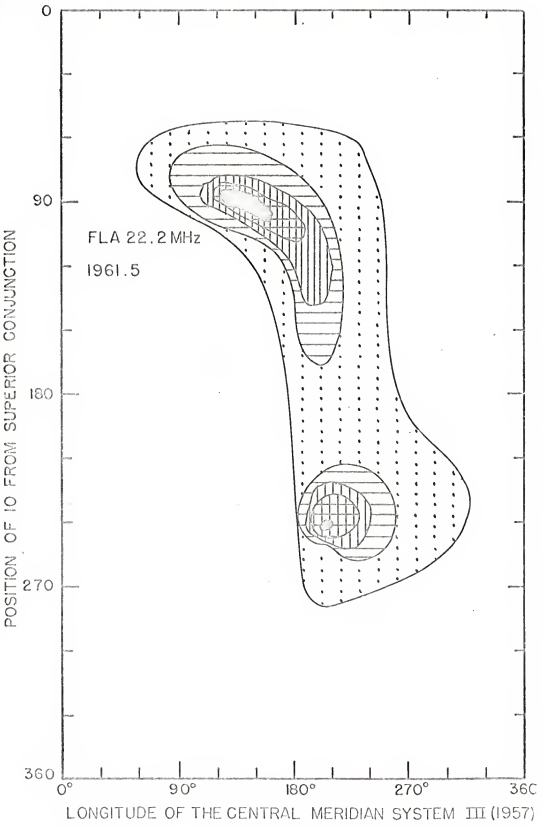
FLA 22.2 MHz
1961.5
POSITION OF IO FROM SUPERIOR CONJUNCTION
0
90
180
270
360
0°
90°
180°
270°
360
LONGITUDE OF THE CENTRAL MERIDIAN SYSTEM III (1957)

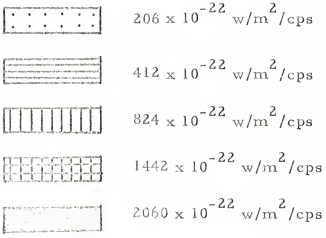

Fig. 44. Two-dimensional contour map of the flux density* at 22.2 MHz at Florida for the 1963.8 apparition.

*For definition of "flux density" as employed here, see discussion on page 38.

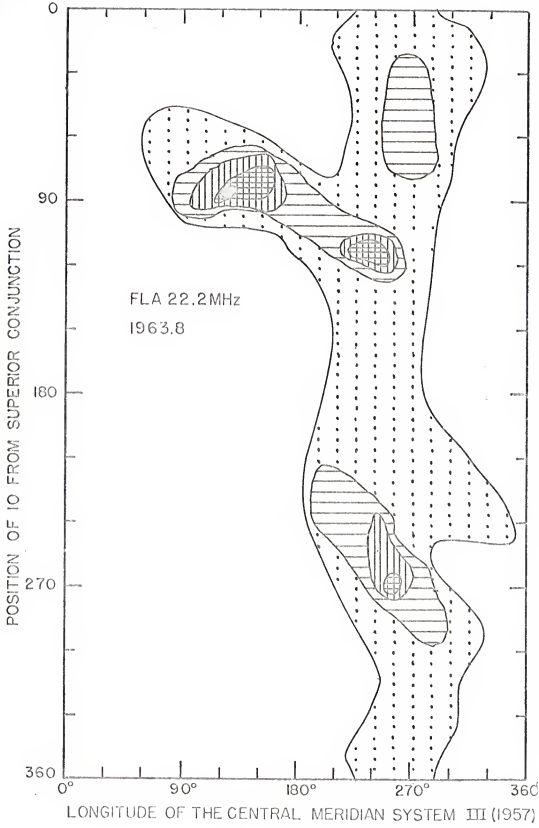
FLA 22.2MHz
1963.8
POSITION OF IO FROM SUPERIOR CONJUNCTION
0
90
180
270
360
0°
90°
180°
270°
360°
LONGITUDE OF THE CENTRAL MERIDIAN SYSTEM III (1957)

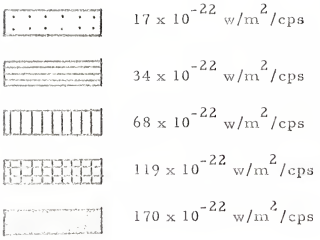

Fig. 45. Two-dimensional contour map of the flux density* at 18 MHz at Florida for the 1957.1 apparition.

*For definition of "flux density" as employed here, see discussion on page 38.

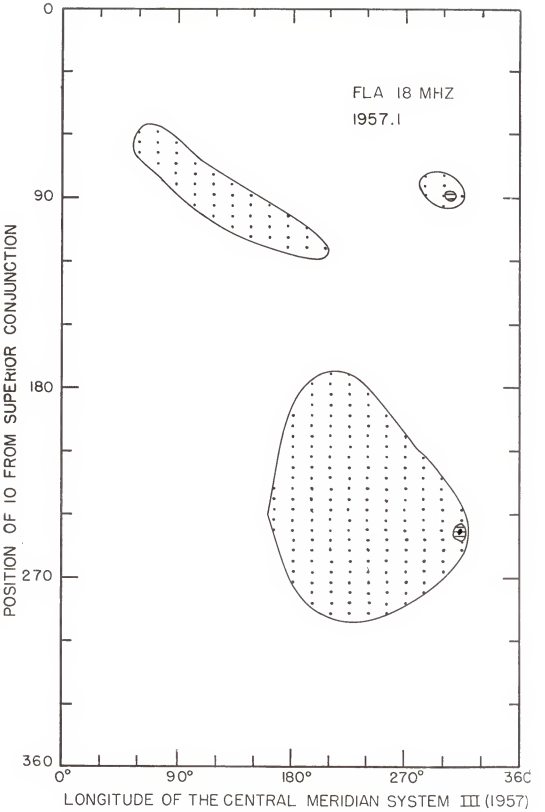
FLA 18 MHZ
1957.1
0
90
180
270
360
POSITION OF IO FROM SUPERIOR CONJUNCTION
0°
90°
180°
270°
360°
LONGITUDE OF THE CENTRAL MERIDIAN SYSTEM III (1957)

Fig. 46. Two-dimensional contour map of the flux density* at 18 MHz at Florida for the 1964.8 apparition.

*For definition of "flux density" as employed here, see discussion on page 38.

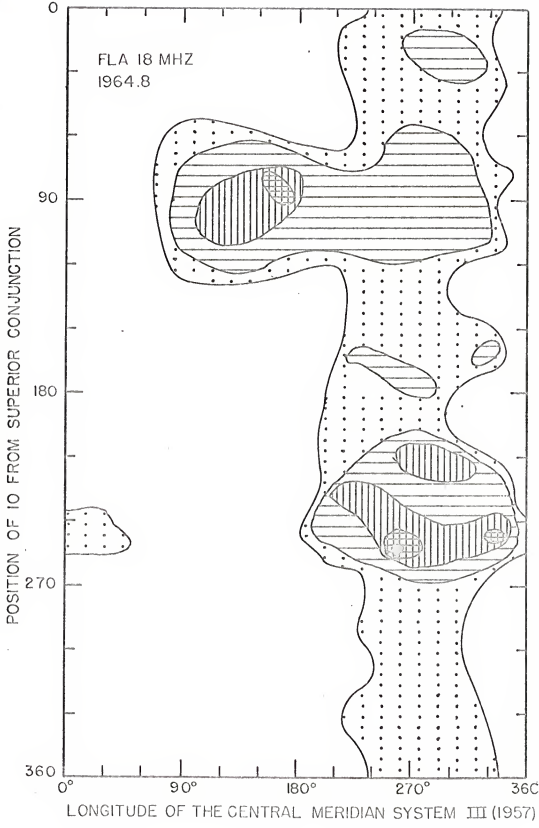
FLA 18 MHZ
1964.8
0
90
180
270
360
POSITION OF IO FROM SUPERIOR CONJUNCTION
0°
90°
180°
270°
360
LONGITUDE OF THE CENTRAL MERIDIAN SYSTEM III (1957)

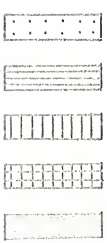

Fig. 47. Two-dimensional contour map of the flux density* at 18 MHz at Florida for the 1965.9 apparition.

*For definition of "flux density" as employed here, see discussion on page 38.

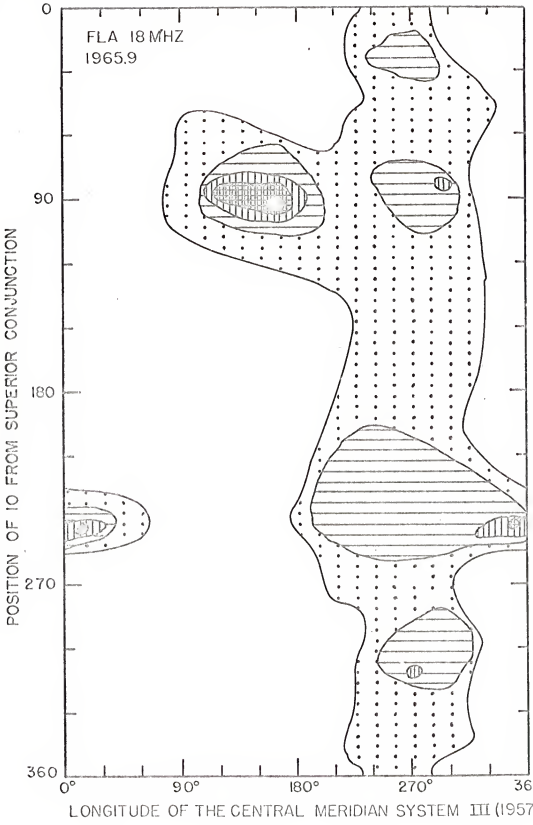
FLA 18 MHZ
1965.9
0
90
180
270
360
POSITION OF IO FROM SUPERIOR CONJUNCTION
0°
90°
180°
270°
360
LONGITUDE OF THE CENTRAL MERIDIAN SYSTEM III (1957)

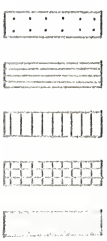

Fig. 48. Two-dimensional contour map of the flux density* at 18 MHz at Florida for the 1969.0 apparition.

*For definition of "flux density" as employed here, see discussion on page 38.

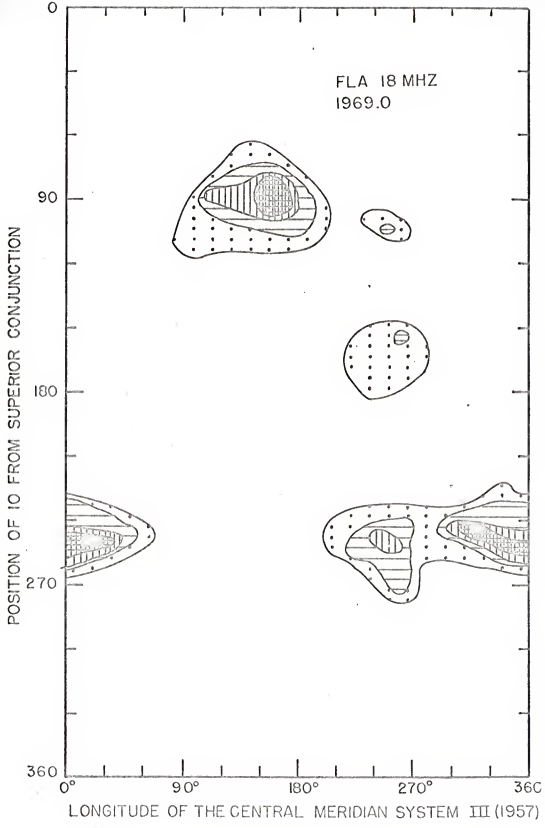
FLA 18 MHZ
1969.0
0
90
180
270
360
POSITION OF IO FROM SUPERIOR CONJUNCTION
0°
90°
180°
270°
360
LONGITUDE OF THE CENTRAL MERIDIAN SYSTEM III (1957)

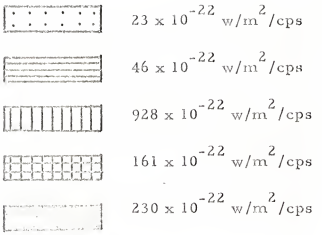

Fig. 49. Two-dimensional contour map of the flux density* at 18 MHz at Maipu for the 1966.0 apparition.

*For definition of "flux density" as employed here, see discussion on page 33.

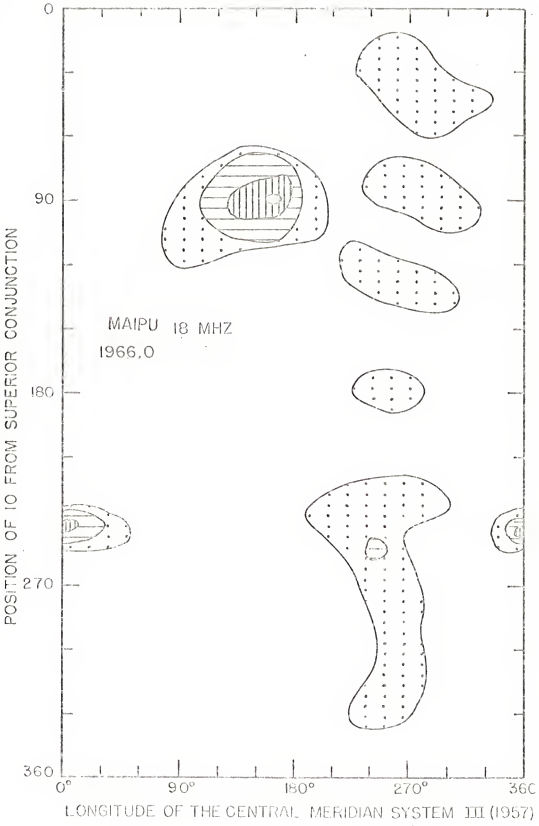
MAIPU 18 MHZ
1966.0
POSITION OF IO FROM SUPERIOR CONJUNCTION
0
90
180
270
360
0°
90°
180°
270°
360
LONGITUDE OF THE CENTRAL MERIDIAN SYSTEM III (1957)

118×10^{-22} w/m^2/cps

236×10^{-22} w/m^2/cps

472×10^{-22} w/m^2/cps

826×10^{-22} w/m^2/cps

1180×10^{-22} w/m^2/cps

Fig. 50. Two-dimensional contour map of the flux density* at 22.2 MHz at Florida for the 1967.0 apparition.

*For definition of "flux density" as employed here, see discussion on page 38.

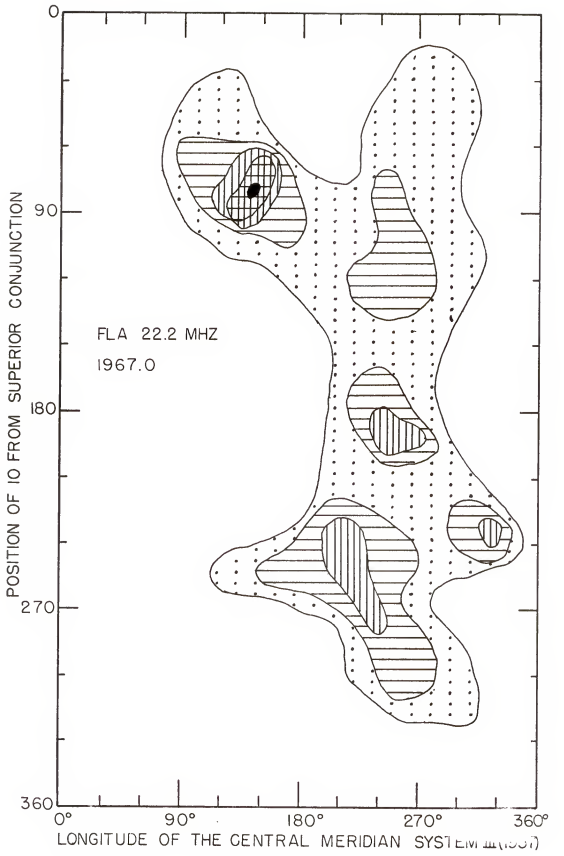
0
90
180
270
360
FLA 22.2 MHZ
1967.0
POSITION OF IO FROM SUPERIOR CONJUNCTION
0°
90°
180°
270°
360°
LONGITUDE OF THE CENTRAL MERIDIAN SYSTEM III(1957)

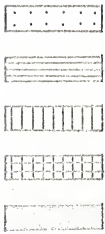

Fig. 51. Two-dimensional contour map of the flux density* at 22.2 MHz at Maipu for the 1965.9 apparition.

*For definition of "flux density" as employed here, see discussion on page 38.

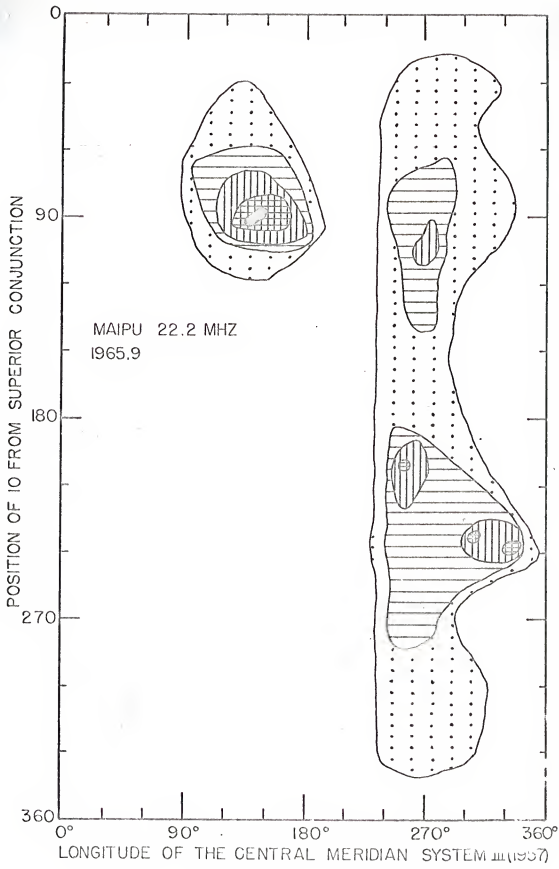
0
90
180
270
360
POSITION OF IO FROM SUPERIOR CONJUNCTION
MAIPU 22.2 MHZ
1965.9
0°
90°
180°
270°
360°
LONGITUDE OF THE CENTRAL MERIDIAN SYSTEM III (1957)

Fig. 52. Two-dimensional contour map of the flux density* at 27.6 MHz at Maipu for the 1965.9 apparition.

*For definition of "flux density" as employed here, see discussion on page 38.

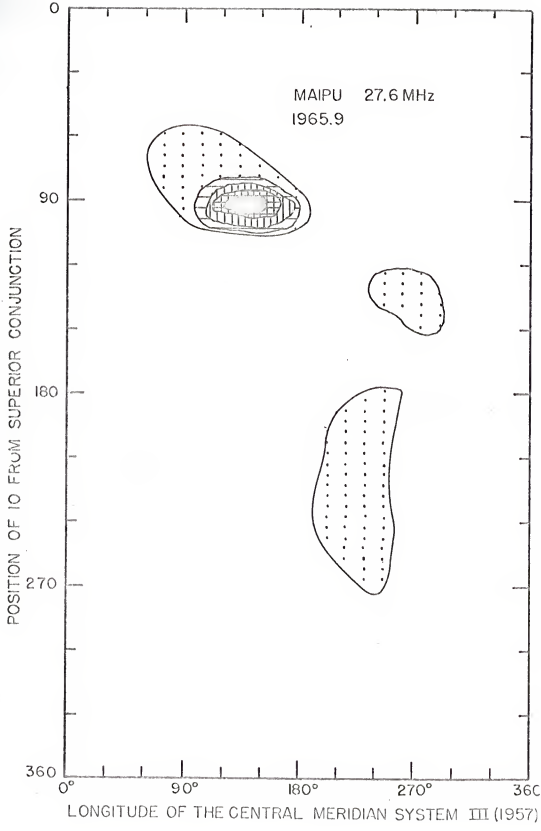
MAIPU 27.6 MHz
1965.9
0
90
180
270
360
POSITION OF IO FROM SUPERIOR CONJUNCTION
0°
90°
180°
270°
360
LONGITUDE OF THE CENTRAL MERIDIAN SYSTEM III (1957)

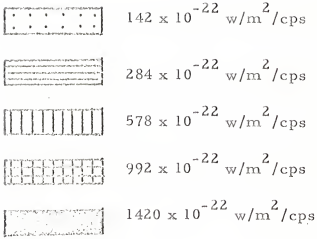

Fig. 53. Two-dimensional contour map of the flux density* at 22.2 MHz at Florida for the 1962.8 apparition.

*For definition of "flux density" as employed here, see discussion on page 38.

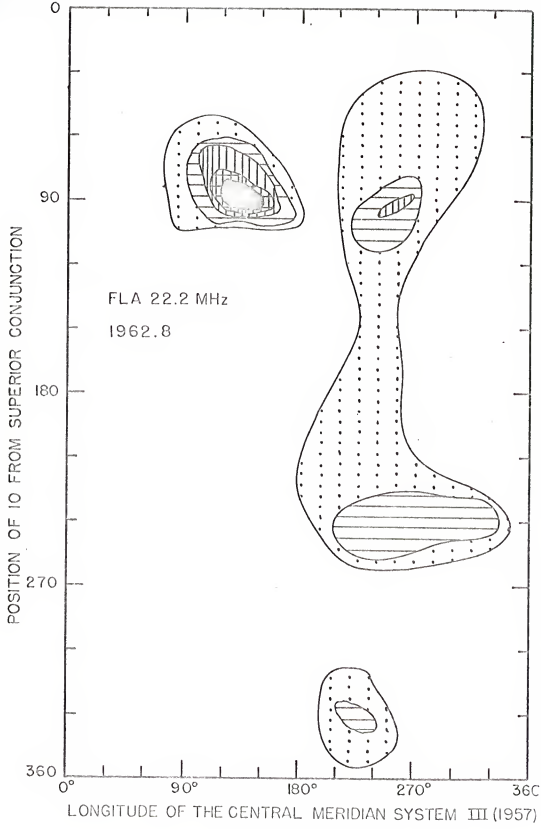
0
90
180
270
360
FLA 22.2 MHz
1962.8
POSITION OF IO FROM SUPERIOR CONJUNCTION
0°
90°
180°
270°
360
LONGITUDE OF THE CENTRAL MERIDIAN SYSTEM III (1957)

received from this source may be helpful in determining whether this is a part of the Io-related source A or not.

A number of other small localizations of the flux density should be mentioned. One is centered about Io=35° and the central meridian longitude = 330°±30° (Figs. 41, 46, 47, and 54). This source was observed only at frequencies of 15 MHz and 18 MHz.

Another localization of the flux density is observed for Io=60° and central meridian longitude = 270° (Figs. 41, 45, 55, 56, and 57). This source was observed only at the frequencies 18 MHz and 22.2 MHz.

A number of other two-dimensional contour maps of the flux density has been produced which show the general permanent features associated with the position of Io from superior geocentric conjunction and the longitude of the central meridian. These maps are presented in Figs. 58-77 for completeness.

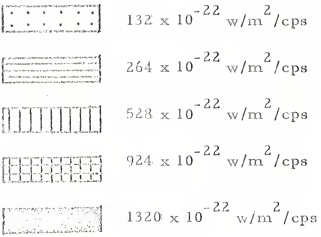

Fig. 54. Two-dimensional contour map of the flux density* at 15 MHz at Florida for the 1963.8 apparition.

*For definition of "flux density" as employed here, see discussion on page 38.

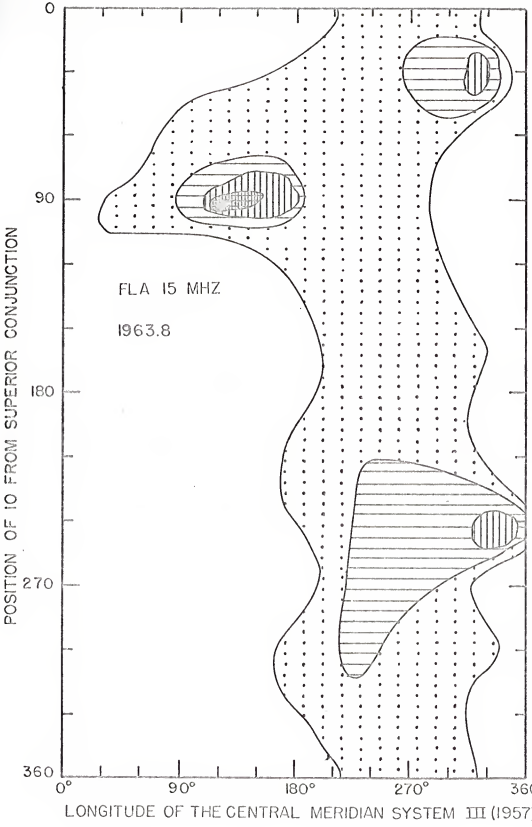
0
90
180
270
360
POSITION OF IO FROM SUPERIOR CONJUNCTION
FLA 15 MHZ
1963.8
0°
90°
180°
270°
360
LONGITUDE OF THE CENTRAL MERIDIAN SYSTEM III (1957)

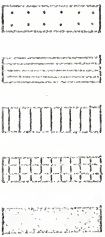

Fig. 55. Two-dimensional contour map of the flux density* at 18 MHz at Florida for the 1960.2 apparition.

*For definition of "flux density" as employed here, see discussion on page 38.

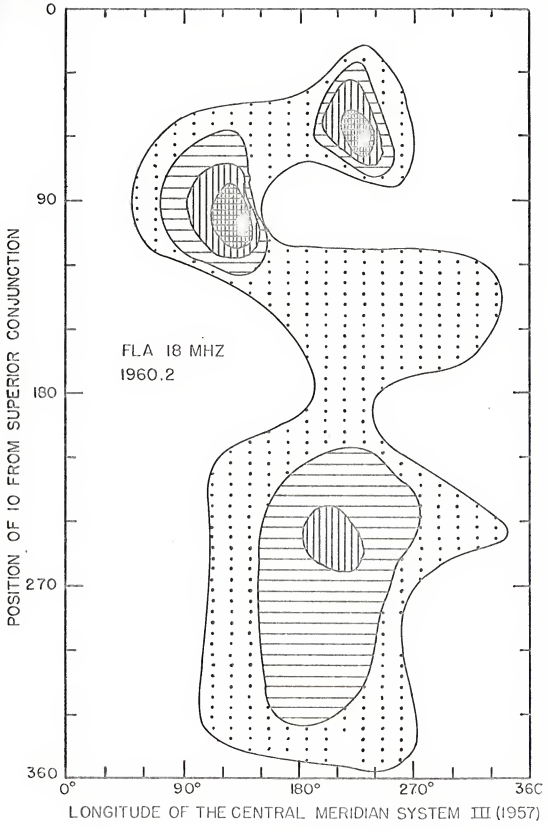
0
90
180
270
360
FLA 18 MHZ
1960.2
POSITION OF IO FROM SUPERIOR CONJUNCTION
0°
90°
180°
270°
360
LONGITUDE OF THE CENTRAL MERIDIAN SYSTEM III (1957)

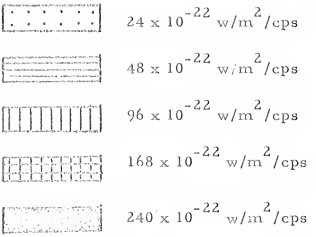

Fig. 56. Two-dimensional contour map of the flux density* at 22.2 MHz at Florida for the 1960.2 apparition.

*For definition of "flux density" as employed here, see discussion on page 38.

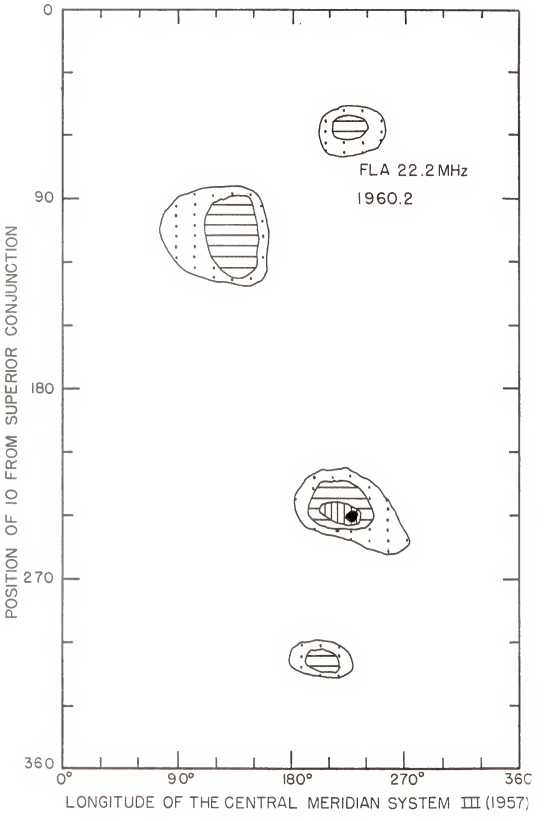
FLA 22.2MHz
1960.2
0
90
180
270
360
POSITION OF IO FROM SUPERIOR CONJUNCTION
0°
90°
180°
270°
360
LONGITUDE OF THE CENTRAL MERIDIAN SYSTEM III (1957)

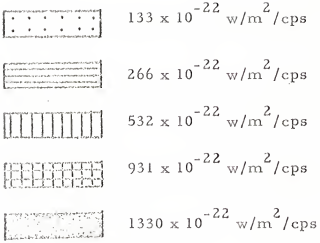

Fig. 57. Two-dimensional contour map of the flux density* at 22.2 MHz at Florida for the 1965.9 apparition.

*For definition of "flux density" as employed here, see discussion on page 38.

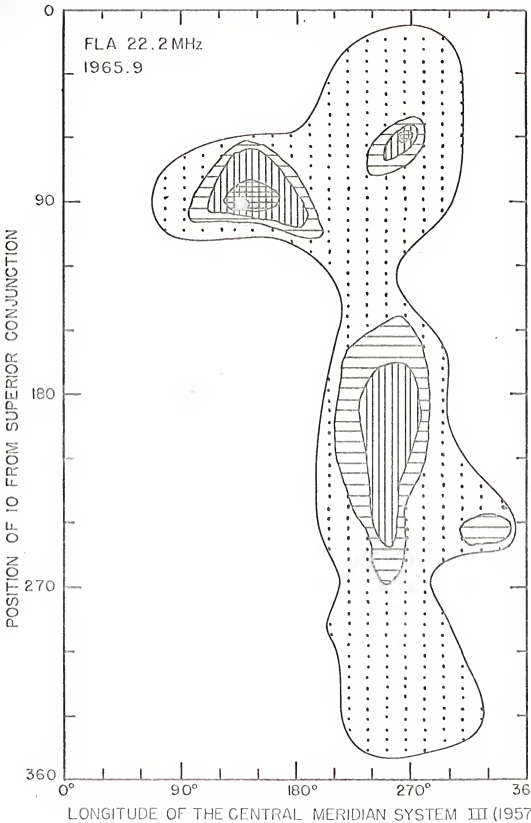
FLA 22.2 MHz
1965.9
0
90
180
270
360
POSITION OF IO FROM SUPERIOR CONJUNCTION
0°
90°
180°
270°
360
LONGITUDE OF THE CENTRAL MERIDIAN SYSTEM III (1957)

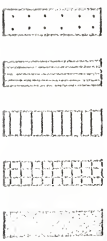

Fig. 58. Two-dimensional contour map of the flux density* at 15 MHz at Florida for the 1962.7 apparition.

*For definition of "flux density" as employed here, see discussion on page 38.

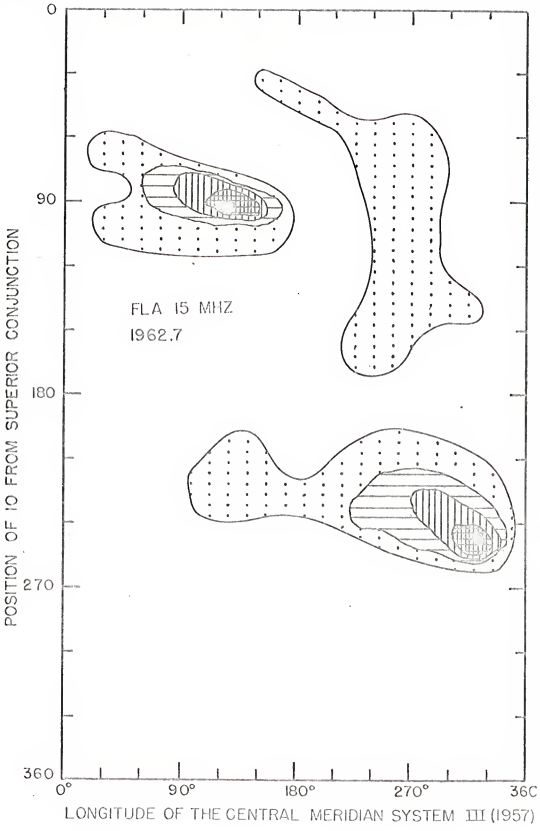
0
90
180
270
360
POSITION OF IO FROM SUPERIOR CONJUNCTION
FLA 15 MHZ
1962.7
0°
90°
180°
270°
360
LONGITUDE OF THE CENTRAL MERIDIAN SYSTEM III (1957)

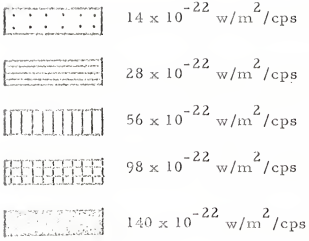

Fig. 59. Two-dimensional contour map of the flux density* at 18 MHz at Florida for the 1958.1 apparition.

*For definition of "flux density" as employed here, see discussion on page 38.

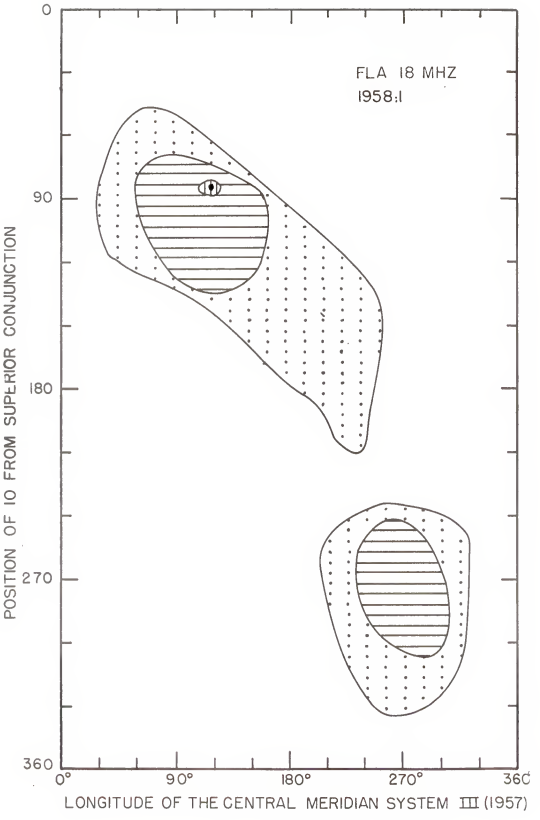
FLA 18 MHZ
1958.1
0
90
180
270
360
POSITION OF IO FROM SUPERIOR CONJUNCTION
0°
90°
180°
270°
360
LONGITUDE OF THE CENTRAL MERIDIAN SYSTEM III (1957)

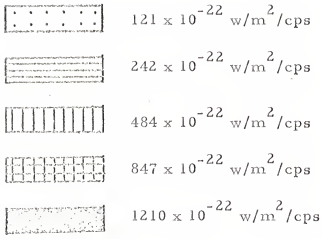

Fig. 60. Two-dimensional contour map of the flux density* at 18 MHz at Florida for the 1963.3 apparition.

*For definition of "flux density" as employed here, see discussion on page 38.

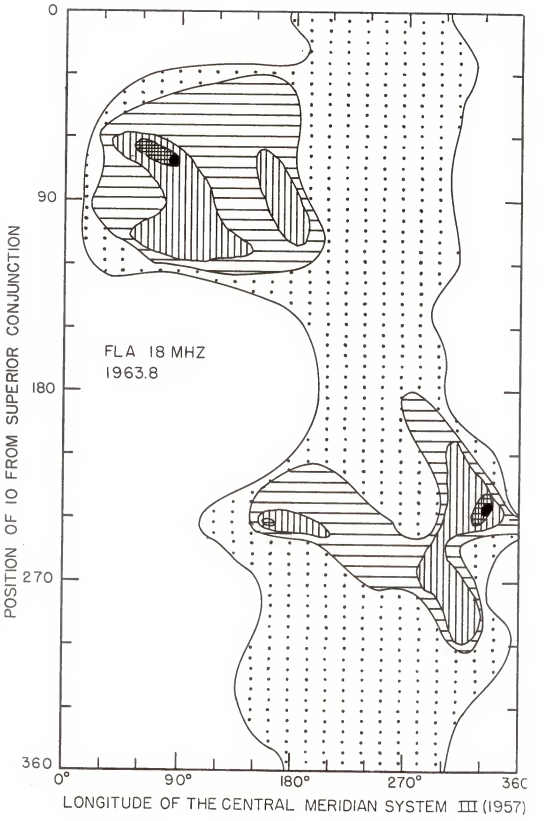
0
90
180
270
360
POSITION OF IO FROM SUPERIOR CONJUNCTION
FLA 18 MHZ
1963.8
0°
90°
180°
270°
360
LONGITUDE OF THE CENTRAL MERIDIAN SYSTEM III (1957)

Fig. 61. Two-dimensional contour map of the flux density* at 22.2 MHz at Florida for the 1958.1 apparition.

*For definition of "flux density" as employed here, see discussion on page 38.

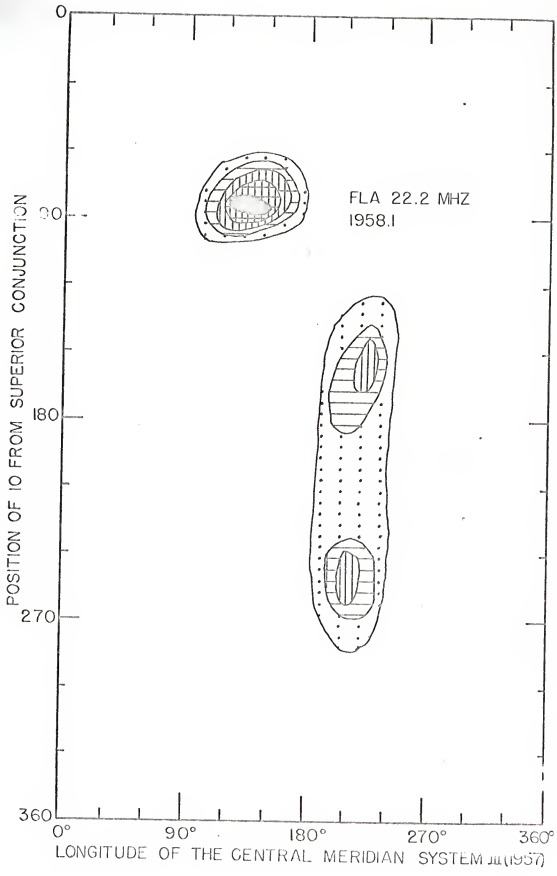
FLA 22.2 MHZ
1958.1
POSITION OF IO FROM SUPERIOR CONJUNCTION
0
90
180
270
360
0°
90°
180°
270°
360°
LONGITUDE OF THE CENTRAL MERIDIAN SYSTEM III (1957)

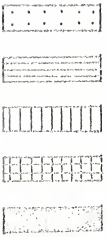

Fig. 62. Two-dimensional contour map of the flux density* at 22.2 MHz at Florida for the 1959.2 apparition.

*For definition of "flux density" as employed here, see discussion on page 38.

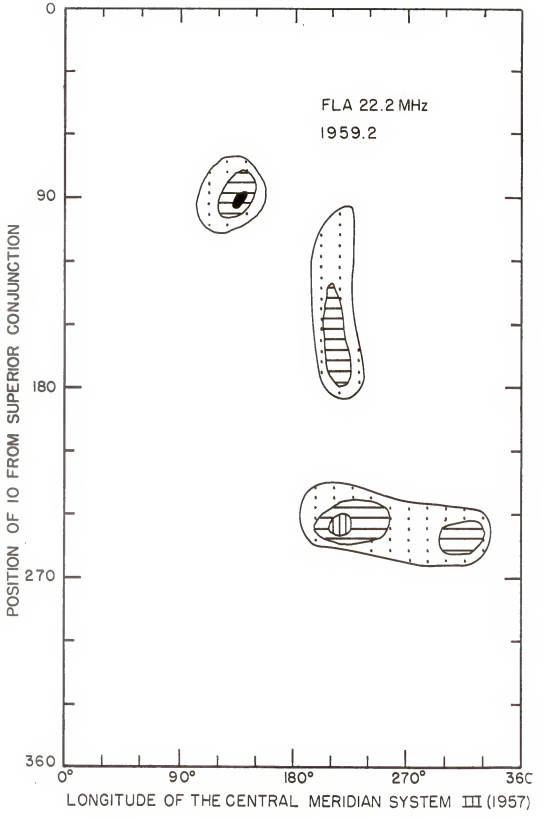
FLA 22.2 MHz
1959.2
0
90
180
270
360
POSITION OF IO FROM SUPERIOR CONJUNCTION
0°
90°
180°
270°
360
LONGITUDE OF THE CENTRAL MERIDIAN SYSTEM III (1957)

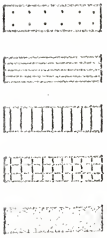

Fig. 63. Two-dimensional contour map of the flux density*at 22.2 MHz at Florida for the 1964.8 apparition.

*For definition of "flux density" as employed here, see discussion on page 38.

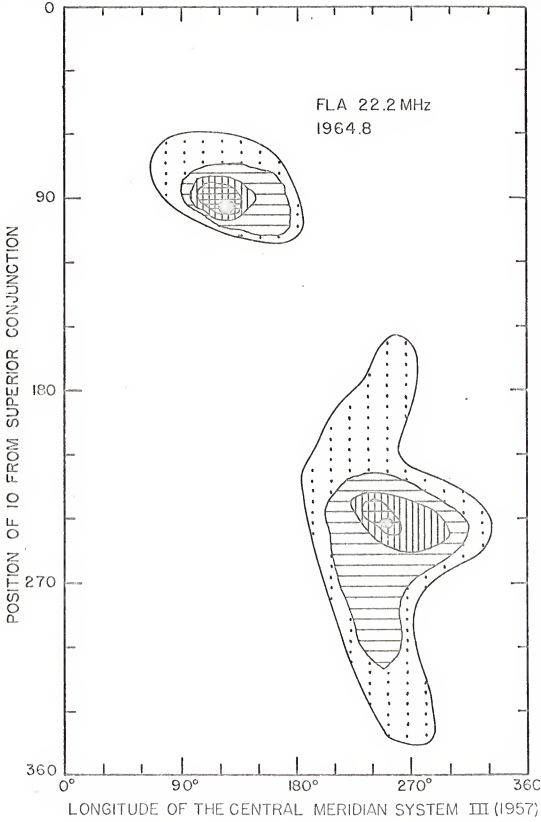
FLA 22.2 MHz
1964.8
0
90
180
270
360
POSITION OF IO FROM SUPERIOR CONJUNCTION
0°
90°
180°
270°
360
LONGITUDE OF THE CENTRAL MERIDIAN SYSTEM III (1957)

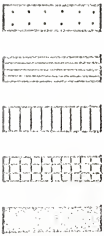

Fig. 64. Two-dimensional contour map of the flux density* at 22.2 MHz at Florida for the 1968.0 apparition.

*For definition of "flux density" as employed here, see discussion on page 38.

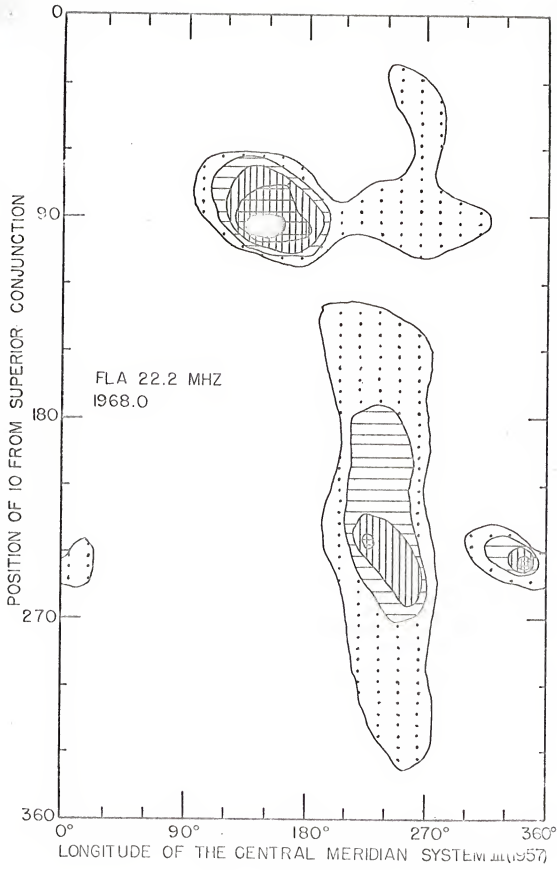
0
90
180
270
360
POSITION OF IO FROM SUPERIOR CONJUNCTION
FLA 22.2 MHZ
1968.0
0°
90°
180°
270°
360°
LONGITUDE OF THE CENTRAL MERIDIAN SYSTEM III(1957)

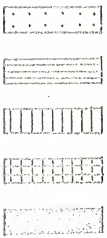

Fig. 65. Two-dimensional contour map of the flux density* at 22.2 MHz at Florida for the 1969.0 apparition.

*For definition of "flux density" as employed here, see discussion on page 38.

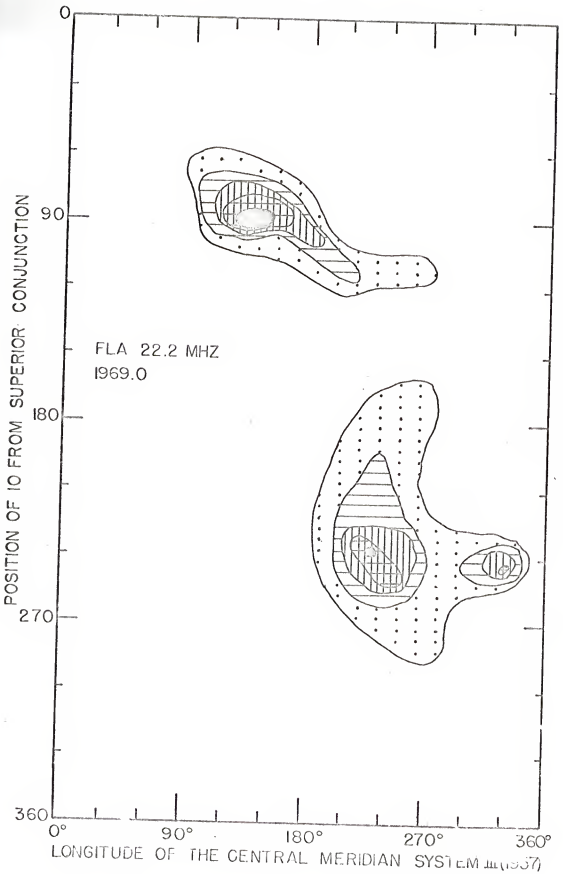
0
90
180
270
360
POSITION OF IO FROM SUPERIOR CONJUNCTION
FLA 22.2 MHZ
1969.0
0°
90°
180°
270°
360°
LONGITUDE OF THE CENTRAL MERIDIAN SYSTEM III(1957)

Fig. 66. Two-dimensional contour map of the flux density*at 22.2 MHz at Maipu for the 1960.4 apparition.

*For definition of "flux density" as employed here, see discussion on page 38.

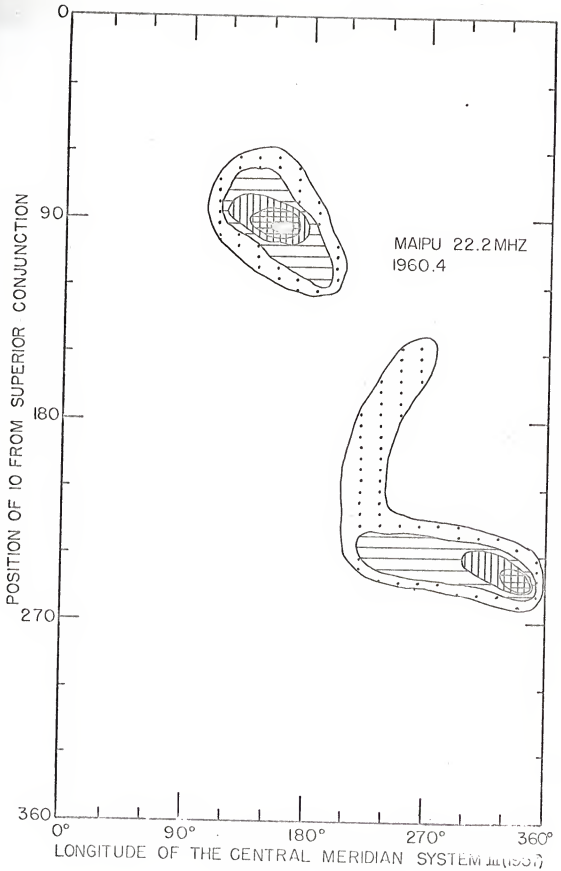
0
90
180
270
360
POSITION OF IO FROM SUPERIOR CONJUNCTION
MAIPU 22.2MHZ
1960.4
0°
90°
180°
270°
360°
LONGITUDE OF THE CENTRAL MERIDIAN SYSTEM III(1957)

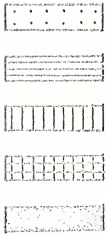

Fig. 67. Two-dimensional contour map of the flux density* at 22.2 MHz at Maipu for the 1961.5 apparition.

*For definition of "flux density" as employed here, see discussion on page 38.

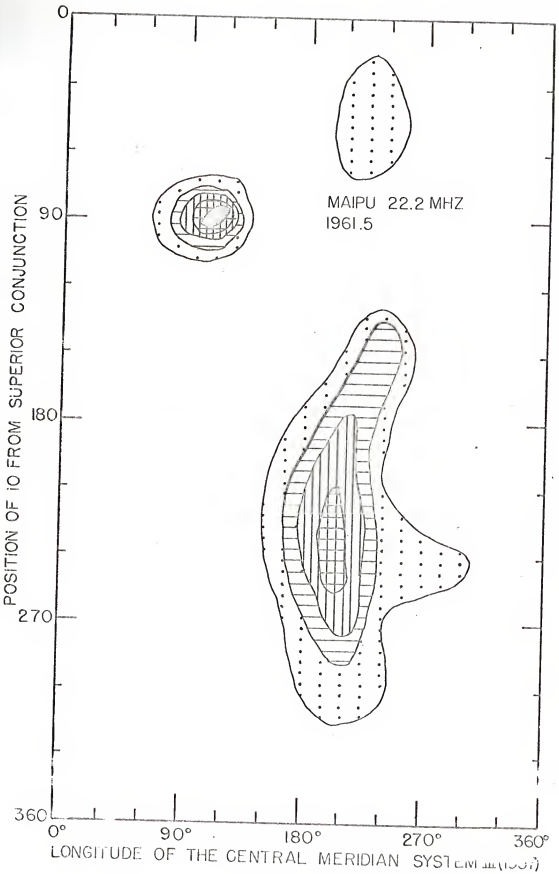
MAIPU 22.2 MHZ
1961.5
POSITION OF IO FROM SUPERIOR CONJUNCTION
0
90
180
270
360
0°
90°
180°
270°
360°
LONGITUDE OF THE CENTRAL MERIDIAN SYSTEM III (1957)

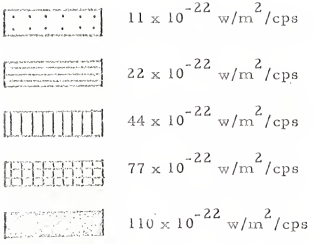

Fig. 68. Two-dimensional contour map of the flux density* at 22.2 MHz at Maipu for the 1963.7 apparition.

*For definition of "flux density" as employed here, see discussion on page 38.

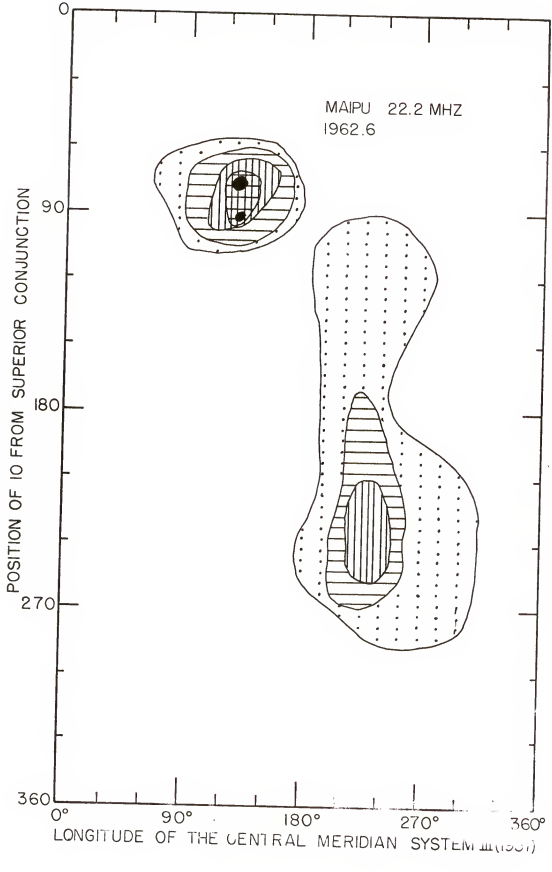
MAIPU 22.2 MHZ
1962.6
POSITION OF IO FROM SUPERIOR CONJUNCTION
0
90
180
270
360
0°
90°
180°
270°
360°
LONGITUDE OF THE CENTRAL MERIDIAN SYSTEM III(1957)

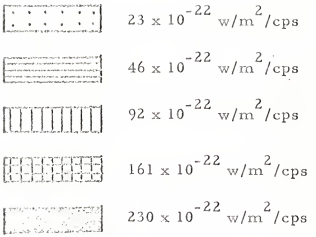

Fig. 69. Two-dimensional contour map of the flux density* at 27.6 MHz at Florida for the 1961.6 apparition.

*For definition of "flux density" as employed here, see discussion on page 38.

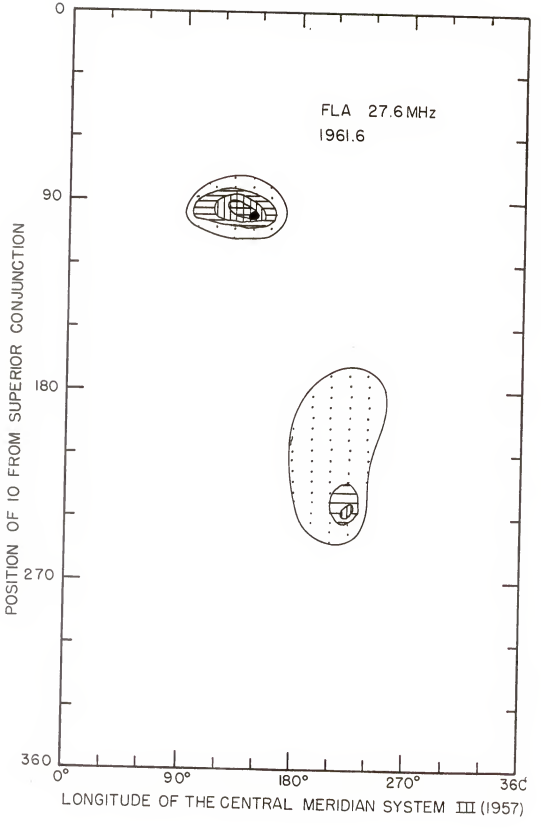
FLA 27.6 MHz
1961.6
0
90
180
270
360
POSITION OF IO FROM SUPERIOR CONJUNCTION
0°
90°
180°
270°
360
LONGITUDE OF THE CENTRAL MERIDIAN SYSTEM III (1957)

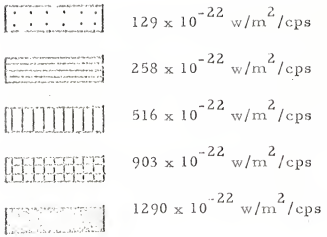

Fig. 70. Two-dimensional contour map of the flux density* at 27.6 MHz at Florida for the 1962.7 apparition.

*For definition of "flux density" as employed here, see discussion on page 38.

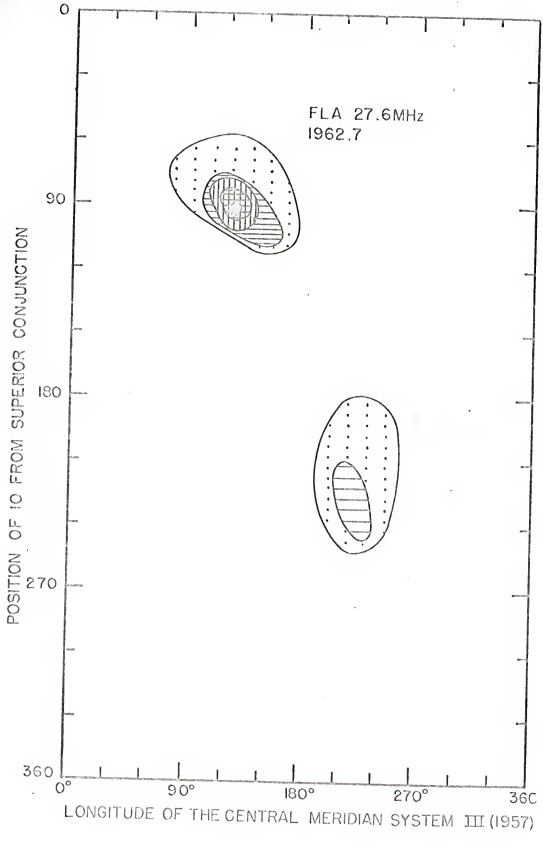
FLA 27.6MHz
1962.7
0
90
180
270
360
POSITION OF IO FROM SUPERIOR CONJUNCTION
0°
90°
180°
270°
360
LONGITUDE OF THE CENTRAL MERIDIAN SYSTEM III (1957)

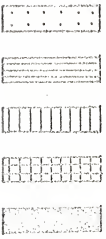

Fig. 71. Two-dimensional contour map of the flux density* at 27.6 MHz at Florida for the 1963.8 apparition.

*For definition of "flux density" as employed here, see discussion on page 38.

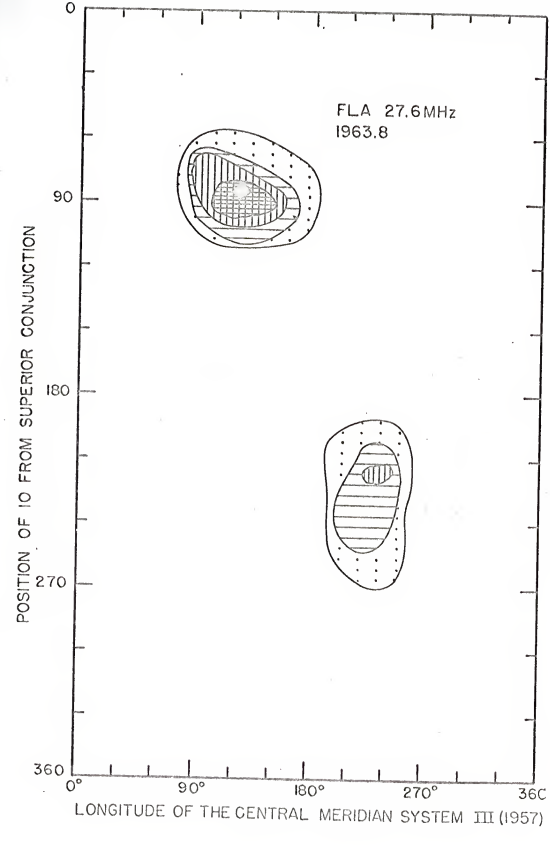
FLA 27.6MHz
1963.8
0
90
180
270
360
POSITION OF IO FROM SUPERIOR CONJUNCTION
0°
90°
180°
270°
360
LONGITUDE OF THE CENTRAL MERIDIAN SYSTEM III (1957)

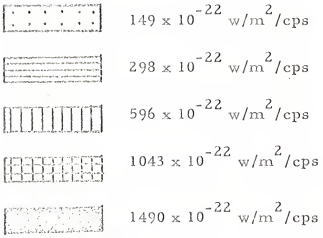

Fig. 72. Two-dimensional contour map of the flux density* at 27.6 MHz at Florida for the 1964.8 apparition.

*For definition of "flux density" as employed here, see discussion on page 38.

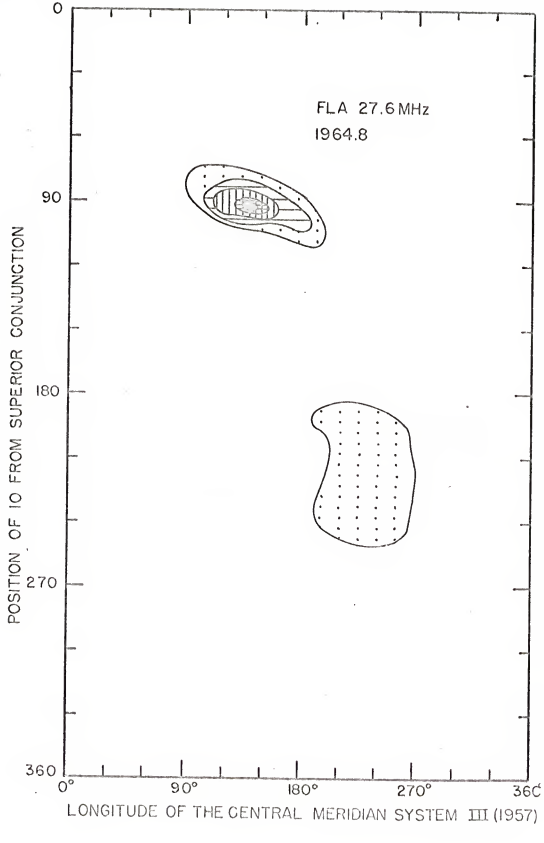
FLA 27.6 MHz
1964.8
0
90
180
270
360
POSITION OF IO FROM SUPERIOR CONJUNCTION
0°
90°
180°
270°
360
LONGITUDE OF THE CENTRAL MERIDIAN SYSTEM III (1957)

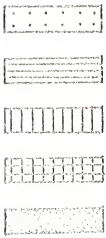

Fig. 73. Two-dimensional contour map of the flux density* at 27.6 MHz at Florida for the 1965.9 apparition.

*For definition of "flux density" as employed here, see discussion on page 38.

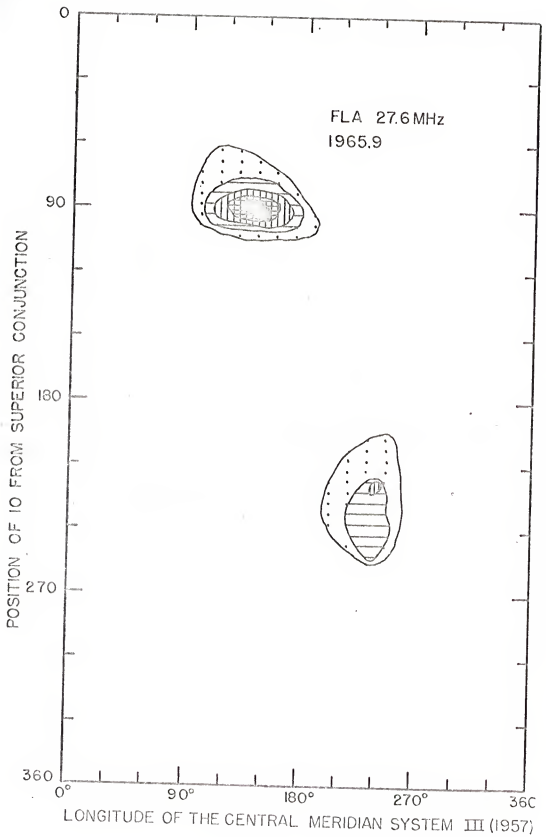
FLA 27.6 MHz
1965.9
0
90
180
270
360
POSITION OF IO FROM SUPERIOR CONJUNCTION
0°
90°
180°
270°
360
LONGITUDE OF THE CENTRAL MERIDIAN SYSTEM III (1957)

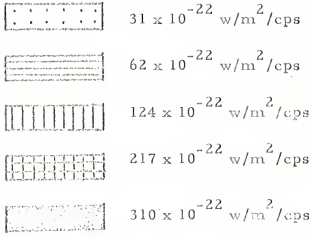

Fig. 74. Two-dimensional contour map of the flux density* at 27.6 MHz at Florida for the 1968.0 apparition.

*For definition of "flux density" as employed here, see discussion on page 38.

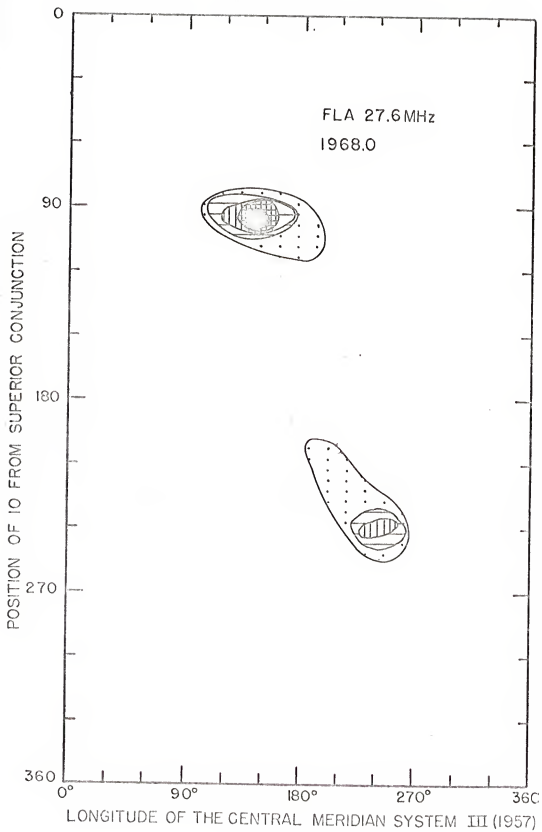
FLA 27.6MHz
1968.0
0
90
180
270
360
POSITION OF IO FROM SUPERIOR CONJUNCTION
0°
90°
180°
270°
360
LONGITUDE OF THE CENTRAL MERIDIAN SYSTEM III (1957)

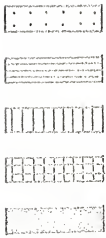

Fig. 75. Two-dimensional contour map of the flux density* at 27.6 MH at Florida for the 1969.0 apparition.

*For definition of "flux density" as employed here, see discussion on page 38.

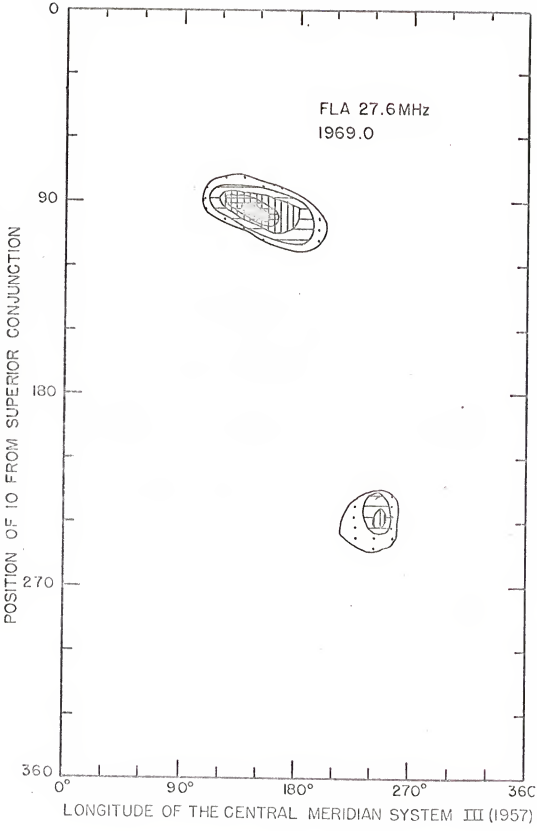
FLA 27.6MHz
1969.0
0
90
180
270
360
POSITION OF IO FROM SUPERIOR CONJUNCTION
0°
90°
180°
270°
360
LONGITUDE OF THE CENTRAL MERIDIAN SYSTEM III (1957)

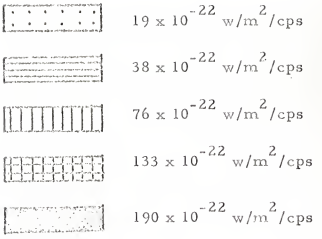

Fig. 76. Two-dimensional contour map of the flux density* at 27.6 MHz at Maipu for the 1962.5 apparition.

*For definition of "flux density" as employed here, see discussion on page 38.

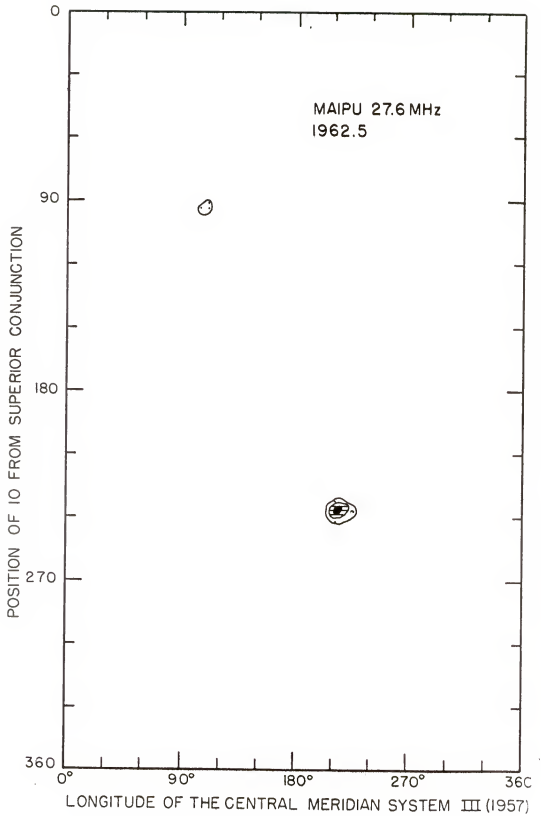
MAIPU 27.6 MHz
1962.5
0
90
180
270
360
POSITION OF IO FROM SUPERIOR CONJUNCTION
0°
90°
180°
270°
360
LONGITUDE OF THE CENTRAL MERIDIAN SYSTEM III (1957)

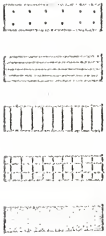

Fig. 77. Two-dimensional contour map of the flux density* at 27.6 MHz at Maipu for the 1963.7 apparition.

*For definition of "flux density" as employed here, see discussion on page 38.

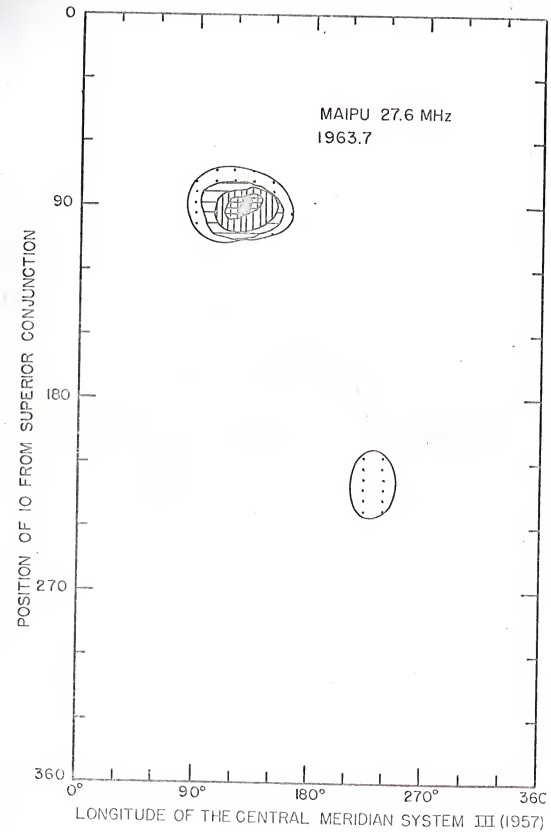
MAIPU 27.6 MHz
1963.7
0
90
180
270
360
POSITION OF IO FROM SUPERIOR CONJUNCTION
0°
90°
180°
270°
360
LONGITUDE OF THE CENTRAL MERIDIAN SYSTEM III (1957)

CHAPTER IV

INDIRECT INFLUENCE OF EUROPA AND GANYMEDE ON THE JOVIAN RADIATION

The previous work of Lebo, Register, and others indicates that Europa and Ganymede have no marked direct effect, similar to that found for Io, on the Jovian decametric radiation. This does not rule out the possibility of simultaneous positions of pairs of the satellites occurring for which the radiation is enhanced.

Two-dimensional contour maps of the flux density have been drawn for the position of Io from superior geocentric conjunction versus the position of Europa from superior geocentric conjunction, and for the position of Io from superior geocentric conjunction versus the position of Ganymede from superior geocentric conjunction (Figs. 78-81).

Since the periods of Io, Europa and Ganymede have a harmonic relationship, the simultaneous positions of any two are restricted over several months of time. If one plots the simultaneous positions of Io and Europa for several months, a band is traced out at 45° on the Io-Europa plane, indicating the simultaneous positions permitted these two satellites. Register[32] previously found that this band of positions slowly shifts with time and requires 11 years for a complete cycle.

Fig. 78. Two-dimensional contour map of position of Io from superior geocentric conjunction versus position of Europa from superior geocentric conjunction for flux density* at a frequency of 18 MHz at Maipu from 1960-1966 and at Florida from 1957-1969.

*For definition of "flux density" as employed here, see discussion on page 38.

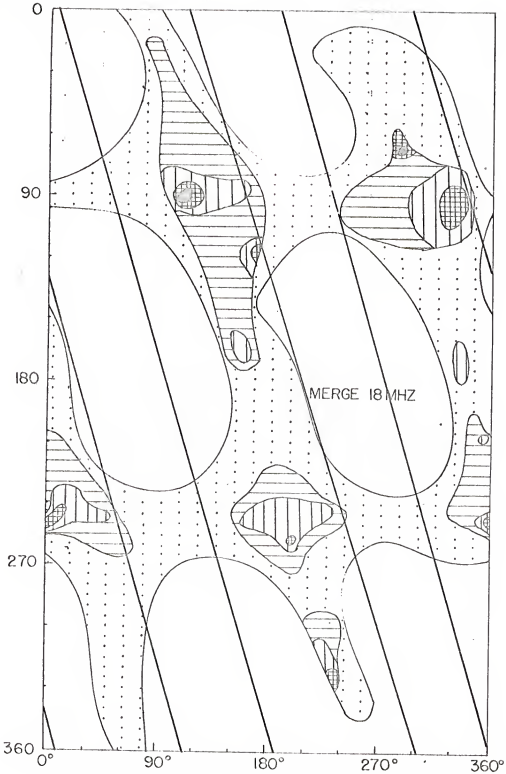
0
90
180
270
360
0°
90°
180°
270°
360°
MERGE 18 MHZ
POSITION OF IO FROM SUPERIOR GEOCENTRIC CONJUNCTION
POSITION OF EUROPA FROM SUPERIOR GEOCENTRIC CONJUNCTION

Fig. 79. Two-dimensional contour map of position of Io from superior geocentric conjunction versus position of Europa from superior geocentric conjunction for flux density* at a frequency of 22.2 MHz at Maipu from 1960-1965 and at Florida from 1958-1969.

*For definition of "flux density" as employed here, see discussion on page 38.

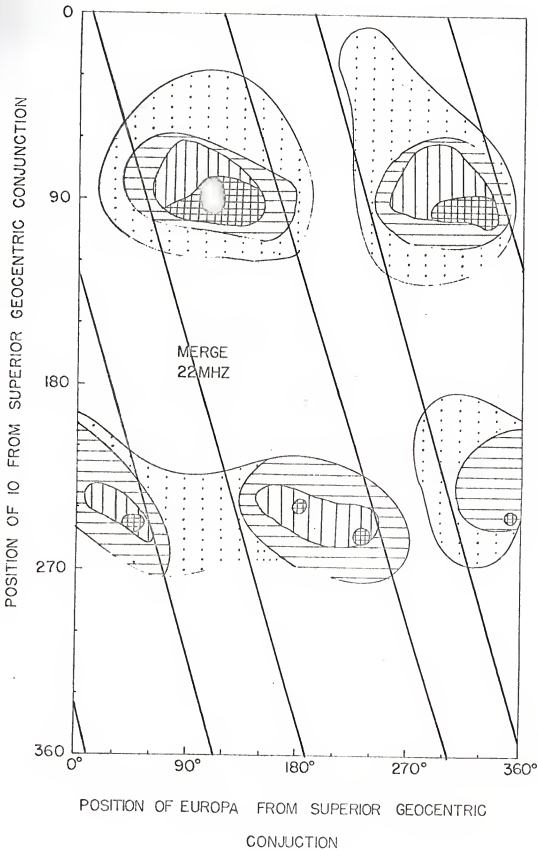
MERGE
22MHZ
0
90
180
270
360
0°
90°
180°
270°
360°
POSITION OF IO FROM SUPERIOR GEOCENTRIC CONJUNCTION
POSITION OF EUROPA FROM SUPERIOR GEOCENTRIC CONJUCTION

Fig. 80. Two-dimensional contour map of position of Io from superior geocentric conjunction versus position of Europa from superior geocentric conjunction for flux density* at a frequency of 27.6 MHz at Maipu from 1962-1964 and at Florida from 1961-1969.

*For definition of "flux density" as employed here, see discussion on page 38.

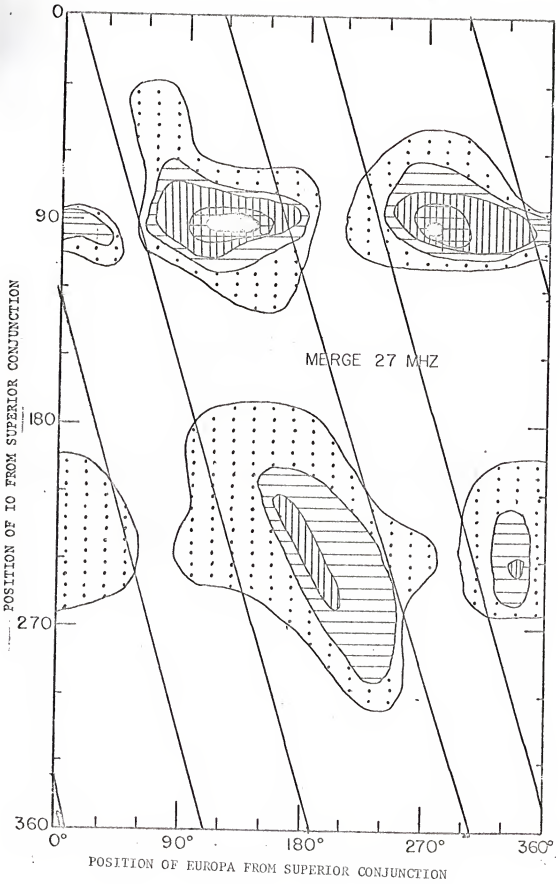
0
90
180
270
360
MERGE 27 MHZ
POSITION OF IO FROM SUPERIOR CONJUNCTION
0°
90°
180°
270°
360°
POSITION OF EUROPA FROM SUPERIOR CONJUNCTION

Fig. 81. Two-dimensional contour map of position of Io from superior geocentric conjunction versus position of Ganymede from superior geocentric conjunction for flux density* at a frequency of 18 MHz at Maipu from 1960-1966 and at Florida from 1957-1969.

*For definition of "flux density" as employed here, see discussion on page 38.

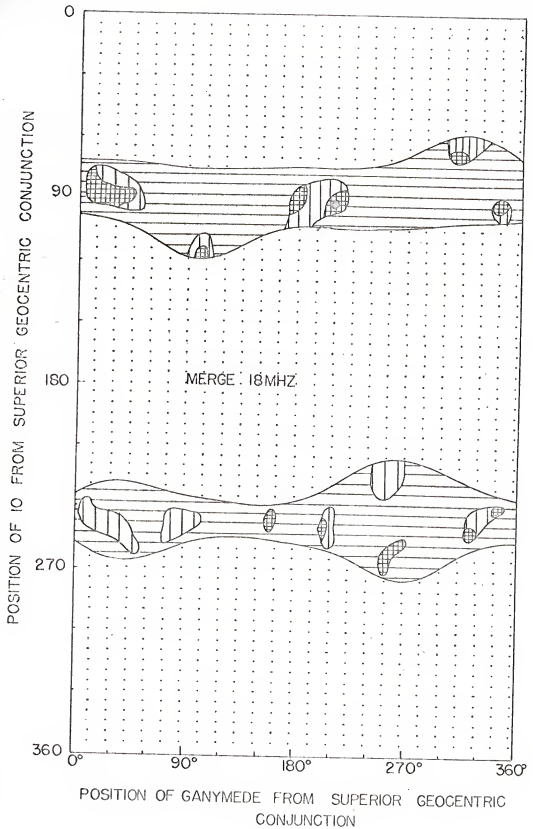
0
90
180
270
360
MERGE 18MHZ
POSITION OF IO FROM SUPERIOR GEOCENTRIC CONJUNCTION
0°
90°
180°
270°
360°
POSITION OF GANYMEDE FROM SUPERIOR GEOCENTRIC CONJUNCTION

If one draws the bands of permissible positions for Io and Europa for the 1963.8 and 1964.8 apparitions, it is obvious that nearly all of the flux received at 18 MHz from 1957 to 1969 occurs in these bands. The same behavior is observed at 22.2 MHz from 1958 to 1969 and at 27.6 MHz from 1961 to 1969.

At first glance, the above behavior is rather puzzling. Why should the two apparitions for which the bands were drawn contain such a large percentage of the received flux? The answer is obvious. These apparitions occur near the maximum probability of emission for the decametric radiation in its eleven-year cycle. Therefore, the apparent Europa-related "peaks" observed on the two-dimensional contour maps are in fact most likely due to an increased probability of emission. However, it would be necessary to observe a number of periods of the bands to determine if the peaks are definitely due to the increased probability of emission or if they are actually Europa-related sources.

A two-dimensional contour map of the flux received at a frequency of 18 MHz at Maipu from 1960 to 1966 and at Florida from 1957 to 1969 was drawn for the position of Io from superior geocentric conjunction (Fig. 81). The Io-related bands of flux centered near Io=90^{o} and 240^{o} from superior geocentric conjunction are obvious. However, no Ganymede-related sources are observed. Apparently there is no significant effect due to Io and Ganymede being situated at simultaneous, favorable positions.

CHAPTER V

FLUX CORRELATION STUDIES

In previous studies,[2, 32, 52] the planet-wide emission probability of the decametric radiation from Jupiter has been observed to be periodic with a period of approximately ten years. Gallet[56] first suggested that the emission probability was negatively correlated with the smoothed sunspot number. Numerous investigators[57, 58, 59, 60] have observed this apparent negative correlation. A second possibility, first mentioned by Carr,[61] is that the variation in the emission probability is due to the change in the Jovicentric declination of the Earth, D_E. Recently, Balasubrahmanyan and Venkatesan[62] have found evidence of a positive correlation between the darkness of Jupiter's red spot and solar activity. They suggest that an appropriate index of solar activity is the brightness of the Fe XIV 5303 Å emission line of the corona. The brightness of this line exhibits a double maximum with a pronounced minimum in between during an eleven-year cycle which corresponds to the sunspot cycle. It seems possible that solar activity as measured by the brightness of the coronal line might have a significant effect upon the decametric radiation received from Jupiter. It has proven to be very difficult to determine which of the above possibilities (if any) are correct, since the mean period of the sunspot cycle is eleven years

while the period of the Jovicentric declination of the Earth is 11.86 years.

In hope of clarifying the question of whether the sunspot cycle, solar activity as indicated by the brightness of the coronal 5303 Å line, or the Jovicentric declination of the Earth is the more important parameter, studies were undertaken of the normalized flux density summed over all longitudes. Two normalization procedures were used. In one, the summed flux density at a fixed frequency was normalized to equal periods of listening time for each apparition. This allows one to compensate for Jupiter having been observed for different lengths of time for each apparition. For example, assume that Jupiter is observed for 500 hours in one apparition, during which time a summed flux density S is recorded. If Jupiter is observed for 1000 hours in a second apparition in which a summed flux density S' is recorded, the normalized summed flux density for the second apparition would be S'/2. This normalization represents the total flux received for hypothetical apparitions in which Jupiter is observed for equal amounts of time.

In the second normalization procedure, the summed flux density at a fixed frequency was normalized to equal periods of active time for each apparition. Active time is defined as that amount of time during which decametric radiation is received. For example, assume that decametric radiation is received for a total time of ten hours in one apparition and twenty hours in a

second apparition with summed flux densities of S and S' respectively. The normalization procedure would credit the second apparition with a summed flux density of S'/2. If one calculates the summed flux density for apparitions of equal active time, one then has an indication of the average intensity of the decametric radiation received.

The results of the two normalizations versus the sunspot cycle, the brightness of the coronal 5303 Å line, and the Jovicentric declination are shown in Figs. 82-89 .

There is very little correlation, positive or negative, between the total flux and either the sunspot cycle or the Jovicentric declination of the earth at the frequencies 15 MHz, 22.2 MHz, and 27.6 MHz. It should be noted, however, that the average intensity appears to oscillate with a greater amplitude (Fig. 84) and more rapidly (Fig. 85) than the total flux.

When the curve for the total flux versus the sunspot cycle and Jovicentric declination of the Earth is studied at 18 MHz, a strong positive correlation is observed between the total flux and the Jovicentric declination of the Earth, and a strong negative correlation between the total flux and the sunspot cycle. It appears from the 18 MHz data that the sunspot cycle correlations are favored over the Jovicentric declination correlations.

When the curves for the total flux are compared to the brightness of the coronal 5303 Å line, no strong correlations are observed.

Fig. 82. The behavior of the intensity (Jupiter A. T.) and the total flux (Jupiter L. T.) are compared to both the cyclic change of the Jovicentric declination of the Earth (D_E) and the sunspot cycle for the radiation received at a frequency of 15 MHz at Maipu from 1961-1964 and at Florida from 1960-1969.

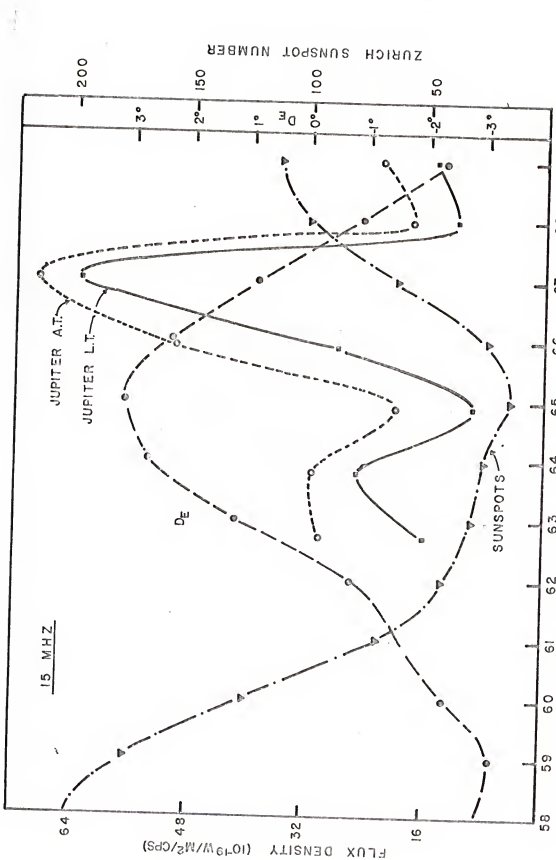
15 MHZ.
JUPITER A.T.
JUPITER L.T.
D_E
SUNSPOTS
FLUX DENSITY (10^{-19}W/M^2/CPS)
YEAR
ZURICH SUNSPOT NUMBER
D_E

Fig. 83. The behavior of the intensity (Jupiter A. T.) and the total flux (Jupiter L. T.) are compared to both the cyclic change of the Jovicentric declination of the Earth (D_E) and the sunspot cycle for the radiation received at a frequency of 18 MHz at Maipu from 1960-1966 and at Florida from 1957-1969.

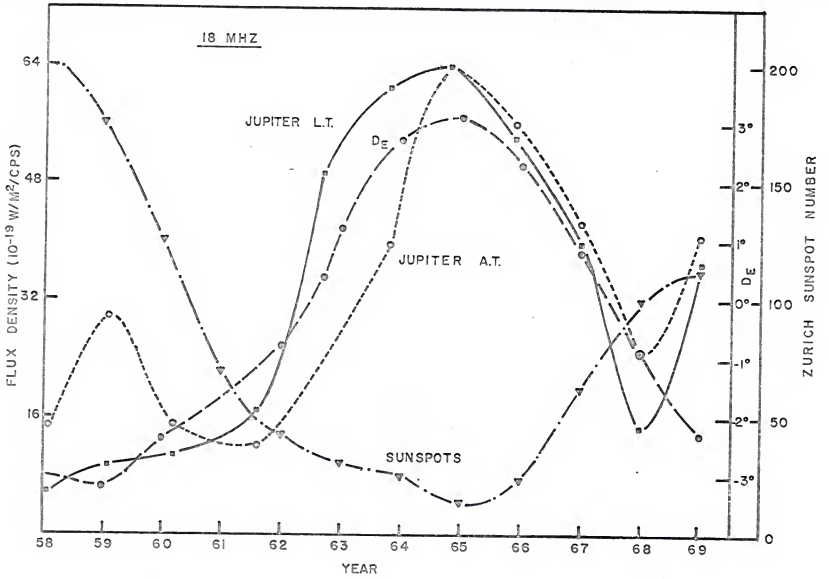
18 MHZ
JUPITER L.T.
D_E
JUPITER A.T.
SUNSPOTS
FLUX DENSITY (10^{-19} W/M^2/CPS)
64
48
32
16
D_E
3°
2°
1°
0°
-1°
-2°
-3°
200
150
100
50
0
ZURICH SUNSPOT NUMBER
58
59
60
61
62
63
64
65
66
67
68
69
YEAR

Fig. 84. The behavior of the intensity (Jupiter A. T.) and the total flux (Jupiter L. T.) are compared to both the cyclic change of the Jovicentric declination of the Earth (D_E) and the sunspot cycle for the radiation received at a frequency of 22.2 MHz at Maipu from 1960-1965 and at Florida from 1958-1969.

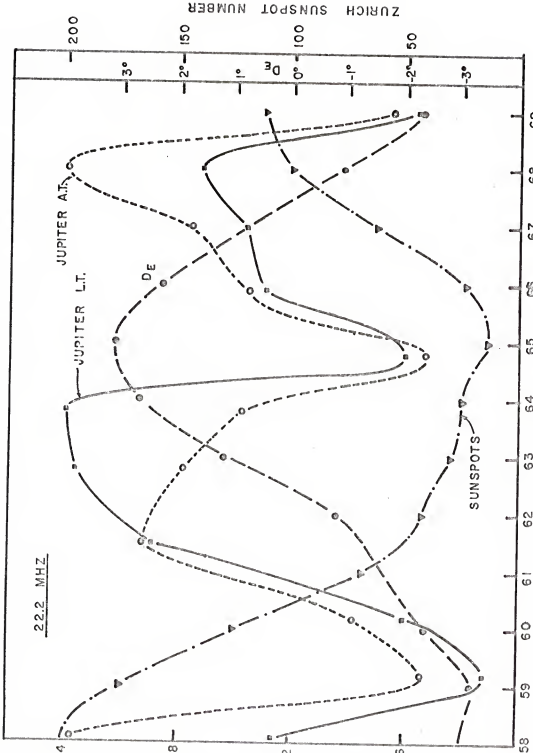
22.2 MHZ
JUPITER A.T.
JUPITER L.T.
D_E
SUNSPOTS
FLUX DENSITY (10^{-19} W/M^2/CPS)
64
48
32
16
DE
3°
2°
1°
0°
-1°
-2°
-3°
ZURICH SUNSPOT NUMBER
200
150
100
50
58
59
60
61
62
63
64
65
66
67
68
69
YEAR

Fig. 85. The behavior of the intensity (Jupiter A. T.) and the total flux (Jupiter L. T.) are compared to both the cyclic change of the Jovicentric declination of the Earth (D_E) and the sunspot cycle for the radiation received at a frequency of 27.6 MHz at Maipu from 1962-1964 and at Florida from 1961-1969.

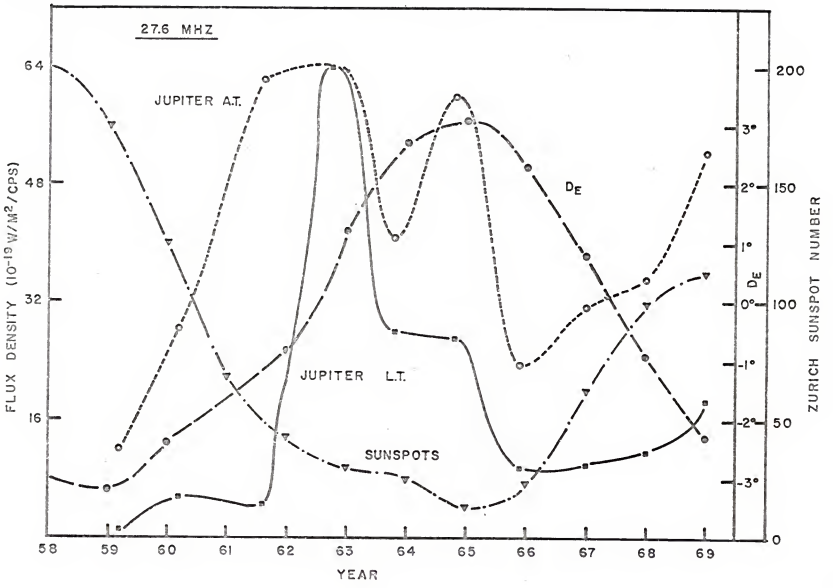
27.6 MHZ
JUPITER A.T.
JUPITER L.T.
SUNSPOTS
D_E
FLUX DENSITY (10^{-19} W/M^2/CPS)
ZURICH SUNSPOT NUMBER
YEAR
64
48
32
16
200
150
100
50
0
3°
2°
1°
0°
-1°
-2°
-3°
58
59
60
61
62
63
64
65
66
67
68
69

Fig. 86. The behavior of the intensity (Jupiter A. T.) and the total flux (Jupiter L. T.) are compared to the cycle of solar activity, as measured by the brightness of the coronal 5303 Å emission line. The data from Maipu (1961-1964) and from Florida (1960-1969) at a frequency of 15 MHz were used in this analysis.

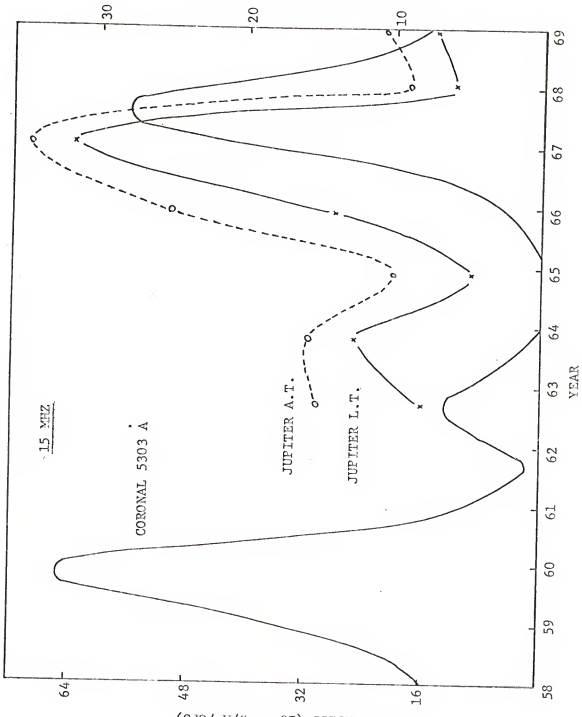
BRIGHTNESS OF CORONAL LINE
10
20
30
FLUX DENSITY (10^{-19} W/M^2/CPS)
16
32
48
64
58
59
60
61
62
63
64
65
66
67
68
69
YEAR
JUPITER L.T.
JUPITER A.T.
CORONAL 5303 Å
.15 MHZ

Fig. 87. The behavior of the intensity (Jupiter A. T.) and the total flux (Jupiter L. T.) are compared to the cycle of solar activity, as measured by the brightness of the coronal 5303 Å emission line. The data from Maipu (1960-1966) and from Florida (1957-1969) at a frequency of 18 MHz were used in this analysis.

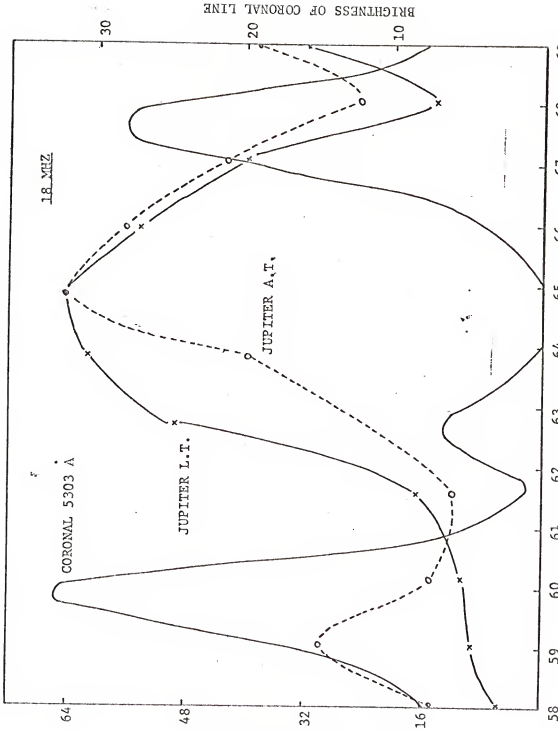
18 MHZ
CORONAL 5303 Å
JUPITER L.T.
JUPITER A.T.
FLUX DENSITY (10^{-19} W/M^2/CPS)
BRIGHTNESS OF CORONAL LINE
YEAR
64
48
32
16
30
20
10
58
59
60
61
62
63
64
65
66
67
68
69

Fig. 88. The behavior of the intensity (Jupiter A. T.) and the total flux (Jupiter L. T.) are compared to the cycle of solar activity, as measured by the brightness of the coronal 5303 Å emission line. The data from Maipu (1960-1965) and from Florida (1958-1969) at a frequency of 22.2 MHz were used in this analysis.

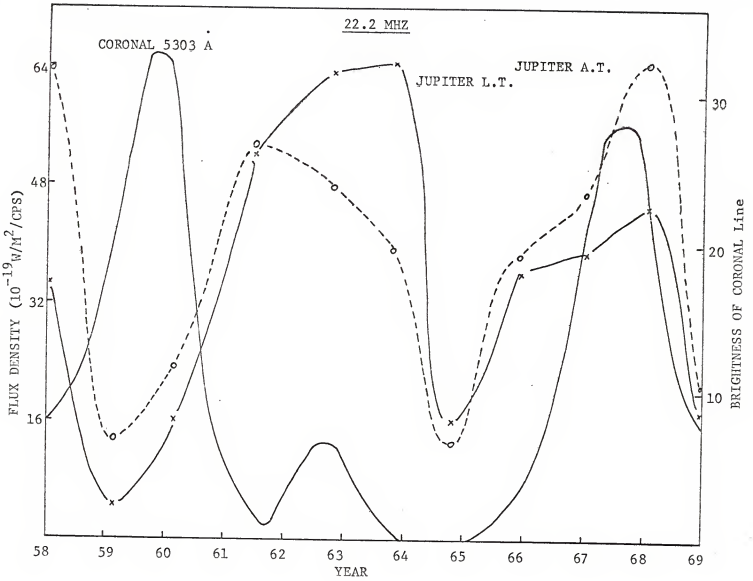
22.2 MHZ
CORONAL 5303 A
JUPITER A.T.
JUPITER L.T.
64
48
32
16
30
20
10
58
59
60
61
62
63
64
65
66
67
68
69
YEAR
FLUX DENSITY (10^{-19} W/M^2/CPS)
BRIGHTNESS OF CORONAL Line

Fig. 89. The behavior of the intensity (Jupiter A. T.) and the total flux (Jupiter L. T.) are compared to the cycle of solar activity, as measured by the brightness of the coronal 5303 Å emission line. The data from Maipu (1962-1964)and from Florida (1961-1969) at a frequency of 27.6 MHz were used in this analysis.

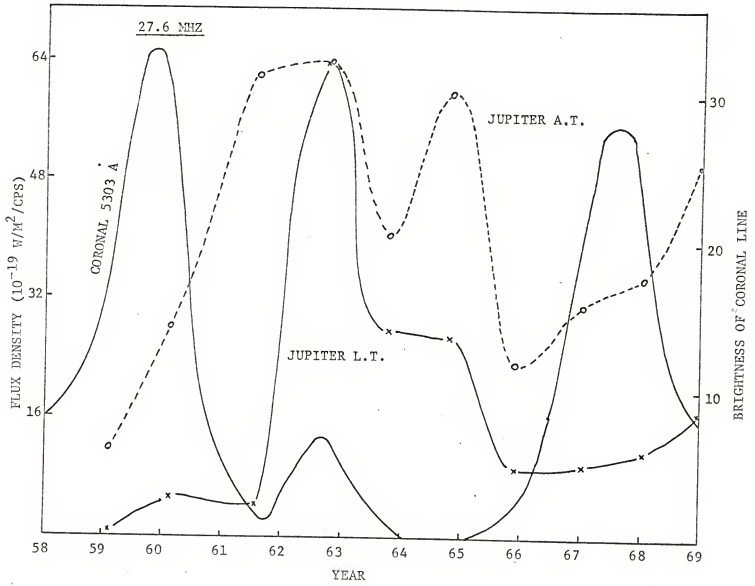
27.6 MHZ
64
48
32
16
FLUX DENSITY (10^{-19} W/M^2/CPS)
CORONAL 5303 Å
JUPITER A.T.
JUPITER L.T.
30
20
10
BRIGHTNESS OF CORONAL LINE
58
59
60
61
62
63
64
65
66
67
68
69
YEAR

However, when the curves for the average intensity are compared to the brightness of the coronal line, there appears to be a positive correlation at all frequencies except 18 MHz (Figs. 86-89). These correlations suggest that although the total flux received from Jupiter for a given apparition is apparently unaffected by solar activity, as monitored by the coronal 5303 Å line, the intensity of the radiation is modulated by the solar activity.

In light of the present analysis, it appears that effects due to the 11-year cycle of solar activity, although perhaps not the sunspot cycle explicitly, are more important with respect to the total flux received at decametric wavelengths than is the Jovicentric declination of the earth. However, the arguments presented here are not conclusive and a more detailed study of the variation of the summed flux density as a function of other solar parameters needs to be done.

CHAPTER VI

PULSE HEIGHT ANALYSIS

A pulse height analysis was performed on the decametric pulses received from Jupiter at frequencies of 15 MHz, 18 MHz, 22.2 MHz, and 27.6 MHz, with the results shown in Figs. 90-93. In most pulse height analyses, the number of pulses and the energy of the pulses are the two parameters analyzed. In the present analysis, the number of five-minute intervals for which activity was observed and the flux density are the parameters investigated.

A number of similarities were noticed for all frequencies investigated. It was observed that the pulse height spectrum out to flux densities of approximately 70×10^{-22} w/m^2/cps could be computer-fitted to a curve of the form

$$N = A(S+B)^C \text{ EXP-}5(S+B)^D + 15 \qquad (16)$$

where N is the number of five-minute intervals containing flux density S. The values of the parameters A, B, C, and D are shown in Table 3 for all four frequencies.

TABLE 3

Parameter Values

Frequency	A	B	C	D
15 MHz	3333.9	4.01	2.6925	0.2901
18 MHz	3623.7	3.46	2.6298	0.2880
22.2 MHz	3497.6	4.25	2.6518	0.2878
27.6 MHz	1159.9	2.79	3.2226	0.3592

Fig. 90. A plot of the number of five-minute intervals in which decametric radiation is received at 15 MHz at Florida (1962-1969) as a function of the mean flux density* for the five-minute interval.

*For definition of "flux density" as employed here, see discussion on page 38.

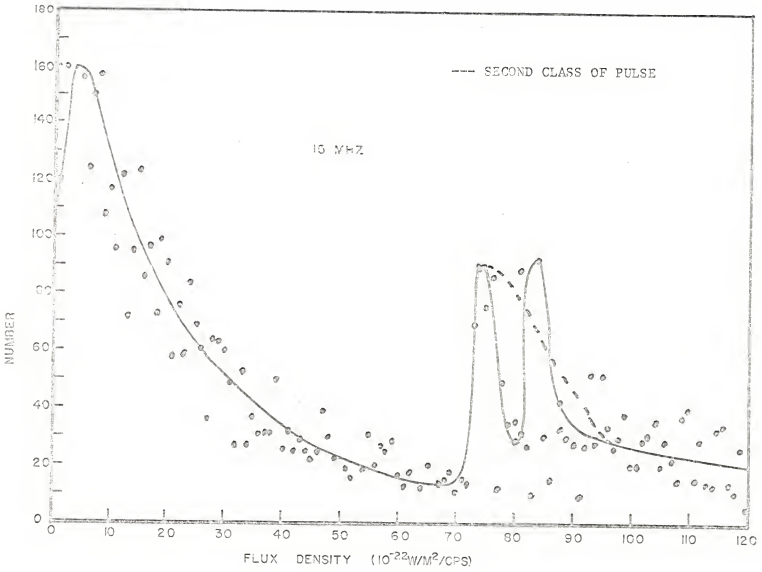
--- SECOND CLASS OF PULSE
15 MHZ
NUMBER
FLUX DENSITY (10⁻²²W/M²/CPS)
0
20
40
60
80
100
120
140
160
180
10
30
50
70
90
110

Fig. 91. A plot of the number of five-minute intervals in which decametric radiation is received at 18 MHz at Florida (1962-1969) as a function of the mean flux density* for the five-minute interval.

*For definition of "flux density" as employed here, see discussion on page 38.

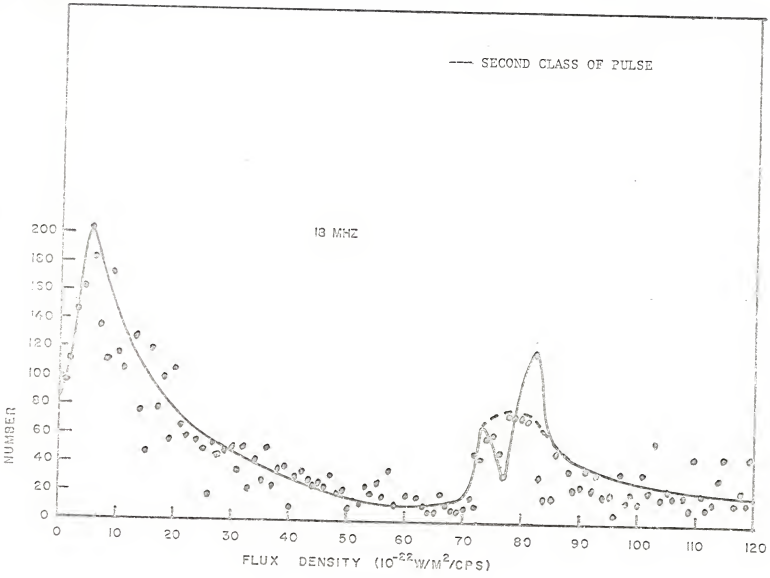
SECOND CLASS OF PULSE
13 MHZ
NUMBER
FLUX DENSITY (10^{-22}W/M^2/CPS)
0
20
40
60
80
100
120
140
160
180
200
10
30
50
70
90
110

Fig. 92. A plot of the number of five-minute intervals in which decametric radiation is received at 22.2 MHz at Florida (1962-1969) as a function of the mean flux density* for the five-minute interval.

*For definition of "flux density" as employed here, see discussion on page 38.

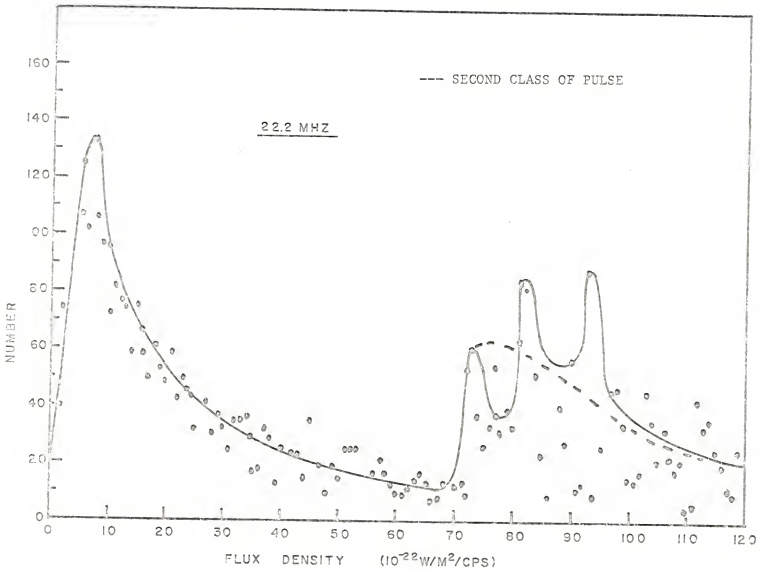
--- SECOND CLASS OF PULSE
22.2 MHZ
NUMBER
0
20
40
60
80
100
120
140
160
0
10
20
30
40
50
60
70
80
90
100
110
120
FLUX DENSITY (10⁻²²W/M²/CPS)

Fig. 93. A plot of the number of five-minute intervals in which decametric radiation is received at 27.6 MHz at Florida (1962-1969) as a function of the mean flux density* for the five-minute interval.

*For definition of "flux density" as employed here, see discussion on page 38.

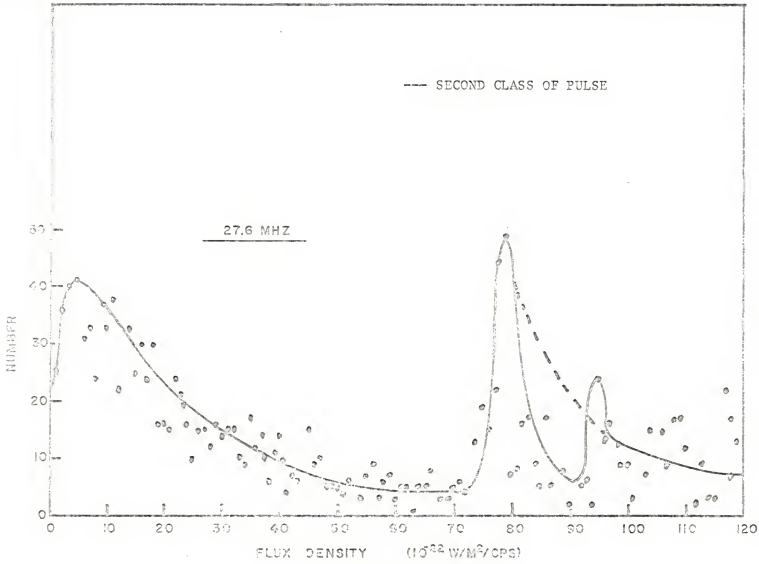
--- SECOND CLASS OF PULSE
27.6 MHZ
NUMBER
0
10
20
30
40
50
60
70
80
90
100
110
120
FLUX DENSITY (10^-22 W/M^2/CPS)

The parameters C and D are of particular interest, since they are the exponents of the flux density in the leading multiplying term and in the exponential term, respectively. There is very good agreement at the frequencies 15 MHz, 18 MHz, and 22.2 MHz for the values of C and D. There is a noticeable difference in these values at 27.6 MHz, which may be due to much less data being available at this frequency.

Another very striking feature of each of the pulse height spectrums is the groups of two or three very sharp peaks which appear for flux densities greater than 70×10^{-22} $w/m^2/cps$. There appears to be a very sharp departure from the behavior indicated by Eq. (16) at a precise value of the flux density of 73×10^{-22} $w/m^2/cps$ for the frequencies 15 MHz, 18 MHz, and 22.2 MHz. At 27.6 MHz, this departure occurs at 74×10^{-22} $w/m^2/cps$. This sudden departure from the behavior described by Eq. (16) may indicate that another class of pulses is being received with an anomalously high value of the flux density. If this assumption is valid, it appears that the number of these pulses also decreases exponentially as the flux density increases.

At the present time, there is some doubt as to the validity of the observed peaks due to the manner in which the data were reduced. The flux densities of the pulses in the above analysis were calculated by dividing the time of Jupiter activity into five-minute intervals, calculating and averaging the flux density of the

three peak pulses in the interval, and calling this average the flux density for that five-minute interval. To establish if Figs. 90-93 exhibit the true character of the distribution, a pulse-by-pulse calculation must be done. If the general features of the curves are still the same, it would be of interest to investigate the possible mechanisms which could be responsible either for the resonance-like behavior at flux densities greater than 70×10^{-22} $w/m^2/cps$ or that would generate another class of pulses with a much higher flux density.

CHAPTER VII

SUMMARY

The Jovian decametric radiation received from 1957 to 1969 at the University of Florida and its associated field station at Maipu, Chile, has been analyzed at frequencies ranging from 15 MHz to 27.6 MHz. A consistent analysis of the flux density was undertaken for approximately seventy-five yearly sets of data in order that the individual and joint effects of several geometrical parameters could be determined. The flux density analysis describes the characteristics of the decametric radiation in terms of its observed intensity. Previous extensive analyses of this radiation have largely been confined to the emission probability, rather than flux density.

A two-dimensional analysis of the flux density as a simultaneous function of the longitude of the central meridian, System III (1957), and the position of Io from superior geocentric conjunction was made. The well-known Io-related "sources," A, B, and C, which were observed in previous probability studies were also recognized in the present analysis of the flux density. However, there were both similarities and differences observed in the structure and amplitude of these sources when the results of the two analyses were compared.

At 15 MHz, Io-related source B appears to be concentrated at higher longitude positions in the flux density analysis than was observed in the probability studies. Io-related sources C and D were observed in both analyses. Io-related source C appears as a relatively stronger source in the probability studies than in the flux density analysis, while Io-related source D appears to be a stronger source when analyzed in terms of the flux density. Source A was observed to exhibit very little Io dependence in either analysis.

At 18 MHz, Io-related sources A, B, and C appear to be of comparable strength in the probability studies, while in the flux density analysis the intensity of the radiation received from Io-related sources B and C is noticeably stronger than that associated with Io-related source A. The intensity of the radiation received from Io-related source C also appears to be much stronger in the longitude region from 0^{o} to 30^{o} than is indicated by the probability analysis. The strength and location of non-Io-related source A as determined from the flux density analysis agrees quite well with that determined from the probability studies.

At 22.2 MHz, the flux density analysis indicates that Io-related source B is the dominant source, while probability studies have indicated that Io-related sources A and B are of comparable strength. Io-related source B is more sharply defined in Io position when analyzed in terms of the emission probability rather than in terms of the flux density. In the flux density analysis, Io-related

sources A and C are of comparable strength, while the probability analysis indicates that Io-related source A is a great deal stronger than Io-related source C. In the flux density analysis, Io-related source A is observed over a much wider range of Io positions than was determined from the probability studies. Io-related source C is apparent for a much smaller range of longitudes when analyzed in terms of the flux density than when it is analyzed in terms of the emission probability. Both analyses, however, indicate a decrease in the radiation received from non-Io-related source A at 22.2 MHz relative to that received at 15 MHz or 18 MHz.

At 27.6 MHz, Io-related source B appears as the only prominent source, with Io-related source A just detectable in the flux density analysis. However, in the probability analysis, Io-related source A is definitely observed, although it is not as strong as Io-related source B. In both analyses, Jo-related source C has essentially disappeared. The flux density analysis indicates a stronger non-Io-related source A component than the probability analysis, although in both analyses the radiation from this source has diminished considerably from that observed at lower frequencies.

It should be noted that the flux density analysis indicates that Io-related source B is the only consistent peak in the frequency range from 15 MHz to 27.6 MHz, and that Io-related source C decreases in strength with increasing frequency until it has essentially disappeared at 27.6 MHz. These characteristics are in good agreement with the

previous probability studies. However, the bifurcation of Io-related source B which had previously been reported in the probability studies was not observed in the flux density analysis.

It is of interest to determine the dependence of the absolute flux density upon the frequency in the range from 15 MHz to 27.6 MHz, In particular, let us look at the behavior of the flux density associated with Io-related source B. If we examine the values obtained for the peaks representing this source in Figs. 24-27, it is found that the flux reaches a maximum value at 18 MHz, and then falls off to approximately 70% of this value at 15 MHz. At 22.2 MHz, the flux density has diminished to 80% of the value observed at 18 MHz. However, at 27.6 MHz, the flux density has fallen to a value of only 30% of that observed at 18 MHz.

A much more limited flux density analysis has previously been performed by G. R. Lebo.[52] Io-related source A was observed to be much stronger at frequencies of 22.2 MHz and 27.6 MHz than is indicated by the present analysis. Io-related source C, which was not observed in the present analysis at a frequency of 27.6 MHz, was apparent in the previous analysis. This earlier analysis also indicated that Io-related sources A and B are of comparable strength at frequencies of 15 MHz and 18 MHz, while Io-related source C continues to increase in intensity with decreasing frequency until it is the most conspicuous source observed at 15 MHz. This is in general agreement with the present analysis except that Io-related sources B and C are

now observed to be of comparable strength at 15 MHz and 18 MHz. Io-related source A, while not observed to be as strong as Io-related sources B and C, is still very apparent at both of these frequencies.

The two-dimensional analysis of the flux density was also used in an attempt to determine if there exist simultaneous favorable positions of Io and Europa and Io and Ganymede for which the intensity of the radiation is enhanced. It appears that there is no applicable effect due either to Europa or Ganymede.

A definite symmetry about the Earth-Jupiter line was observed which appears to be associated with these four sources. It was noted that if the positions of Io and Jupiter's north magnetic pole associated with Io-related source A are reflected through the Earth-Jupiter line, they are then located at positions for which radiation associated with Io-related source B is highly probable. A similar relationship relative to the Earth-Jupiter line exists for Io-related sources C and D where the parameters which are reflected are the position of Io and the position of Jupiter's south magnetic pole. This strongly suggests that Io's position relative to the Earth is the important factor with regard to the reception of the decametric radiation from Jupiter.

It is obvious that Io's distance from either the north or south magnetic pole varies from some minimum distance to a maximum distance as Io revolves about Jupiter. If one believes the general radiation model proposed by Goldreich and Lynden-Bell,[42] the plasma trapped in the flux tube attached to Io should be compressed as Io

approaches either of the magnetic poles. This compression would change the charge density and the electric field associated with it inside the flux tube. One may speculate that this compression may be the source of the anomalies in the current flowing along the flux tube which apparently is the origin of the decametric bursts. It has been observed in the present work that the volume contained in the northern half of Io's flux tube is at or near a minimum when sources B and C are observed. It has also been observed that the volumes of the northern and southern halves of the flux tube are approximately equal when sources A and D are observed.

A study was made of the flux density versus sunspot number, Jovicentric declination of the earth, and brightness of the coronal 5303 Å line (which is widely used as an index of solar activity) in an attempt to determine which of these parameters appears to have more influence on the observed 11-year cycle of the Jovian emission probability. A limited amount of positive correlation was observed between the flux density and the brightness of the coronal line, indicating that solar activity may exert a more important influence on the decametric radiation than the Jovicentric declination. However, the results presented here are far from conclusive.

A pulse-height analysis of the Jupiter data was also carried out. In this pulse height analysis, the number of five-minute intervals in which the average of the three peak pulses equaled a given flux density was plotted as a function of flux density. It was found that the number decreased exponentially as the flux density increased, out to

a value of 73×10^{-22} $w/m^2/cps$. At this point, the number of five-minute intervals in which the flux density exceeded the previously mentioned value suddenly increased. This jump may be due either to some resonance phenomenon, or it may result from a different class of pulses. The analysis is not complete enough at the present time to determine which of the above-mentioned possibilities is more likely.

LIST OF REFERENCES

1. B. F. Burke and K. L. Franklin, "Observations of a Variable Radio Source Associated With the Planet Jupiter," Journal of Geophysical Research 60, 213 (1955).
2. I. Shever, "Influence of Io on Jovian Decametric Radiation." (Ph. D. Dissertation, University of Florida, 1967).
3. T. D. Carr, A. G. Smith, R. Pepple, and C. H. Barrow, "18 Megacycle Observations of Jupiter in 1957," Astrophysical Journal 127, 274-283 (1958).
4. T. D. Carr and A. G. Smith, "Radio Frequency Emission from the Planet Jupiter," Astronomical Journal 64, 39-21 (1959).
5. R. M. Gallet, " The Results of Observations of Jupiter's Radio Emissions of 18 and 20 MC/S in 1956 and 1957," Transactions of the Institute of Radio Engineers AP-5, 327 (1957, Abstract).
6. R. M. Gallet, "Radio Observations of Jupiter 11," Planets and Satellites, edited by G. P. Kuiper and B. M. Middlehurst, Chapter 4 (University of Chicago Press, 1961).
7. K. L. Franklin and B. F. Burke, "Radio Observations of Jupiter," Astronomical Journal 61, 177 (1956, Abstract).
8. J. F. Firor, W. C. Erickson, H. W. Wells, B. F. Burke, and K. L. Franklin, "Radio Astronomy," Carnegie Institute of

Washington Year Book, 74-76 (1956).

9. B. F. Burke, "Radio Astronomy," Carnegie Institute of Washington Year Book, 90 (1957).

10. K. L. Franklin and B. F. Burke, "Radio Observations of the Planet Jupiter," Journal of Geophysical Research 63, 807-824 (1958).

11. J. D. Kraus, "Some Observations of the Impulse Radio Signals from Jupiter," Astronomical Journal 61, 182-183 (1956, Abstract).

12. J. D. Kraus, "Planetary and Solar Emission at 11 Meters Wavelength," Proceedings of the Institute of Radio Engineers 46, 266-274 (1958).

13. J. D. Kraus, "Radio Observations of Jupiter," Proceedings of the Institute of Radio Engineers (Correspondence) 47, 82 (1959).

14. J. N. Douglas and H. J. Smith, "Decametric Radiation from Jupiter," Astronomical Journal 68, 163 (1963).

15. J. N. Douglas and H. J. Smith, "Change in Rotation Period of Jupiter's Decameter Radio Sources," Nature 199, 1080 (1963).

16. J. W. Warwick, "The Position and Sign of Jupiter's Magnetic Moment," Astrophysical Journal 137, 1317 (1963).

17. J. W. Warwick and W. T. Kreiss, IGY Solar Activity Report 20 - Boulder, Colorado (1964).

18. J. W. Warwick and G. A. Dulk, IGY Solar Activity Report 32 and 34 - Boulder, Colorado (1966).

19. J. N. Douglas, "Decametric Radiation From Jupiter," IFFF Transactions on Military Electronics MIL-8, 173-187 (1964).

20. C. H. Mayer, T. P. McCullough, and R. N. Sloanaker, "Observations of Mars and Jupiter at a Wavelength of 3.15 Cm," Astrophysical Journal 127, 11 (1958).

21. J. S. Hey, "Solar Radiations in the 4-6 Metre Radio Wave-Length Band," Nature 157, 47 (1946).

22. V. Radhakrishnan and J. A. Roberts, "Polarization and Angular Extent of the 960-Mc/sec Radiation from Jupiter," Physical Review Letters 4, 493 (1960).

23. G. B. Field, "The Source of Radiation from Jupiter at Decimeter Wavelengths," Journal of Geophysical Research 64, 1169 (1959); 65, 1661 (1960); 66,1395 (1961).

24. J. A. Roberts and G. J. Stanley, "Radio Emission from Jupiter at a Wavelength of 31 Cm," Publications of the Astronomical Society of the Pacific 71, 485 (1959).

25. C. A. Shain, "18.3 Mc/s Radiation from Jupiter," Australian Journal of Physics 9, 61-73 (1956).

26. T. D. Carr, A. G. Smith, H. Bollhagen, N. F. Six, and N. E. Chatterton, "Recent Decameter-Wavelength Observations of Jupiter, Saturn, and Venus," The Astrophysical Journal 134, 105-125 (1961).

27. T. D. Carr, A. G. Smith, R. Pepple, and C. H. Barrow, "18-Megacycle Observations of Jupiter in 1957," The Astrophysical Journal 127, 274-283 (1958).

28. International Astronomical Union Information Bulletin 8, March 1962.

29. A. G. Smith, G. R. Lebo, N. F. Six, T. D. Carr, H. Bollhagen, J. May, and J. Levy, "Decameter-Wavelength Observations of Jupiter: The Apparitions of 1961 and 1962," Astrophysical Journal 141, 457 (1965).

30. S. Gulkis and T. D. Carr, "Radio Rotation of Jupiter," Science 154, 257-259 (1966).

31. T. D. Carr and F. F. Donivan, "Jupiter's Decametric Rotation Period," The Astrophysical Journal 157, 65-68 (1969).

32. H. I. Register, "Decameter-Wavelength Radio Observations of the Planet Jupiter 1957-1968 (Ph. D. Dissertation, University of Florida, 1968).

33. T. D. Carr, NASA Conference on Jupiter, New York (1962).

34. J. N. Douglas, "Decametric Radiation From Jupiter," IFFF Transactions on Military Electronics MIL-8, 173-187 (1964).

35. E. K. Bigg, "Influence of the Satellite Io on Jupiter's Decametric Radio Emission," Nature 203, 1008 (1964).

36. G. R. Lebo, A. G. Smith, and T. D. Carr, "Jupiter's Decametric Emission Correlated With the Longitudes of the First Three Galilean Satellites," Science 148, 1724-1725 (1965).

37. G. A. Dulk, Io-Related Radio Emission From Jupiter (Ph. D. Thesis, University of Colorado, 1965).

38. G. A. Dulk, "Lack of Effects of Satellites Europa, Ganymede, Callisto, and Amalthea on the Decametric Radio Emission of Jupiter," The Astrophysical Journal 148, 239-248 (1967).

39. J. A. Gledhill, The Structure of Jupiter's Magnetosphere and the Effect of Io on its Decametric Radio Emission (Goddard Space Flight Center Report X-615-67-296, 1967).

40. G. R. A. Ellis and P. M. McCullough, "The Decameter Radio Emissions of Jupiter," Australian Journal of Physics 16, 380 (1963).

41. J. W. Warwick, "Radio Physics of Jupiter," Space Science Reviews 6, 841-891 (1967).

42. P. Goldreich and D. Lynden-Bell, "Io, A Jovian Unipolar Generator," The Astrophysical Journal 156, 59-78 (1969).

43. T. D. Carr, Studies of Radio Frequency Radiation from the Planets (Ph.D. Dissertation, University of Florida, 1958).

44. N. E. Chatterton, Spectral Characteristics of the Radio-Frequency Outbursts of the Planet Jupiter (Ph.D. Dissertation, University of Florida, 1963).

45. N. F. Six, Jr., Analysis of the Decameter-Wavelength Radio Emission from the Planet Jupiter (Ph.D. Dissertation, University of Florida, 1963).

46. G. R. Lebo, Decameter-Wavelength Radio Observations of the Planets in 1962 (Ph.D. Dissertation, University of Florida, 1964).

47. T. D. Carr and S. Gulkis, "The Magnetosphere of Jupiter," Annual Review of Astronomy and Astrophysics 7, 577-618 (1969).

48. A. G. Smith, "The Radio Spectrum," Science 145, 380-382 (1964).

49. J. D. Kraus, Radio Astronomy (McGraw-Hill Book Company, 1966).

50. J. D. Kraus, Antennas (McGraw-Hill Book Company, 1967).

51. D. J. Kennedy, Polarization of the Decametric Radiation from Jupiter (Ph.D. Dissertation, University of Florida, 1969).

52. G. R. Lebo (unpublished data, 1965).

53. C. F. Tiberi and T. D. Carr (unpublished data, 1965).

54. N. F. Six, Jr., Analysis of the Decameter-Wavelength Radio Emission from the Planet Jupiter (Ph.D. Dissertation, University of Florida, 1963).

55. C. N. Olsson and A. G. Smith, "Delineation of Jovian Decametric Sources by Millisecond Pulses," Nature 214, 999-1001 (1967).

56. R. M. Gallet, "Radio Observations of Jupiter II," Planets and Satellites, edited by G. P. Kuiper and B. M. Middlehurst, Chapter 4 (University of Chicago Press, 1961).

57. A. G. Smith, T. D. Carr, and N. F. Six, "Results of Recent Decameter-Wavelength Observations of Jupiter," La Physique Des Planets 7, 543-553 (1963).

58. T. D. Carr, A. G. Smith, and H. Bollhagen, "Evidence for the Solar Corpuscular Origin of the Decameter Wavelength Radiation from Jupiter," Planetary Space Science 13, 997-1001 (1965).

59. J. W. Warwick, "Relation of Jupiter's Radio Emission at Long Wavelengths to Solar Activity," Science 132, 1250-1252 (1960).

60. A. J. Plourde, Statistical Investigation of the Occurrence of Noise Emission from the Planet Jupiter (Master's Thesis, University of Florida, 1960).

61. T. D. Carr, NASA Conference on Jupiter, New York (1962).

62. V. K. Balasubrahmanyan and D. Venkatesan, "Solar Activity and the Great Red Spot of Jupiter," Astrophysical Letters 6, 123-126 (1970).

BIOGRAPHICAL SKETCH

Hugh Richard Miller was born in Springfield, Tennessee, on March 13, 1943, the son of Mr. and Mrs. Hugh R. Miller. After living in Tennessee until the age of twelve, he and his family moved to Bay City, Texas, and lived there three months. This was followed by eight months of residence in New Orleans, Louisiana. Then, in the fall of 1956, he moved to Richmond, Kentucky, where he continued his education and graduated from Madison Central High School in June, 1961. He attended Eastern Kentucky State College and received the Bachelor of Science degree in June, 1965. The following September he enrolled in the Graduate School of the University of Florida where he received the Master of Science degree in March, 1969. He is currently employed as an assistant professor of physics and astronomy at Georgia State University in Atlanta, Georgia. His wife is the former Beverly Ann Brumfield, who he married August 31, 1963.

Hugh Richard Miller is a member of the AIP student section. He is also a member of Sigma Pi Sigma and served as President of the University of Florida chapter during the 1966-1967 academic year.

This dissertation was prepared under the direction of the chairman of the candidate's supervisory committee and has been approved by all members of that committee. It was submitted to the Dean of the College of Arts and Sciences and to the Graduate Council, and was approved as partial fulfillment of the requirements for the degree of Doctor of Philosophy.

December, 1970.

H. E. Spivey
Dean, College of Arts and Sciences

Dean, Graduate School

Supervisory Committee:

A. G. Smith, Chairman

T. D. Carr

G. R. Lebo

F. B. Wood

F. E. Dunnam